Università degli Studi di Milano
Dipartimento di Chimica Strutturale
e Stereochimica Inorganica
via Venezian 21 - 20133 Milano

CORSO DI DOTTORATO DI RICERCA IN SCIENZE CHIMICHE CICLO XXIII

TESI DI DOTTORATO DI RICERCA

ORGANOMETALLIC CHEMISTRY FROM THE INTERACTING QUANTUM ATOMS APPROACH

sigla del settore scientifico disciplinare
CHIM03

NOME DEL TUTOR
Prof: Angelo Sironi

NOME DEL DOTTORANDO
Davide Tiana

NOME DEL COORDINATORE DEL DOTTORATO
Prof. Silvia Ardizzone

ANNO ACCADEMICO 2009/2010


LINUX POWER
PENGUIN COMPUTING

Index

Introduction

Organometallic chemistry is very important for industrial processes, organic synthesis and "green chemistry". It consists of the study of chemical compounds containing bonds between carbon and metal (M). Situations where metal is bounded to an organic ligand (L) but not directly to C should be instead referred to metal-organic area but, nowadays, these two terms result almost interchangeable. As usual, the presence of electrons in the d shell makes differences in organometallic chemistry of the transition metals (TM) and of the main group (1, 2, 12-18) elements. The TM organometallic chemistry will be treated in this thesis. This can be considered as a subfield of the more general coordination chemistry in which the complexes contain M-C and M-H bond[1]. Nowadays coordination chemistry is treated by the ligand field theory which will be briefly summarized.

The ligand field theory (LFT)

This theory is an improvement of the crystal field theory (CFT) and represents an application of molecular orbital (MO) theory to transition metal complexes. Developed in 1930s, CFT explains compound colors, magnetism and other properties not taking into account the description of TM-L bond. Based on the energy changes of the five d metal orbitals, this theory considers interactions between metal and ligand as purely electrostatic. Depending on the geometry, when ligand approaches TM, L electrons will be closer to some d-electrons than to others. Thus, because of charges repulsion between electrons, d-orbitals divide themselves removing their degeneracy. For instance, in octahedral complexes there are six L around metal: d_{z^2} and $d_{x^2-y^2}$ point to the ligand resulting higher in energy than d_{xy}, d_{xz}, d_{yz},. Thus an energy gap called Δ arises between the two series of d orbitals. The magnitude of delta, which depends on the geometry and ligands nature, determines if a molecule is para or diamagnetic. Indeed, if such gap is low, the high d orbitals will be accessible and the electrons will spread in the maximum spin multiplicity. On the other hand, in an high gap compound, the system would spend too much energy to put electrons in all the d orbitals. Instead of following the Hund's rule, the electrons will tend to lie in the low orbitals coupling each other providing a low spin configuration. Orbitals diagrams related to different geometries are reported in figure 1. Although CFT gives a useful qualitative explanation of metal-organic interaction, it lacks of a

[1] R.H.Crabtree *The Organometallic Chemistry of the Transition Metals* John Wiley & Sons Inc. Publications

real treatment of chemical bond. A more exhaustive model to treat the chemical bond in coordination chemistry is provided by the ligand field theory. Using the MO language, LFT gives an accurate and detailed picture of ML interactions.

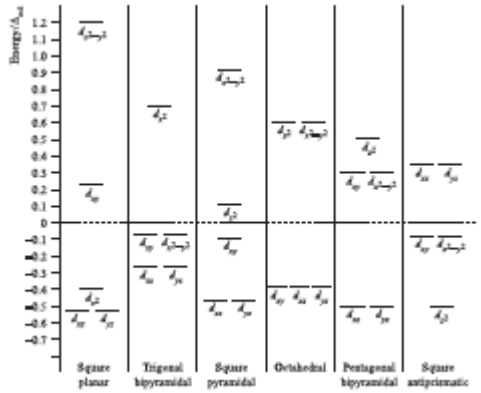

Figure 1: Orbital diagrams for the most common TM compound geometries.
C.E.Housecroft A.G.Sharpe *Inorganic Chemistry* Pearson Ed. Limited

The MO theory is the fundament of modern chemistry and can be succinctly summarized as follow. The Schrödinger equation Ψ contains all the chemical information but it is not exactly solvable for molecules. Introducing some approximations theoreticians developed a method for solving the equation. The Born-Oppheneimer (or adiabatic) approximation decouples nuclei and electrons motions. The former are much more heavier than the latter. Then, it is reasonable to assume that the speed difference is so high that electrons can rearrange instantly to nuclei motions. This implies nuclei can be considered fixed compared with electrons so to simplify the equation and make calculable the solution for H. Solving Ψ for hydrogen atoms provides a series of functions called atomic orbitals (AOs) which are one-electron wave-functions. Considering every electron as belonging to a hydrogen atom, the orbital approximation allows to solve Ψ also for atoms bigger than H. When two atoms are bounded together their AOs mix each other yielding molecular orbitals which can be considered as a linear combination of atomic orbitals (LCAO). Only AOs which overlap each other are able to mix. Thus, only AOs close in energy and with the correct symmetry can join in a MO. It should be notice how, since the first requirement, only the valence electrons will contribute to the chemical bond whereas the core electrons can be considered as inert. Two different situations can arise from the mixture of two atomic orbitals, one will give a lower MO (bonding) and the other a higher MO (antibonding) in energy than the respective atomic orbitals. Coming back to coordination chemistry, figure 2 shows a MO diagram for ML_6 (L = σdonor). Transition metals have nine valence orbitals (5 $(n-1)d$, 1 ns, 3 np). In octahedral complexes ligands approach

along the three axes, then only six of M orbitals (the s, the p and the two d_{z^2}, $d_{x^2-y^2}$) have the correct symmetry and can combine with the ligand ones. When the six ligands approach to bonding distance the combination of such orbitals gives rise to twelve MO: six lower (σ bonding orbitals) and other six (σ^* antibonding) higher in energy. Concerning the three d_π, they do not overlap with L orbitals remaining non-bonding. Notice how the CFT d-orbitals split can be recovered. Now Δ gap increases with the increasing of the strength of σ bonds. Each MO have both ligand and metal character being formed by a mixture of the ligand lone pairs σ orbital and the $Md\sigma$ one. Any MO resembles the parent atomic orbital that lies closest in energy to it which, in this case, are the ligand orbitals. This means that electrons that were purely L lone pairs in the free ligand gain some metal character in the complex, hence the $L\sigma$ lone pairs are partially transferred (donated) to the metal.

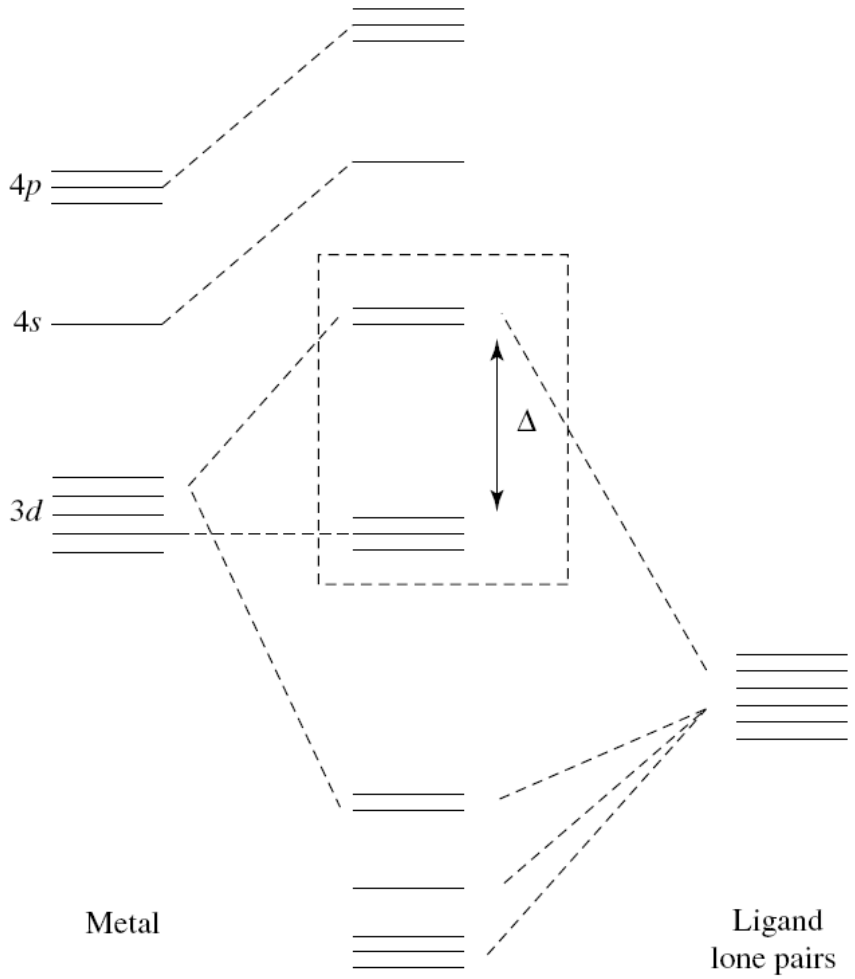

Figure 2: MO of metal ligand bonding in an octahedral ML_6 complex. The box contains the *d* orbitals.
R.H. Crabtree *The Organometallic Chemistry of the Transition Metals*, John Wiley & Sons Inc. Publication

Ligands like the ones of the previous case are called sigma donors. Their highest occupied molecular orbitals (HOMOs) are close in energy and can interact with metal valence orbitals. On the other hand, their lowest unoccupied molecular orbitals (LUMOs) result too high in energy and cannot. In nature another kind of ligands, called π-acceptor, exists. Such genre of L have empty π^* orbitals at a relative low energy. Unlike before, such LUMOs can interact with filled $d\pi$ orbitals as showed in figure 3. Taking for example carbonyl (CO), it has the $2\pi^*$ orbital which are anti-bonding with respect to CO but become bonding between M and C. The MO diagram (figure 4) of $M(CO)_6$ reveals a difference with the previous case. Now the $d\pi$ orbital mixes with the π^* of ligand losing its nonbonding nature and going down in energy. Thus, the $d\pi$ electrons spend some of their time on the ligand resulting in a donation of electron density from M to L. Called back-bonding, this is a key feature of complexes with unsaturated ligands. Such mechanism leads two important consequences. As $d\pi$ are stabilized, the Δ gap increases favoring low-spin configuration. On the other hand, back-bonding is the reason neutral TM compound can be formed. Indeed such metals are rich in electron and cannot accept further electrons from pure σ donor L. Back-donation lightens the charge on the metal allowing donation from ligands.

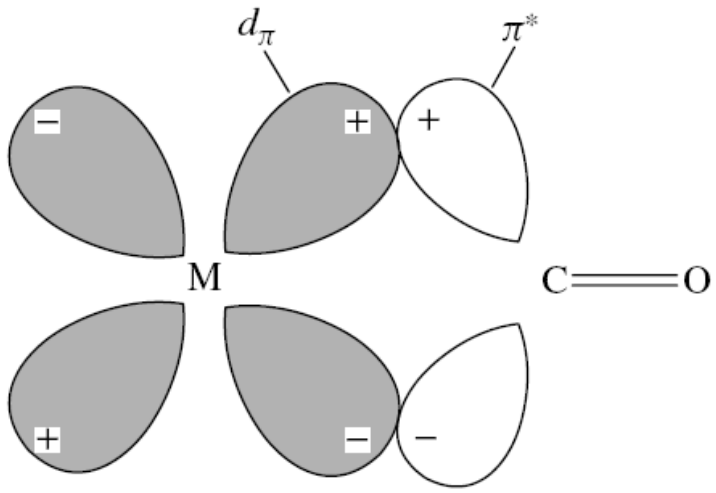

Figure 3: Overlap between a filled metal $d\pi$ orbital and an empty CO π^* orbital to give the π component of the M−CO bond. The shading refers to occupancy of the orbitals and the + and − signs, to the symmetry. R.H. Crabtree *The Organometallic Chemistry of the Transition Metals*, John Wiley & Sons Inc. Publication

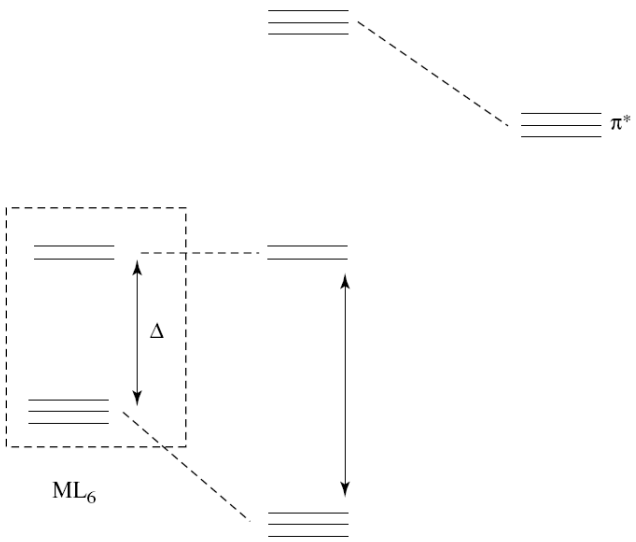

Figure 4: Effect of "turning on" the π interaction between a π-acceptor ligand and the metal. The unoccupied, and relatively unstable $\pi*$ orbitals of the ligand are shown on the right. Their effect is to stabilize the filled $d\pi$ orbitals of the complex and so increase Δ. In $W(CO)_6$, the lowest three orbitals are filled. R.H. Crabtree *The Organometallic Chemistry of the Transition Metals*, John Wiley & Sons Inc. Publication

Summarizing, the coordination chemistry is regulated by the interaction between the HOMO and LUMO of ligands and the metal d orbitals. In all the complexes there is a sigma donation from the L (HOMO) to the M ($d\sigma$) orbital. Moreover, depending on metal and ligand, a back-donation from the metal ($d\pi$) to the L (LUMO) orbital can arise. Such mechanism is the most important interaction of metal-organic chemistry being organometallic ligands like CO, C_2H_4 and H_2 backdonation acceptors.

The chemistry from a real space point of view

The LFT provides a complete and robust theory based on the analysis of the wave-function and molecular orbitals. Concepts like MO and LCAO are common in chemistry and have provided the theoretical fundament of chemical bond since the advent of quantum mechanics. Nevertheless, the use of MO forces the chemist to reason in the Hilbert space and to recover the classic chemical concepts adapting MO results to the real space. In the Nineties a new theory was proposed by Richard Bader. Called quantum theory of atoms in molecules (QTAM)[2] it extracts chemical information by a topological analysis of the electron charge density (CD) ρ. Strictly developed on quantum mechanics rules, QTAM uses a measurable quantity to explain chemistry providing a more realistic description of the chemical bond. Another big advantage of QTAM if compared to MO theory is the possibility to directly compare experimental and theoretical results. Briefly by ρ , $\nabla\rho$ and $\nabla^2\rho$ it is possible to define the "atom domain" inside a

[2] R.F.W.Bader *Atoms in Molecules* 1990 Oxford Univ Press

molecule and then to calculate its atomic charge, to establish if it is bonded with other atoms or not, in which kind of interaction it is involved etc. Having determined when two atoms are bond or not, other information concerning the nature of the bond are required to provide a complete explanation of it. Perfectly integrable with QTAM concepts, the interacting quantum atoms (IQA[3]) approach provides such information. Based on partition of the pair (also called 2nd order) density matrix $\rho(r_1; r_2)$[4], IQA calculates the interacting energy between two atoms and exactly splits it in ionic and covalent contributes. At last, using the QTAM definition of atoms, the domain Fermi hole (DAFH)[5] allows to define which electron pairs are shared between atoms recovering the orbital concepts related to the Lewis idea of chemical bond.

Despite their powerfulness, each of the above techniques alone cannot provide a full description of the chemical bond. On the other hand, combining QTAM with IQA and DAFH concepts could provide an exhaustive theory which could replace the more complicated and counterintuitive MO theory. The purpose of my PhD career was to join these techniques in order to recover and explain classical organometallic concepts from ρ. The first part of my thesis will concern the theory. QTAM, IQA and DAFH are presented and how to combine these techniques will be explained. Moreover it will be showed how some computational problems concerning transition metals were solved. In the second part it will be reported the studies made during my PhD. The fundament of metal-organic chemistry is the σ-donation π-backdonation mechanism which was studied for metal carbonyl (MCO) and metal hydrogen bond (MH). The metal metal (MM) bond was studied in bridged and unbridged $[M_{2(}CO)_n]^n$ molecules as well in MM dimers. Another important interaction consist of the 3c2e one which was investigated in metals hydride bridge systems. In order to test the concepts arisen during my PhD, a possible application as the hydrogen cleavage in $[FeH_2(\eta\text{-}H_2)(PH_3)_3]$ was also studied. The thesis will finish with some appendixes were the code manual and the computational details will be reported.

[3] M.A. Blanco, A.Martìn Pendàs, E.Francisco *J. Chem. Th. Comp.* 2005 **1** 1069
E.Francisco, A.Martìn Pendàs, M.A.Blanco *J. Chem. Th. Comp.* 2006 **2** 90
[4] L.Li, R.G.Parr J. Chem. Phys. 1986 **84** 1074
[5] R.Ponec *J. Math. Chem.* 1997 **21** 323
R.Ponec *J. Math. Chem.* 1998 **23** 85

Part I

Chapter 1: The quantum theory of atoms in molecules (QTAM)

Topological analysis of electron charge density

Developed by R. Bader, QTAM is a quantum mechanics theory based on topological analysis of electronic charge density (CD) $\rho(\boldsymbol{r})$. Obtainable from experiment and theory, $\rho(r)$ is a scalar defined in the real space. In figure 1.1 on the left the charge density of LiH is reported.

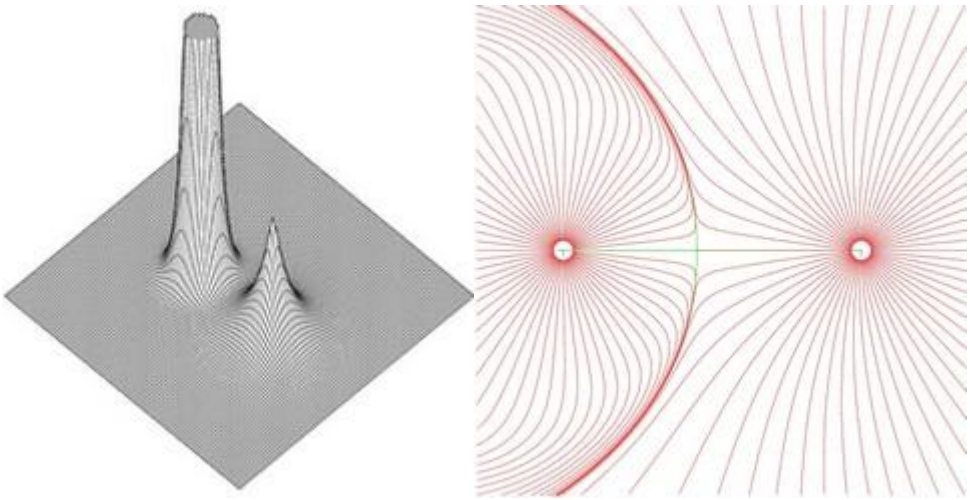

Figure 1.1: 3D plot of ρ of LiH in Li-H bond plane(Li on the left, H on the right) and its vector field

The two peaks are in the nuclei positions (r_N). Those points are local maxima and determine the morphologic structure of ρ in the space. Moreover they have a null gradient of ρ. Points where $\nabla\rho(\boldsymbol{r}) = 0$ are the fundament of QTAM and are called critical points (CPs): they are characterized by rank and sign (rank, sign) of the Hessian matrix. In order to visualize CPs the vector field plot is required as reported in figure1.1 on the right. The local maximum (3,-3), called attractor, is usually found on nuclei positions[6]. Another point, called bond critical point (BCP) is present between Li and H. It is a first order saddle (3,-1) resulting a maximum in a plane and a minimum in the other direction. Two vectors exit from BCP ending in two nuclei. The line linking such nuclei is called bond path (BP) and, if present, is a sufficient and necessary condition for atoms to be bonded each others. Note that, in LiH, the BCP is closer to Li than H. The position depends on the electronegativity of atoms: the BCP will be exactly in the middle for bonds between same atoms and will be closer to the less electronegative atom in

[6] It was found(C.Gatti, P.Fantucci, G.Pacchioni *Theor. Chem. Acc.* 1987 **72** 433) in Lithium clusters, there is a local maximum also in a non nuclear position.

other cases. Another feature of BCP is that they lie on a of a zero flux surface $\nabla\rho(\boldsymbol{r}) = 0$. Such surfaces are not crossed by any vectors and partition the space defining the atomic basins (Ω). Hence, a topological atom is defined by its surface plus its relative attractor. Other two genres of CPs are possible: 2nd order saddle (3,1) called ring critical point and local minimum (3,3) defined cage critical point (CCP). An example of the former is reported in figure 1.2 (diborane) while the latter can be found in molecules like cubane (figure 1.4). All these information can be summarized in plots containing CPs and BPs called molecular graphs (MGs). Looking at the diborane's pictures, two new features catch the eyes. The first one is related to the RCP observable on the top of the picture. The CP between borons is a minimum in yz plane resulting, as wrote before, a saddle of 2nd order. This corroborates the presence of a ring confirming the classic idea for diboranes bond. The other one, visible in the picture below on the left, is related to the bent bond. Looking at the MG of the plane containing the bridge hydrogens, it is clear how the BP between B and H does not result straight, revealing some tension for such bond.

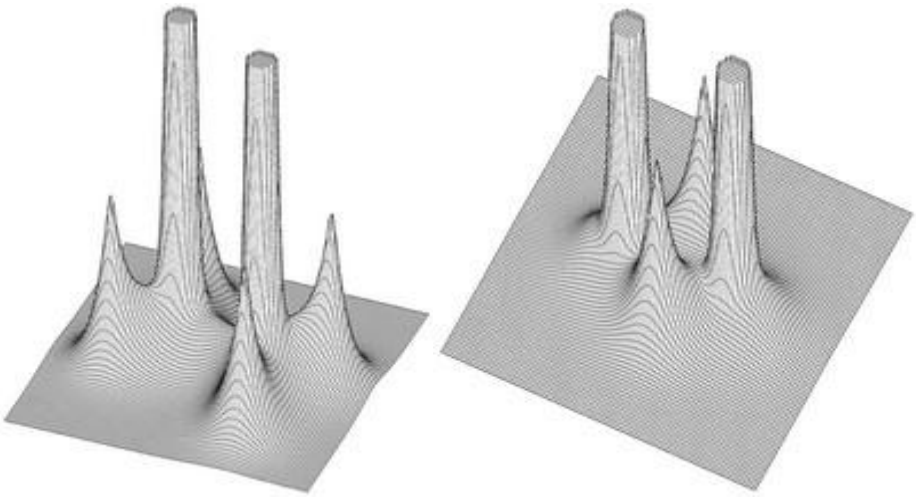

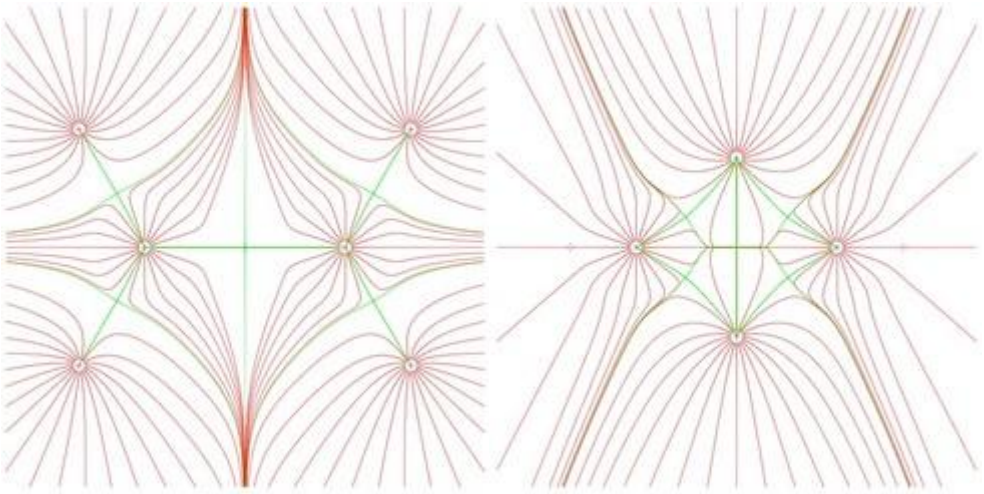

Figure 1.2: Electronic density and it gradient field in plane xy(on the left) and yz(on the right) for B_2H_6

Another example of RCP is reported in figure 1.3 which shows CD and MG of benzene while figure 1.4 reveals the presence of a cage amongst carbons in cubane (C_8H_8).

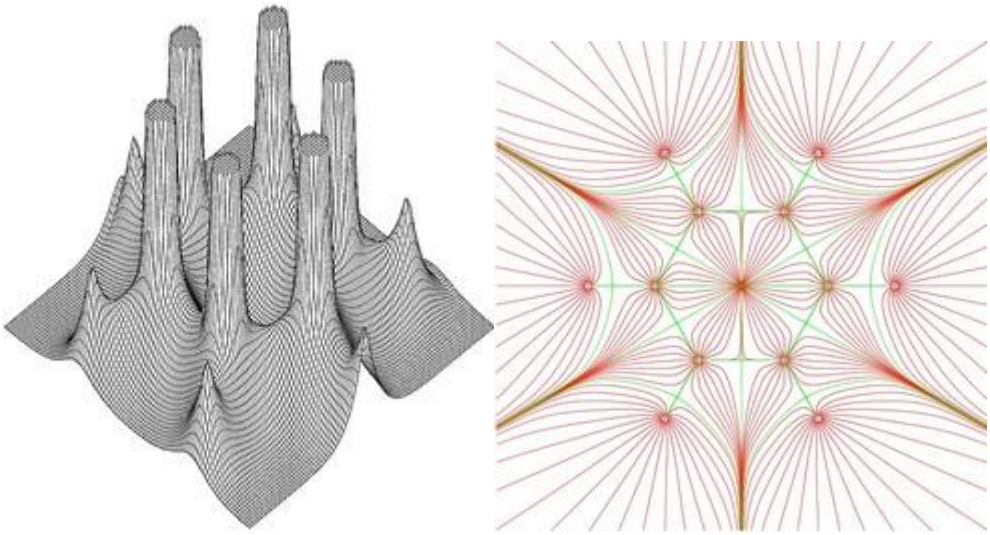

Figure 1.3: Electronic density and it gradient field in the molecular plane for benzene.

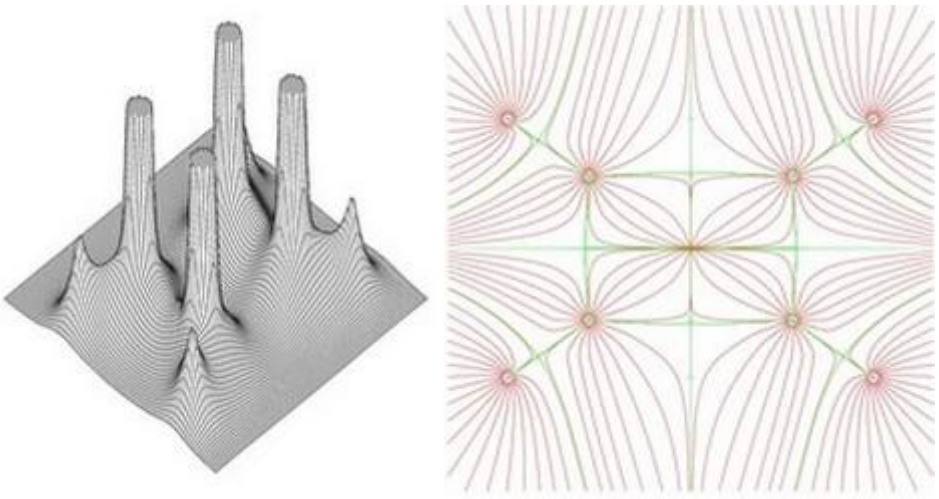

Figure 1.4: Electronic density and it gradient field in plane xy for cubane.

Analysis of the electronic charge density Laplacian

Up to now nothing was said regarding the genre of chemical interaction nor its reactivity. Such information can be recovered from the Laplacian of the charge density $\nabla^2\rho$. This is the trace of the Hessian matrix and provides a measure of where ρ is concentrate or deplected. Measuring the curvature of a function the Laplacian will be positive in zones with low CD and negative where CD is concentrate. Thus, for sake of clarity, $-\nabla^2\rho$ is usually reported[7]. In order to appreciate the difference between ρ and $-\nabla^2\rho$ in figure 1.5 the CD (on the left) and its Laplacian (below) are reported for Cl_2 atom. The charge density shows the normal maximum in the atoms positions and a 1st saddle point (BCP) between atoms which is clearly visible in the molecular graph. Here the BCP lies exactly in the middle of the bond path and the basins are symmetric. The value of $-\nabla^2\rho$ at the BCP is positive revealing an accumulation of CD between atoms in Cl_2. Moreover the electronic configuration of Cl ($1s^2 2s^2 2p^6 3s^2 3p^5$) can be argued looking at the nuclei where these three shells (K, L, M) are easily displayed.

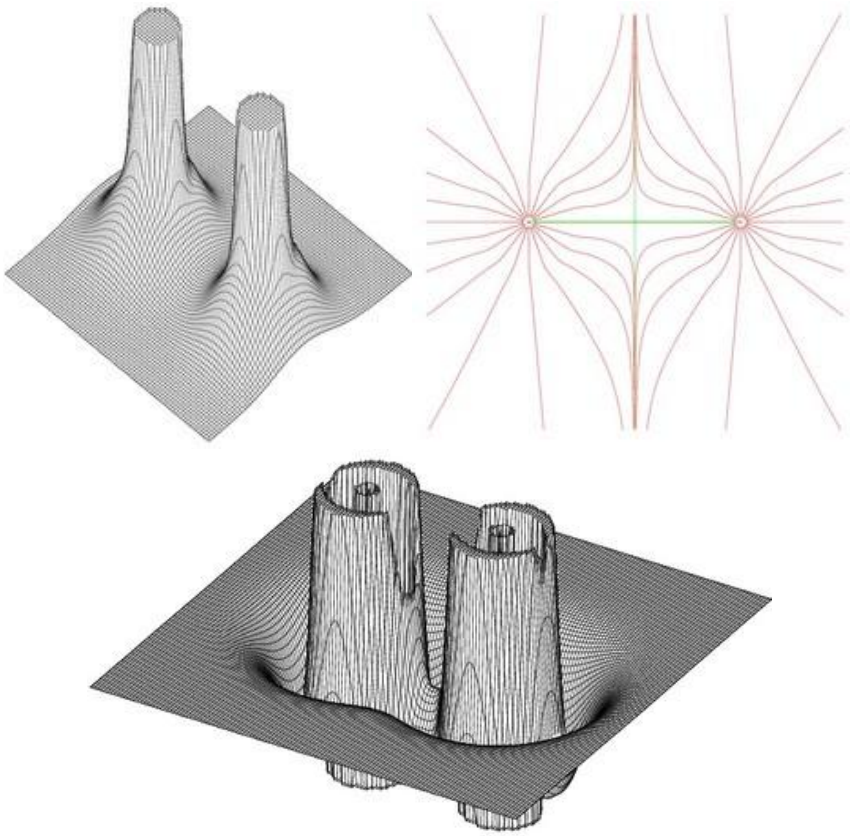

Figure 1.5: Electronic density, its gradient field and laplacian for Cl_2

[7] Hence positive values correspond to accumulation and negative ones coincide to deplection of CD.

Another example is showed in figure 1.6 with NaCl. As usual the peaks of CD reveal the position of atoms sodium (on the left) and Cl (on the right). Chlorine has a bigger basin being more electronegative. For the same reason, the BCP results closer to Na than Cl. These differences are also reflected in the Laplacian. The inner shell of chlorine atom remains almost unchanged if compared to the previous case. In agreement with the chemical concepts of inert core, only the valence changes its shapes. Concerning Na ($1s^2 2s^2 2p^6 3s^1$) it has only two shells. This means it lost one electron supporting the idea of an ionic molecule Na^+ Cl^-. Finally the value at the BCP is negative.

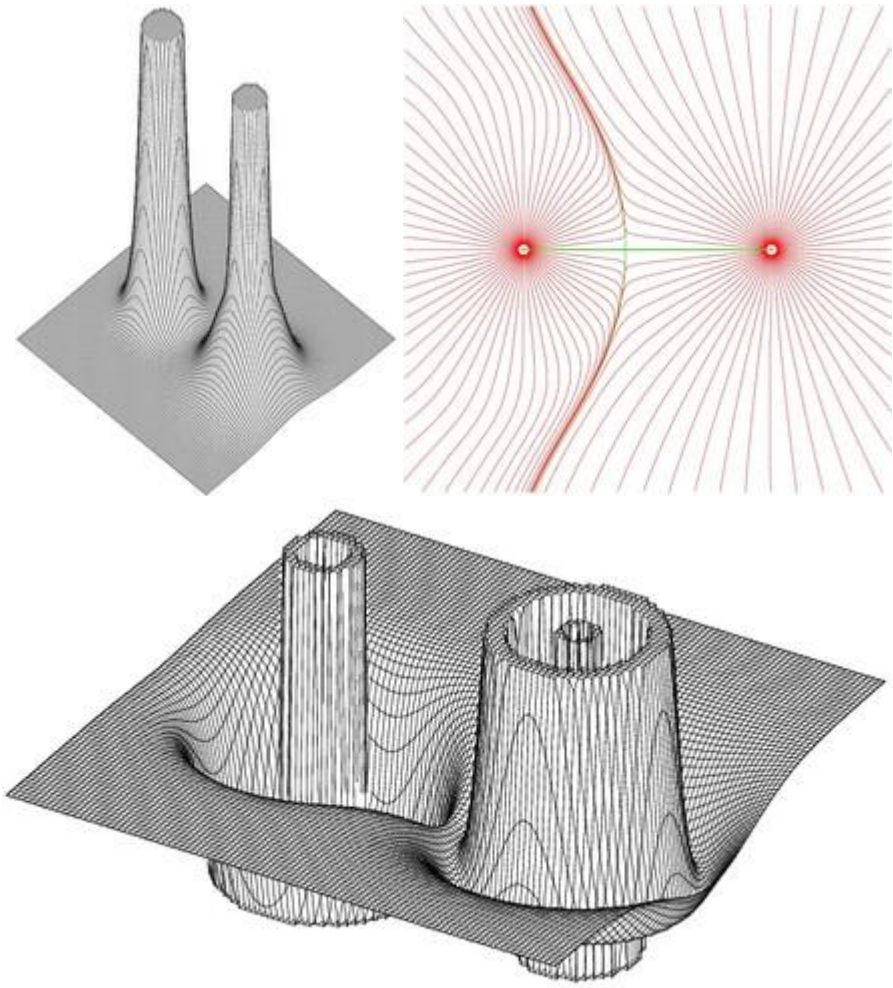

Figure 1.6: Electronic density, its gradient field and laplacian for NaCl(Na on the left, Cl on the right)

Other properties

As said above the space can be partition in basins Ω which, together with their attractor, can be associated to the definition of atoms. Bader showed that medium value of an observable is equal to the sum of atomic contributes.

[1.1] $$O_\Omega = \int_\Omega \rho_O(\boldsymbol{r})\, d\tau \Rightarrow \langle \hat{O} \rangle = \sum_\Omega O_\Omega$$

Valid for mono- and bi-electronics operators, this represents one of the cornerstones of chemistry stating atoms conserve their nature inside molecules and determine the global properties of a system. For instance, being the electronic population operator $\langle \hat{O} \rangle = \hat{1}$, the number of electrons of an atom is equal to $N_\Omega = \int_\Omega \rho(\boldsymbol{r})\, d\tau$ and the atomic charge is $Q_\Omega = (Z_\Omega - N_\Omega)e$.

Other important properties that can be obtained by space partition are the localization (λ) and delocalization (δ) indexes[8]. Related to the partition of the pair density matrix, the former provides the number of electrons completely localized inside a basin whereas the latter gives the number of electrons shared between two different basins.

The last quantity we need to introduce is the energy density which is related to the Laplacian through the virial theorem and describes the covalency in the chemical interaction[9]. The total energy density, $H(r) = V(r) + G(r)$, will be negative at the BCP in case of covalent bonds. Indeed this interaction will be governed by potential energy density $V(r)$ (everywhere negative). On the other hand, due to an excess of kinetic energy density $G(r)$ (everywhere positive), $H(r)$ will be positive at the BCP between two closed shells interaction like ionic or Van der Waals bond.

Summarizing, calculating the charge density, from theory or experiment, it is possible to strictly define if two atoms are bonded or not. A chemical bond exists between two atoms only if there is a bond critical point between them. This lies on a surface which is not crossed by any gradient and represent a maximum for all the trajectories describing the zero-flux surface. On

[8] R.F.W.Bader, M.E.Stephens *J. Am. Chem. Soc.* 1975 **97** 7391
X.Fradera, M.A.Austen, R. F. W. Bader *J. Phys. Chem. A* 1999 **103** 304
[9] D.Cremer, E.Kraka, *Croat. Chem. Acta* 1984 **57** 1259

the other hand, two vectors leave from such CP and finish on the two nuclei constituting a line called bond path where there is a minimum of CD. Thus, a chemical bond can be defined as a line of maximum of the CD which joins two attractors (nuclei) through a BCP lying on a zero flux surface. Hence the charge density is accumulated between nuclei bonded together. If inside the molecule a ring is present a ring critical point arises. Being a minimum of CD in two directions and a maximum in the other one, there are infinite trajectories leaving from this point and ending at the attractors position (the vertexes of the ring). Moreover, there is one vector for each BCP which leaves from RCP to end in it. The surfaces of all those trajectories give the ring surface. If there is a volume enclosed inside rings, a cage is formed and a local minimum of CD arises. Such point is a cage critical point. The number of a critical points inside a molecular graph is regulated by the Poincaré-Hopf relation: $\text{Attractor} - \text{BCP} + \text{RCP} - \text{CCP} = 1$. Having localized and defined when two atoms are bonded together, the analysis of the Laplacian of CD allows to define if this bond is covalent (open shell interaction) or ionic (closed shell interaction). Finally, the delocalization indexes provide a "measure of the bond order" giving the number of electrons shared between atoms.

Chapter 2: The interacting quantum atoms theory (IQA)

Introduction

The partition of energy is a key concept in quantum chemistry. Total, interaction and binding energy are used to explain the interaction amongst atoms and molecules. Under the Born-Oppenheimer approximation McWeeny developed the theory of electronic separability[10] (TES) from which the total energy can be written as the sum over different contributes:

[2.1] $$E = T + V_{el-nucl} + V_{el-el} + V_{nucl-nucl}$$

Li and Parr[11] showed how to decompose the 1st $\rho(\boldsymbol{r},\boldsymbol{r}')$ and 2nd $\rho(\boldsymbol{r}_1,\boldsymbol{r}_2)$ order density matrixes by a space partition and, therefore, how to extract the total energy of the system from those ones.

As seen in the previous chapter, it is possible to partition the space in atomic basins by the zero-flux surface of the kinetic energy T^A. Making the momentum operator hermitian inside the bounded region[12] ensures the kinetic operators $(\frac{\nabla^2}{2}, \frac{\nabla\nabla'}{2})$ to have the same expectation value. Thus, T^A is transferable[13] and fulfills an atomic virial theorem[14]. With this Bader partition the total energy in atomic (one-boby) contributions $E = -\sum_A T^A$. This is only valid at equilibrium and, using only one-body terms, it is not useful in interaction studies.

On the other hand, due to the 6D integral required for the V_{ee} interaction, the common methods used for partitioning the total energy usually neglects this term introducing an approximation in the analysis. An algorithm, developed in Oviedo[15] in 2004, exploits the multipolar approach and the symmetry reducing bi-electronic integral scale up to 4D making the computation more feasible.

---

[10] R.Mcweeny *Methods of Molecular Quantum Mechanics* 1992 Academic Press: London
[11] L.Li, G.Parr *J. Chem. Phys.* 1985 **84** 1704
[12] R.Bader, H.J.Preston *Int. J. Quant. Chem.* 1969 **3** 327
[13] R.Bader, P.M.Beddal *J. Chem. Phys.* 1972 **56** 3320
[14] S.Srebrenik, R.Bader *J. Chem. Phys.* 1975 **63** 3945
[15] A.Martin Pendas, M.A.Blanco, E.Francisco *J. Chem. Phys.* 2004 **120** 4581

The interacting quantum atom theory[16] implements decomposition on the Li-Parr matrix and, based on the TES theory, takes advantage of this algorithm allowing an exhaustive analysis of the total energy at any point of the potential energy surface (PES).
This chapter will follow this scheme: first it will be shown how to reconstruct the total energy from the 1st ρ_1 and 2nd ρ_2 order density matrix. Then the V_{ee} algorithm will be showed and the IQA approach will be explained. At last it will be shown how correlation can be introduced inside the calculation[17].

The total energy from the first and second order density matrix partition

The total energy depends on ρ, on the non-diagonal part of the 1st order density matrix and on the diagonal elements of the 2nd order one[18]. Given a wave function Ψ, they are defined:

[2.2] $$\rho(\boldsymbol{r}) = N_e \int \Psi * \Psi \, d\boldsymbol{r}_1 d\boldsymbol{r}_2 \ldots d\boldsymbol{r}_{Ne}$$

[2.3] $$\rho_1(\boldsymbol{r},\boldsymbol{r}') = N_e \int \Psi * \Psi \, d\boldsymbol{r}_2 \ldots d\boldsymbol{r}_{Ne}$$

[2.4] $$\rho_2(\boldsymbol{r_1},\boldsymbol{r_2}) = N_e(N_e - 1) \int \Psi * \Psi \, d\boldsymbol{r}_3 \ldots d\boldsymbol{r}_{Ne}$$

Imposing the logical conditions that the repulsion between two electrons at point $\boldsymbol{r}$ and $\boldsymbol{r}'$ depends only on their relative position and, similarly, the kinetic energy is independent if the electron is part of an atom or a molecule, Li-Parr showed how to partition the 1st and 2nd order density matrix in a sum of atomic contributions.
Defining a real function $0 \leq \omega_A(\boldsymbol{r}) \leq 1$:

[2.5] $$\omega_A(\boldsymbol{r}) = \frac{\rho_A(\boldsymbol{r})}{\rho(\boldsymbol{r})}$$

The first order density matrix $\rho_1^A(\boldsymbol{r},\boldsymbol{r}')$ can be written:

[2.6] $$\rho_1^A(\boldsymbol{r},\boldsymbol{r}') = \rho_1(\boldsymbol{r},\boldsymbol{r}')\frac{\rho_A(\boldsymbol{r}')}{\rho(\boldsymbol{r})} = \rho_1(\boldsymbol{r},\boldsymbol{r}')\omega_A(\boldsymbol{r}')$$

[2.7] $$\rho_1(\boldsymbol{r},\boldsymbol{r}') = \sum_A \rho_1^A(\boldsymbol{r},\boldsymbol{r}') = \rho_1(\boldsymbol{r},\boldsymbol{r}')\sum_A \omega_A$$

[16] M.A.Blanco, A.Martin Pendas, E.Francisco *J. Chem. Th. Comp.* 2006 **1** 1096
[17] A.Martin Pendas, E.Francisco, M.A.Blanco *J. Comp. Chem.* 2004 **26** 344
[18] A.Martin Pendas, M.A.Blanco, E.Francisco *J. Comp. Chem.* 2006 **28** 161

and the second $\rho_2^{AB}(\boldsymbol{r_1},\boldsymbol{r_2})$:

[2.8] $$\rho_2^{AB}(\boldsymbol{r_1},\boldsymbol{r_2}) = \rho_2(\boldsymbol{r_1},\boldsymbol{r_2})\frac{\rho_A(r_1)\rho_B(r_2)}{\rho(r_1)\rho(r_2)} = \rho_2(\boldsymbol{r_1},\boldsymbol{r_2})\omega_A(\boldsymbol{r_1})\omega_B(\boldsymbol{r_2})$$

[2.9] $$\rho_2(\boldsymbol{r_1},\boldsymbol{r_2}) = \rho_2(\boldsymbol{r_1},\boldsymbol{r_2})\sum_A \omega_A \sum_B \omega_B$$

Therefore, with a given Ψ, the atomic contribution depends only on Ω which partitions ρ, ρ_1, ρ_2. In the previous chapter it was showed how the electrons can be associated to a nucleus to form an atomic basin by a topological analysis of ρ. This partitions the space in an exhaustive way.

[2.10] $$\Omega_A = \begin{cases} 1\ if\ \boldsymbol{r_1} \in \Omega \\ 0\ elsewhere \end{cases}$$

[2.11] $$\sum_A \Omega_A = 1$$

Even if in principle it is possible to use any kind of partition in order to get Ω, it is straightforward the use of the QTAM theory for partitioning the real space and, consequently, obtaining ρ_1 and ρ_2.

Doing this gives the terms of the eq.2.1 related to the density matrices[19].

[2.12] $$E = T + V_{ne} + V_{en} + V_{ee} + V_{nn}$$

[2.13] $$T = \int_{\boldsymbol{r}\to\boldsymbol{r'}} \hat{T}\,\rho_1(\boldsymbol{r},\boldsymbol{r'})d\boldsymbol{r}$$

[2.14] $$V_{ne} = -\sum_A Z_A \int \frac{\rho(\boldsymbol{r})}{|\boldsymbol{r}-\boldsymbol{R_A}|}d\boldsymbol{r}$$

[2.15] $$V_{en} = -\sum_B Z_B \int \frac{\rho(\boldsymbol{r})}{|\boldsymbol{r}-\boldsymbol{R_B}|}d\boldsymbol{r}$$

[2.16] $$V_{ee} = \frac{1}{2}\int \frac{\rho_2(\boldsymbol{r_1},\boldsymbol{r_2})}{r_{12}}d\boldsymbol{r_1}\,d\boldsymbol{r_2}$$

[2.17] $$V_{nn} = \frac{1}{2}\sum_A \sum_{B\neq A} \frac{Z_A Z_B}{R_{AB}}$$

[19] E.Francisco, A.Martin Pendas, M.A.Blanco *J. Chem. Th. Comp.* 2006 **2** 90

The electron-electron repulsion term

The six-dimensional integrals required for computing the bi-electronic interaction are the main reason of the huge computational effort requested to calculate the total interaction energy. As written above V_{ee} is[20]:

[2.18] $$V_{ee} = \frac{1}{2}\iint d\boldsymbol{x}_1 d\boldsymbol{x}_2 \frac{\rho_2(\mathbf{1},\mathbf{2};\mathbf{2}',\mathbf{1}')}{r_{12}}$$

Given an atomic basins space partition, it is possible to separate this integral into the repulsion between an electron and another of the same basin (intra-atomic contribute) and of different ones (inter-atomic contribute):

[2.19] $$V_{ee}^{AA} = \int_{\Omega_A} d\boldsymbol{x}_1 \int_{\Omega_A} d\boldsymbol{x}_2 \frac{}{r_{12}}$$

[2.20] $$V_{ee}^{AB} = \int_{\Omega_A} d\boldsymbol{x}_1 \int_{\Omega_B} d\boldsymbol{x}_2 \frac{\rho_2(\mathbf{1},\mathbf{2};\mathbf{2}',\mathbf{1}')}{r_{12}}$$

Since the space partition from the QTAM theory is exhaustive, the eq.2.18 can be rewritten:

[2.21] $$V_{ee} = \frac{1}{2}\sum_A \int_{\Omega_A} d\boldsymbol{x}_1 \sum_B \int_{\Omega_B} d\boldsymbol{x}_2 \frac{\rho_2(\mathbf{1},\mathbf{2};\mathbf{2}',\mathbf{1}')}{r_{12}} = \sum_A V_{ee}^{AA} + \sum_{B>A} V_{ee}^{AB}$$

At the Hartree-Fock level the electron- electron repulsion is composed by the Coulomb term J and the exchange one K:

[2.22] $$V_{ee}^{AB} = \begin{cases} \frac{1}{2}(J^{AA} - K^{AA}) \; when \; A = B \\ J^{AB} - K^{AB} \; when \; A \neq B \end{cases}$$

with:

[2.23] $$J^{AB} = \iint_{\Omega_A\Omega_B} d\boldsymbol{r}_1 d\boldsymbol{r}_2 \frac{\mathbf{1}}{r_{12}} \rho_2(\mathbf{1},\mathbf{2};\mathbf{2}',\mathbf{1}')\rho(\boldsymbol{r}_1)\rho(\boldsymbol{r}_2)$$

[2.24] $$K^{AB} = \iint_{\Omega_A\Omega_B} d\boldsymbol{x}_1 d\boldsymbol{x}_2 \frac{\mathbf{1}}{r_{12}} |\rho_1(\mathbf{1},\mathbf{2})|^2$$

[20] Notice in the previous paragraph the equation was spin-variable integrated

considering a closed-shell system described by real orbitals φ:

[2.25] $$K^{AB} = 2\sum_{ij}\iint_{\Omega_A\Omega_B} d\boldsymbol{r}_1 d\boldsymbol{r}_2 \frac{\mathbf{1}}{r_{12}} f_{ij}(\boldsymbol{r}_1) f_{ij}(\boldsymbol{r}_2)$$

with $f_{ij} = \varphi_i(\boldsymbol{r})\varphi_j(\boldsymbol{r})$. It should be noticed that, defining a spin-orbital $g_{ij} = \psi(\mathbf{1}) * \psi(\mathbf{1}')$, the 2nd order density matrix can be written as a product expansion of those. Integrating on the spin it becomes a linear combinations of integral I^{AB} with space orbital g_i products:

[2.26] $$I^{AB} = \iint_{\Omega_A\Omega_B} d\boldsymbol{r}_1 d\boldsymbol{r}_2 \frac{\mathbf{1}}{r_{12}} g_i(\boldsymbol{r}_1) g_j(\boldsymbol{r}_2)$$

Both the Coulomb and the exchange-correlation terms can be recovered as linear combinations like this.
In order to simplify the above equation, a variable separation, $\boldsymbol{r}_1$ and $\boldsymbol{r}_2$, is required: this can be done using the Laplace expansion of r_{12} for I^{AA}:

[2.27] $$r_{12}^{-1} = \sum_{l=0}^{\infty} \frac{4\pi}{2l+1} \frac{r_{small}^{l}}{r_{big}^{l+1}} \sum_{m=-l}^{l} S_{lm}(\boldsymbol{r}_1) S_{lm}(\boldsymbol{r}_2)$$

and the Kay, Todd and Silverston[21] bipolar expansion[22] for I^{AB}:

[2.28] $$r_{12}^{-1} = 4\pi \sum_{l_1 m_1}^{\infty} \sum_{l_2 m_2}^{\infty} -1^{l_1} S_{l_1 m_1}(\boldsymbol{r}_1) S_{l_2 m_2}(\boldsymbol{r}_2) \sum_{l_3}^{l_1+l_2} \Delta_{l_1 l_2 l_3}(r_1, r_2, R) Y_{l_1 m_1 l_2 m_2}^{l_3}$$

In eq.2.27 r_{small} and r_{big} denote the smaller and the larger terms between $\boldsymbol{r}_1$ and $\boldsymbol{r}_2$. Hence the discriminant $\frac{r_{big}}{r_{small}}$ is always bigger than 0 and the series is convergent. Calling the above determinants $D(\boldsymbol{r}_1, \boldsymbol{r}_2)$ and putting the expansion in 2.26 gives[23]:

[21] M.G.Kay, H.D.Todd, J.Silverstone *J. Chem. Phys.* 1969 **51** 2363
[22] Δ is a discriminant whose value depends on r_1, r_2, R; Y is the Gaunt coefficient; $l_3 = |l_1 - l_2|$
[23] $g_p = g_q = f$; $l_1 = l_2$

[2.29] $$I^{AB} = \sum_{l_1 m_1}^{\infty} \sum_{l_2 m_2}^{\infty} \int_{\hat{r}_1} S_{l_1 m_1}(\hat{r}_1) d\hat{r}_1 \int_0^{r_{\Omega_A}(r_1)} f(\boldsymbol{r}_1) r_1^2 dr_1$$

$$\int_{\hat{r}_2} S_{l_2 m_2}(\hat{r}_2) d\hat{r}_2 \int_0^{r_{\Omega_B}(r_2)} f(\boldsymbol{r}_2) r_2^2 dr_2 D(r_1, r_2)$$

In an analytical integral the equations 2.27 and 2.28 can be separated in radial (r) and angular ($\hat{r}$) variables but this is not the case. The QTAM integrations derive from numerical methods that handle the atomic surface $r_\Omega(\hat{r})$ like a function of the angular coordinates. Here the form $r_\Omega(\hat{r})$ prevents the reverse of angular and radial integrations order. This can be done defining the function f^Ω:

[2.30] $$f^\Omega = \begin{cases} f(\boldsymbol{r}) \; if \; \boldsymbol{r}_1 \in \Omega \\ 0 \; if \; \boldsymbol{r}_1 \notin \Omega \end{cases}$$

The problematic integration of f within the basin Ω becomes a simpler integration of f^Ω within the whole space. A further angular integration gives:

[2.31] $$R_{lm}^{\Omega}(R) = \sqrt{\frac{4\pi}{2l+1}} \int_{\hat{r}} S_{lm}(\hat{r}) f^{\Omega}(r) d\hat{r}$$

This finally gives the possibility to rewrite eq.2.29

[2.32] $$I^{AB} = \sum_{l_1 m_1}^{\infty} \sum_{l_2 m_2}^{\infty} N_{l_1}^{-1} N_{l_2}^{-1} \int_0^{\infty} R_{l_1 1}^{\Omega}(\boldsymbol{r}_1) r_1^2 d\boldsymbol{r}_1 \int_0^{\infty} R_{l_2 2}^{\Omega}(\boldsymbol{r}_2) r_2^2 d\boldsymbol{r}_2 D(\boldsymbol{r}_1, \boldsymbol{r}_2)$$

The two $R_{lm}^{\Omega}(\boldsymbol{r})$ can be computed independently. This means the equations scales to $2N^4$ instead of N^6 with a considerable computational effort reduction.

The IQA approach

The different contributes of the eq.2.1 can be gathered into one (one-body) and two (two-body) atoms contributes. This lead to the definition of self (or net) energy, which is equivalent to the energy of the atom as if it was isolated, and of interaction energy:

[2.33] $$E^A_{self} = T^A + V^{AA}_{en} + V^{AA}_{ee}$$

[2.34] $$E^{AB}_{int} = V^{AB}_{nn} + V^{AB}_{en} + V^{AB}_{ne} + V^{AB}_{ee} \quad A \neq B$$

The first term includes all the intra-atomic contributions and defines an atom as a quantum physical object which carries its identity in the molecule characterized by the different interaction amongst its atoms. Therefore, the total energy is the sum of all the self energies plus the interaction energy between them:

[2.35] $$E = \sum_A E^A_{self} + \frac{1}{2}\sum_A \sum_{A \neq B} E^{AB}_{int}$$

From the above equations it is also possible to define the effective energy E_{eff}, which includes all the terms dependent by the atom A, and the additive energy E_{add}.

[2.36] $$E^A_{eff} = E^A_{self} + \sum_{B \neq A} E^{AB}_{int}$$

[2.37] $$E^A_{add} = E^A_{self} + \frac{1}{2}\sum_{A \neq B} E^{AB}_{int}$$

It should be observed that $E = \sum_A E^A_{add}$.

The deformation (or promotion) energy E_{def} is defined as the difference between E^A_{self} and the free atom energy[24] E^A_{vac}.

The first term includes all the energy contributions of an isolated atom. Subtracting E^A_{vac} provides a measure of the atom deformation inside the molecule. In detail the changes that happen to an atom inside a molecule consist of two contributes: the charge transfer (CT) between two different atoms and the subsequent charge electron reorganization (CR).

[24] A different reference states such an ion could be chosen for better describing the situation

[2.38] $$E_{def}^{A} = E_{CT}^{A} + E_{CR}^{A}$$

Regarding the interaction energy, it is composed of two different terms: $E_{int}^{AB} = V_{cl}^{AB} + V_{xc}^{AB}$. The first arises from the classical Coulomb (electrostatic term) interactions V_{cl}^{AB}, the other, the exchange-correlate contribute V_{xc}^{AB}, from the quantum-mechanics (covalent term).

The Coulomb term is equal to $\rho_2^C = \rho(\boldsymbol{r}_1)\rho(\boldsymbol{r}_2)$: this lead to the possibility of partitioning the 2nd order density matrix $\rho_2 = \rho_2^C + \rho_2^{xc}$. Thus V_{ee}^{AB} becomes $V_{ee}^{AB} = V_C^{AB} + V_{xc}^{AB}$ and the classic interaction energy V_{cl}^{AB} can be defined as follow:

[2.39] $$V_{cl}^{AB} = V_{nn}^{AB} + V_{ne}^{AB} + V_{en}^{AB} + V_C^{AB}$$

Reminding all the contributes can be written as a multi-polar expansion, a long range interaction energy V_{C-lr}^{AB} can be defined from the classical electrostatic terms as a multipoles expansion:

[2.40] $$V_{C-lr}^{AB} = \sum_{l_1 m_1}^{\infty} \sum_{l_2 m_2}^{\infty} C_{l_1 m_1 l_2 m_2}(\hat{R}) \frac{Q_{l_1 m_1}^{A} Q_{l_2 m_2}^{B}}{R^{l_1 + l_2 + 1}}$$

On the other hand, when a multi-determinants correlated wave-function is used, V_{xc} can be further partitioned as it will be shown in the next paragraph. Remarkable is the correlation between V_{xc}^{AB} and the delocalization index[25] δ_{AB}:

[2.41] $$V_{xc}^{AB} = \iint [\rho_2^{AB}(\boldsymbol{r}_1, \boldsymbol{r}_2) - \rho_A(\boldsymbol{r}_1)\rho_B(\boldsymbol{r}_1)] \frac{1}{r_{12}} d\boldsymbol{r}_1 d\boldsymbol{r}_2$$

[2.42] $$\delta_{AB} = 2\left| \iint [\rho_2^{AB}(\boldsymbol{r}_1, \boldsymbol{r}_2) - \rho_A(\boldsymbol{r}_1)\rho_B(\boldsymbol{r}_1)] d\boldsymbol{r}_1 d\boldsymbol{r}_2 \right|$$

At the end of this paragraph it should be noticed that the above concept can be exported from the atoms level to the functional groups one. This is done defining the fragment density as a sum of all its components $\rho_F(\boldsymbol{r}_1) = \sum_{A \in F} \rho_A$. Thus, given a functional group *F*, its 1st order

[25] R.Bader, M.E.Stephens *J. Am. Chem. Soc.* 1975 **97** 7391

density matrix is just the sum of all the atoms inside the fragment. Concerning ρ_2 it is composed of two terms: the intra-fragment ρ_2^{AA}, containing the intra-atomic terms of its atoms, and the inter-atomic ρ_2^{AB}, composed by the atoms A lying in the F group and the atoms B of another functional group (which can be composed of a single atom):

[2.43] $$E = \sum_F E^F_{self} + \frac{1}{2}\sum_F \sum_{G \neq F} E^{FG}_{int}$$

[2.44] $$E^F_{self} = \sum_{A \in F} E^A_{self} + \frac{1}{2}\sum_{A \in F}\sum_{B \neq A\ B \in F} E^{AB}_{int}$$

[2.45] $$E^{FG}_{int} = \sum_{A \in F}\sum_{B \in G} E^{AB}_{int}$$

The correlation inside the IQA

E.R.Davidson[26] showed how to factorize a general two-body matrix into one-particle terms by a monadic diagonalization of them[27]. Doing this with the second order density matrix allows us to use a multi-configurational self-consistent field (MCSCF) and so to introduce the electrons correlation.

Briefly, writing the wave-function as a spin-orbitals products expansion $\psi_i(1)\,\psi_j(2)\ldots\psi_N(N)$, squaring and integrating over all electron coordinates gives[28]:

[2.46] $$\rho_2(1,2) = \sum^n_{abcd} \mu_{abcd}\psi_a(1)\psi_b(1)\psi_c(2)\psi_d(2)$$

defining a set of coefficients $\epsilon_{abcd} = \mu_{abcd} + \mu_{bacd}\Delta_{ab} + \mu_{abdc}\Delta_{cd} + \mu_{badc}\Delta_{ab}\Delta_{dc}$ with $\Delta = 1 - \delta_{ab} = \begin{cases} 0 & a = b \\ 1 & a \neq b \end{cases}$ leads to:

[2.47] $$\rho_2(1,2) = \sum_{a \geq b, c \geq d} \varepsilon_{abcd}\psi_a(1)\psi_b(1)\psi_c(2)\psi_d(2)$$

which, when diagonalized[29], produces the monadic decomposition required[30]:

[2.48] $$\rho_2(1,2) = \sum^n_{a \geq b} d_{ab} f_{ab}(1) f_{ab}(2)$$

---

[26] E.R.Davidson *Chem. Phys. Lett.* 1995 **246** 209
[27] A.Coleman *J. Rev. Mod. Phys.* 1963 **35** 668
[28] μ_{abcd} is a symmetric matrix in the (a, b) and (c, d) pairs
[29] Using the basis of products of spin orbitals $\psi_a(\boldsymbol{x}_1)\psi_b(\boldsymbol{x}_2);\ a \geq b$
[30] f eigenfunctions are linear combinations of the above products

Integrating over the spin coordinates an equivalent expression with the spatial orbital ϕ is obtained. This produces a decomposition of ρ_2 in terms of[31] $\frac{m(m+1)}{2}$ one-electron functions.

Remembering that:

[2.49] $$\rho_2(1,2) = \rho_1(1)\rho_1(2) - \rho_1(2,1)\rho_1(1,2)$$

the second order density matrix can be written[32]:

[2.50] $$\rho_2(\boldsymbol{r}_1,\boldsymbol{r}_2) = \rho_1(\boldsymbol{r}_1)\rho_1(\boldsymbol{r}_2) - \sum_{a\geq b}^{m}\lambda_{ab}\phi_a(\boldsymbol{r}_1)\phi_b(\boldsymbol{r}_1)\phi_a(\boldsymbol{r}_2)\phi_b(\boldsymbol{r}_2)$$

The first term gives the Coulomb part of V_{ee}, the second its exchanges contribute.

In general, the interelectronic repulsion terms are defined as:

[2.51] $$\rho_2^C = \rho_1(1)\rho_1(2)$$

[2.52] $$\rho_2^x = -\rho_1(2,1)\rho_1(1,2)$$

[2.53] $$\rho_2^{corr} = \rho_2(1,2) - \rho_2^C - \rho_2^x$$

A monadic diagonalization of ρ_2^x allows to calculate all the above terms. Given a MCSCF wavefunction, the non-diagonal 1st order density matrix $\rho_1(1,2)$ can be written as an expansion[33]:

[2.54] $$\rho_1(1,2) = \sum_{ij}^{N\,det} c_i^* c_j (ij|12) = \sum_{ab}^{n} c_{ab}\delta_{m_s a}\delta_{m_s b}\psi_a(1)\psi_b(2)$$

Using this and integrating out the spin, the exchange matrix becomes[34]:

---

[31] m is the number of spatial orbital (partially) occupied in the wave-function

[32] $\lambda_{ab} = 2 + 2\Delta_{ab}$

[33] In order to preserve the total M_s spin mixing is forbidden when $i \neq j$. c_{ab} coefficients are constructed using the Slater rules

[34] $c_{cd} = c_{dc}$ and $d_{abcd} = c_{ac}^{\alpha\alpha}c_{bd}^{\alpha\alpha} + c_{ac}^{\beta\beta}c_{bd}^{\beta\beta}$

[2.55] $$-\rho_2^x(1,2) = \sum_{ij}^{Ndet} c_{ab}\delta_{m_s a m_s b} c_{cd}\delta_{m_s c m_s d}\psi_a(1)\psi_c(1)\psi_b(2)\psi_d(2)$$

[2.56] $$-\rho_2^x(1,2) = \sum_{abcd}^{m} d_{abcd}\phi_a(\boldsymbol{r}_1)\phi_c(\boldsymbol{r}_1)\phi_b(\boldsymbol{r}_2)\phi_d(\boldsymbol{r}_2)$$

[2.57] $$-\rho_2^x(1,2) = \sum_{a\geq b, c\geq d}^{m} x_{abcd}\phi_a(\boldsymbol{r}_1)\phi_b(\boldsymbol{r}_1)\phi_c(\boldsymbol{r}_2)\phi_d(\boldsymbol{r}_2)$$

[2.58] $$x_{abcd} = d_{abcd} + d_{abdc}\Delta_{ab} + d_{badc}\Delta_{ab}\Delta_{cd}$$

Chapter 3: The domain averaged Fermi hole (DAFH)

One of the most significant concepts in chemistry is the chemical bond. As stressed in the previous chapters, all the chemical information can be recovered by charge density ρ and its n-order matrixes. Particularly, Lewis concepts can be extracted using the 1st $\rho(r)$ and 2nd $\rho(r_1, r_2)$ ones in the so called DAFH[35].

The probability of finding a single electron in a fixed point r is given by the 1st order density matrix: $\rho = N \int \Psi^2(1,2,\dots,N) dr_1 dx_2, dx_3, \dots dx_N$.

On the other hand, $\rho(r_1, r_2) = \frac{N(N-1)}{2} \int \Psi^2(1,2,\dots,N) dr_1 dr_2, dx_3, \dots dx_N$ provides the probability to find the first electron of the pair at r_1 and the second one at r_2. Thus, fixing one of the two electrons in a point r_2, the probability of finding the other at r_1 is $P_{r2}(r_1) = \frac{2\varrho(r_1,r_2)}{\varrho(r_2)}$.

The Fermi hole[36] defined as:

[3.1] $$h_{r2}(r_1) = \varrho(r_1) - P_{r2}(r_1)$$

was introduced in chemistry by Luken[37]. Providing the difference between the full electron density at r_2 and the conditional density that an electron lies at $r_2$when another electron is at r_1, it shows the effect of electron pairing giving a measure of correlation arisen from antisymmetry principle.

The assignment of the reference electron in a fixed position is in contrast with Heisenberg principle hence, instead of definition of eq.3.1, it is preferable to use the integrated Fermi hole:

[3.2] $$h_\Omega(r_1) = \varrho(r_1) - P_\Omega(r_1)$$

Now the reference electron is not fixed but contained in a defined region Ω which can be defined as QTAM atomic basin providing a chemical meaningful issue.

---

[35] R.Ponec *J. Math. Chem.* 1997 **21** 323

[36] E.Wigner, F.Seitz *Phys. Rev.* 1933 **43** 804
J.R.Boyd, C.A.Coulson *J. Phys. B* 1974 **7** 1805

[37] W.L.Luken, D.N.Beratan *Theor. Chem. Acc.* 1982 **61** 265

The probability $P_\Omega(r_1) = \frac{2\int_\Omega \varrho(r_1,r_2)dr_2}{\varrho(r_2)dr_2}$ satisfies the normalization $\int P_\Omega(r_1)dr_1 = N-1$ thus $\int h_\Omega(r_1) = 1$.

Taking into account that, in a real molecule, a region Ω is not populated by only one electron but by N_Ω, a last correction is required. The "charge-weighted" Fermi hole (g_Ω) is nothing but h_Ω statistically corrected for the of electrons inside Ω[38].

[3.3] $$g_\Omega = N_\Omega h_\Omega$$

[3.4] $$g_\Omega = N_\Omega$$

g_Ω can be written as an expansion:

[3.4] $$g_\Omega = \sum_{\mu\nu} G^\Omega_{\mu\nu}\phi_\mu(r)\phi_\nu(r)$$

Effective one-electron functions may be defined by diagonalizing the DAFH in the basis of occupied orbitals. In this way, $G^\Omega = \sum_i n_i|\phi_i|^2$, being ϕ_i one-electron functions called DAFH orbitals (or domain natural orbitals, DNOs), and n_i a set of occupation numbers that reconstruct by summation N_Ω. A nice link (exact for single determinant descriptions) between these DNOs, their occupation numbers and the statistics of domain electron population exists[39]. It establishes that the effective electrons described by the DNOs are statistically independent, so that $P(n_\Omega,n_{\Omega'})$, the probability of finding n_Ω electrons in basin Ω, and $n_{\Omega'} = N - n_\Omega$ electrons in basin $\Omega' = \mathrm{R}^3 - \Omega$ is given by a binomial distribution constructed from a set of N independent events (or coin tosses). Each of the electrons, described by one different ϕ_i, has a probability $p_i(\Omega) = n_i = \int_\Omega |\phi_i|^2$ of being found in basin Ω (so that $p_i(\Omega') = 1 - n_i$). It should be noticed[40] that the statistics of basin electron populations is intimately linked to electron localization and delocalization, and thus to chemical bonding.

---

[38] As stated in the first chapter the number of electrons inside a basin are obtained integrating the CD: $N_\Omega = \int_\Omega \varrho(r_1)$

[39] E.Francisco, A.Martin Pendas, M.A.Blanco *J. Chem. Phys.* 2009 **131** 124125

[40] A.Martin Pendas, E.Francisco, M.A.Blanco *Phys. Chem. Chem. Phys.* 2007 **9** 1087

The DNOs obtained for a given basin Ω come out in three basic flavors. Each ϕ may be either extremely localized in Ω, with $n_i \approx 1$, extremely localized in Ω', with $n_i \approx 0$, or partially delocalized between both, with an extreme case being $n_i = 0.5$.

DNOs display the local symmetry of the Ω basin. In high symmetry situations this property is undesirable, and it is customary to break it by performing an isopycnic localization[41]. This is a linear non-unitary transformation, that transforms the DNOs into a different set, the isopycnic orbitals, which fulfill three important properties: i) they preserve the diagonal form of the one-particle density matrix, provided this is expressed in terms of the natural orbitals of the system; ii) they transform according to the point group of the molecule, and iii) they preserve the basic DNO properties (including their degree of localization) at the cost of mutual orthogonality, that is rigorously lost. Nevertheless, this nonorthogonality is almost always residual in single determinant descriptions.

Remembering that $\rho_{xc}(\boldsymbol{r_1},\boldsymbol{r_2}) = 4\sum_i^{N/2} \phi_i\ (\mathbf{r_1})\phi_j^*(\mathbf{r_1})\,\phi_i^*(\mathbf{r_2})\phi_j\ (\mathbf{r_2})$ and $V_{xc}^{\Omega\Omega'} = \int_{\Omega\Omega'} \frac{\rho_{xc}(\boldsymbol{r_1},\boldsymbol{r_2})}{r_{12}} d\boldsymbol{r_1} d\boldsymbol{r_2}$, the exchange correlation energy can be approximated as the sum of contributes of delocalized (and so bonding) DNOs. Indeed, the orthogonality of the DNOs in both Ω and Ω' will make the non-diagonal ($i \neq j$) contributions to $V_{xc}^{\Omega\Omega'}$ very small (strictly vanishing in the absence of the r_{12} denominator. Moreover, the diagonal ($i = j$) terms will be dominated, by large, by orbitals delocalized between Ω and Ω'. DNOs localized either in Ω or in Ω' will contribute to one of the $\boldsymbol{r_1}$ or $\boldsymbol{r_2}$ domains, respectively, but not to the other. In the end, the total $V_{xc}^{\Omega\Omega'}$ energy will mainly come from diagonal delocalized, i.e. bonding, terms, and the expression 3.5 recover about 90% of the covalent energy in standard cases.

[3.5] $$V_{xc}^{\Omega\Omega'} = \sum_{\phi i\ bonding} V_{xc}^{\Omega\Omega'}(ii)$$

[41] J.Cioslowsky *Int. J. Quantum Chem.* 1990 **S24** 15

Chapter 4: Using pseudopotentials within the IQA approach[42]

Introduction

IQA analyses, necessarily based on numerical integration techniques, are computationally intensive, power scaling with the number of electrons, basis set functions, and (partially) occupied orbitals. Moreover, small numerical errors when integrating the core regions of heavy atoms amplify themselves to large energetic uncertainties that may decrease the IQA interaction energies accuracy that is needed for chemical bonding problems. Before my PhD, IQA had only been applied to small molecular systems composed of light atoms. Thus, my studies were focused on how to extend such theory to larger molecules with heavier atoms. This is particularly true in the case of transition metal compounds, natural home of a number of key concepts in the modern theory of the chemical bond. Among them we may just cite the nature of formally multiple metal-metal bonds[43] or of agostic interactions[44], and concepts like back-donation[45], the versatility of the metal-carbon bond[46], etc.

Most modern electronic structure calculations in heavy atom molecules also struggle with the problem posed by the large number of chemically inert core electrons. This is almost invariably tackled by using either pseudopotentials (PP)[47] or, in general, effective core potentials (ECPs)[48], one-electron operators that act on valence electrons and prevent them to collapse onto core states. The absence of cores would contribute to solve the numerical problems described above and to reduce the time required for a calculation. On the other hand, this very absence has also an obvious drawback within the QTAM, for the electron density ρ constructed from pseudo-valence orbitals lacks the maxima (cusps, rigorously speaking) at the nuclear positions that define the atomic basins within the theory. This means that even though the PP energetics is well-behaved, the topology of the valence-only density, $\rho_{pp}(\boldsymbol{r})$, may be completely

[42] D.Tiana, E.Francisco, M.A.Blanco, A.Martin Pendas *J. Phys. Chem. A* 2009 **113** 7963
[43] G.Frenking *Science* 2005 **3**10
L.Gagliardi, P.Pyykkö, B.Roos *Phys. Chem. Chem. Phys.* 2005 **7** 2415
[44] M.Brookhart, M.Green, *J. Organomet. Chem.* 1983 **500** 127
[45] M.Dewar *Bull. Soc. Chim. Fr.* 1951 **18** C79
J.Chatt, L.A.Duncanson *J. Chem. Soc*. 1953 2939
[46] F.Wheinhold, C.Landis *Valency and Bonding. A Natural Bond Orbital-Donor Prespective*. Cambridge Press 2005
[47] C.J.Philips, L.Kleinman *Phys. Rev.* 1959 **116** 287
[48] S.Huzinaga A.A.Cantu *J. Chem. Phys.* 1971 **55** 5543

different from that obtained with the all-electron $\rho(\boldsymbol{r})$. This difficulty is well-known in literature, and several works[49] have been devoted to elucidate how to by-pass it.

In this chapter it will be shown how the correct topology can be obtained from PP calculations. Then, in order to analyze problems arising in IQA neglecting the core, results obtained for CH_4, SiH_4, GeH_4 using both all-electron (AE) and ECP wavefunctions will be reported. At last it will be explained how to implement ECP approximation inside IQA.

The topology of ρ from pseudopotential calculations

The absence of core electrons in PP or ECP electronic structure calculations poses some important problems on determining the topology of ρ. The key feature of valence-only densities is the lack of (3,-3) critical points at the nuclear positions affected by core removal, which are sometimes substituted by (3,+3) CPs. Since the Poincaré-Hopf (or Morse) topological invariant must retain its value and the indices of (3,-3) and (3,+3) CPs are of opposite sign, the substitution of a maximum by a minimum must be necessarily accompanied by the creation of other compensating CPs, including at least either one maximum or one (3,+1) ring CP. As ρ is relatively unaffected at r points far enough the removed cores, these new CPs are expected to lie in the proximity of the latter, and the topology of ρ_{pp} to closely resemble that of the AE density in the chemically relevant valence regions.

In their paper Vyboishchikov *et al.* showed that correct topologies may be obtained from core-reconstructed pseudo-AE densities. Two different procedures were analyzed. In the first, called augmented, the pseudo-AE density is obtained adding a core density (generated in an independent atomic calculation) to the ECP (which contains only the valence) one: $\rho_{aug} = \rho_{core} + \rho_{ecp}$. In the second, the core orbitals are orthogonalized to the valence ones, and the pseudo-AE density, ρ_{orth}, is derived from the orthogonalized determinant. Orthogonalized densities yielded no clear-cut improvement over either the local properties at critical points or the integrated ones over atomic basins. Indeed, atomic populations and bond orders were shown to worsen considerably with respect to AE values, this effect being traced to the diffuse tails induced in the core orbitals upon orthogonalization. Moreover, using this procedure gives computationally cost required to an IQA/AE calculation equivalent. Hence it was not considered. In table 4.1 topologies parameters of all electron (AE), pseudo-valence (ECP) and core-reconstructed (Aug) for methane, silane and germane are reported.

[49] J.Ciosslowski, P.Piskorz *Chem. Phys. Lett.* 1996 **255** 315
S.Voyboishchikov, A.Sierraalta, G.Frenking *J. Comp. Chem.* 1996 **18** 416

$X(XH_4)$	CP	position	x(y)	d	ρ	Lapl ρ	H
C(AE)	-1	(x,x,x)	0.7394	1.2807	0.2815	-1.0118	-0.2974
C(ECP)	3	(0,0,0)		0.0000	9.00E-05	28.1304	-0.1295
	1	(x,x,x)	0.3361	0.5821	0.2358	-0.7615	-0.8228
	-1	(0,0,x)	0.6177	0.6177	0.2547	-1.1119	-0.8196
	-3	(x,x,x)	0.4409	0.7637	0.294	-1.4904	-0.6208
	-1	(x,x,x)	0.7243	1.2545	0.2797	-1.1088	-0.3005
C(aug)	-1	(x,x,x)	0.7266	1.2585	0.2798	-1.0006	-0.2986
Si(AE)	-1	(x,x,x)	0.7724	1.3378	0.1195	0.3018	-0.0711
Si(ECP)	-3	(0,0,0)		0.0000	5.00E-008	-0.8607	-0.2154
	3	(x,x,x)	0.0273	0.0473	4.00E-008	0.0004	-0.0002
	1	(x,y,y)	0.0319(-0.0251)	0.0516	4.00E-008	0.0005	-0.0002
	3	(0,0,x)	0.055	0.0550	9.00E-008	0.0022	-0.0004
	1	(x,x,y)	0.0186(-0.0500)	0.0565	1.00E-008	0.0024	-0.0002
	3	(x,x,x)	-0.0336	0.0582	7.00E-008	0.0027	-0.0004
	1	(x,x,x)	-0.7526	1.3035	0.0338	-0.0251	-0.0228
	-1	(0,0,x)	1.3835	1.3835	0.0508	-0.0536	-0.0392
Si(aug)	-1	(x,x,x)	0.7957	1.3782	0.1222	0.1997	-0.0595
Ge(AE)	-1	(x,x,x)	0.9688	1.6780	0.1342	0.0581	-0.0878
Ge(ECPl)	-3	(0,0,0)		0.0000	1.00E-006	-1.0549	-0.2637
	3	(x,x,x)	-0.0067	0.0116	1.00E-010	0.0083	0.0000
	-3	(x,x,x)	0.0152	0.0263	2.00E-007	-0.0028	-0.0009
	-1	(x,x,x)	-0.0181	0.0314	2.00E-007	-0.0022	-0.0008
	1	(x,y,y)	0.0018(0.0250)	0.0354	1.00E-006	0.0246	-0.0004
	3	(0,0,x)	0.0389	0.0389	8.00E-010	0.0056	0.0000
	1	(x,x,x)	-0.8174	1.4158	0.0368	-0.0453	-0.0302
	-1	(0,0,x)	1.4851	1.4851	0.0484	-0.0769	-0.0377
Ge(ECPs)	-3	(0,0,0)		0.0000	1.00E-006	-1.0497	-0.2624
	-1	(x,y,y)	0.1941(0.0711)	0.2186	0.1329	0.0157	-0.0905
	3	(0,0,x)	0.2836	0.2836	7.4371	-312.22	-356.2900
	-3	(x,x,x)	-0.1638	0.2837	7.468	-319.93	-357.2200
	-3	(x,x,x)	0.166	0.2875	0.3674	-21.539	-5.3861
	-1	(x,x,x)	0.9505	1.6463	0.1329	0.0151	-0.0905
Ge(augl)	-1	(x,x,x)	0.9825	1.7017	0.1364	0.0369	-0.0820
Ge(augs)	-1	(x,x,x)	0.9794	1.6964	0.1359	0.0389	-0.0849

Table 4.1: Molecular geometries are fixed at the AE-optimized values. All CPs are nondegenerate, classified according to their signatures with nuclear cusps ignored, and ordered according to their distance to the X nucleus, *d*. Only nonequivalent by symmetry CPs, together with their densities, laplacians, and energy densities, are reported. The multiplicities of CPs are 1, 4, 6, and 12 for the $(0,0,0)$, (x,x,x), $(x,0,0)$ and (x,x,y) special positions, respectively. All data are in au

The calculation was made using CRENBL[50] ECP at Hartree-Fock level using standard 6-311G(d,p) basis-set[51]. Two and ten electron cores have been used for C and Si, respectively, while both large (l, 28 e) and small (s, 18 e) cores are presented for Ge. In order to isolate the effect that the use of ECPs has on the topology from geometry optimization issues, all systems were fixed at the AE optimized geometries. Looking at the table some interesting points could be noticed. All ECP topologies contain spurious CPs, whose number tends to increase with the size of the ECP core. In both CH_4 and the small core GeH_4 cases, it is possible to define a sphere

[50] F.L.Pacios, P.A.Christiansen *J. Chem. Phys.* 1985 **82** 2664
M.M Hureley, F.L.Pacios, P.A.Christiansen, R.Ross, W.Ermler *J. Chem. Phys.* 1986 **84** 6840

[51] Note that changing the basis-set, the level of the calculation or the ECP recipe does not alter the results

which completely contains the "core" CPs. However it should be noticed how the ECP topology of these systems are different. In the first molecule, the carbon nuclear cusp has been substituted by a cage CP, whereas a very small, though clearly developed, maximum is found in germane.

The valence topology outside the confinement sphere coincides with that in the AE calculation, although the quantitative details may differ. For instance, the position of the X-H bond critical points, together with their electron densities and energy densities, are recovered within 3% error. On the other hand, more sensitive properties like $\nabla^2\rho$ are found to accumulate much larger errors. This behavior is typical of very compact cores. The situation for other cases (SiH_4 and large core GeH_4) is more complex. In both silane and germane the confinement sphere cannot be defined, since the AE valence topology is severely affected. No CP is found in the valence region along the bond directions. In fact, ρ grows monotonously from the X core towards the H maxima, and four (x, x, x) ring CPs appear in the rear bond directions at about the same distance from X as the AE BCPs. Well developed BCPs appear between every pair of H's, in accord with the results of Vyboishchikov's paper. A QTAM partitioning based upon these ρ_{ecp} would fail by assigning completely unphysical basins to the quantum atoms. This behavior is usual for larger cores that clearly penetrate the valence, and for highly charged quantum atoms, like Si in silane (see table 4.2). Addition of core densities, obtained by solving the ground state electronic structure of the neutral isolated X atom with the same basis set used in the ECP calculation, recovers the AE topology in every case. The errors in ρ and H are less than 2 and 16%. However, although the errors in $\nabla^2\rho(\boldsymbol{r}_{bcp})$ decrease upon adding core densities, they may be as large as 40%. Since our goal is to compare integrated properties, a question remains. Finally, the surfaces of analyzed systems were calculated finding that the AE interatomic surfaces are rather faithfully reconstructed using ρ_{aug}, both in the small and large core cases. This is quite a general result that allows us to conclude that the usage of $\rho_{aug} = \rho_{core} + \rho_{ecp}$ provides an enough accurate framework to perform IQA integrations on ECP-based electronic structure calculations. Furthermore, when a confinement sphere may be defined, like in the GeH_4 small ECP model, the interatomic surfaces obtained from just ρ_{ecp} might also be trustful.

IQA partitioning from ECP pseudo-wavefunctions

Most modern ECPs or PPs are modeled as one-electron non-local operators acting on the valence electrons with the following algebraic structure[52,53]:

[4.1] $$V_{eff} = V_L(r) + \sum_{\lambda=0}^{L-1}\sum_{\mu=-\lambda}^{\lambda}|Y_{\mu\lambda})V_{\lambda-L}(r)(Y_{\lambda\mu}|$$

$$V_{\lambda-L}(r) = V_\lambda(r) - V_L(r)$$

ECP pseudo-energies do not contain, manifestly, core self-energy contributions. Moreover, core-valence interactions are introduced in a mean-field manner through the effective one-electron potentials. ECP descriptions are not strictly compatible with the first and second order density matrix partition provided by IQA. If we partition Tr $\rho\, V_{eff}$ in real space into basin contributions, the resultant atomic effective potentials, $V_{eff}^A = \int_{\Omega_A} Tr\, \rho\, V_{eff}\, d\mathbf{r}$ will contain a mixture of effective one and two electron contributions. This violates the IQA spirit, in which every energetic quantity has both a clear physical meaning and a well defined one or two electron nature. Since the total expectation value of V_{eff} plays no role in ECP calculations, we deem that no chemical meaning should be assigned to the atomic V_{eff}^A. Thus, it was not considered in IQA-ECP protocol.

Taking into account these constraints, together with the results of the previous paragraph, we have devised three computational strategies. They all start by using an ECP pseudo-wavefunction to determine the interatomic surfaces (i.e. the atomic basins) of ρ_{aug} obtained by adding the core densities ρ_{core} of all the ECP atoms to ρ_{ecp}, as described before. In the first strategy, IQA integrations are performed on first and second order density matrices, ρ_{ecp} and $\rho_{2,ecp}$, derived from the pseudo-valence wave function Ψ and completely ignoring the energetic role of core electrons, which are, in a way, collapsed onto their corresponding nuclei. From a practical point of view, the nuclear charge of each ECP atom is decreased by the number of core

[52] P.K.L.R.Baybutt, G.D.Truhlar *J. Chem. Phys.* 1976 **65** 3826

[53] $L-1$ is the maximum angular momentum of the excluded core electrons. $l = \lambda - L$. All the spherical harmonics and radial functions are centered at the position of the atomic nucleus of the excluded core, and the $V_l(r)$ potentials are expressed as linear combinations of Gaussians $V_l(r) = \sum_{i=1}^{N} B_i^l r^{n_i^l} e^{-\alpha_i^l r^2}$

electrons, $Z_{eff}^{A} = Z_A - n_{core}^{A}$, and a normal IQA calculation is performed afterwards. These IQA-ECP (or simply ECP) results scale with a power of the number of valence electrons, n_{val}, which was the original purpose. A second possibility is to obtain pseudo all electron first and second order matrices constructed by augmenting the pseudo-valence with suitable core orbitals. The cleanest procedure to do this, mutually orthogonalizing the chosen core orbitals to the pseudo-valence ones, leads to the errors commented above, and has to be abandoned. Neglecting the orthogonality requirements, we arrive at $\rho_{aug} = \rho_{core} + \rho_{ecp}$. Since $\rho_{2,aug}$ can be written as $\rho_{2,aug} = \rho_{2,aug}^{C} + \rho_{2,aug}^{xc}$, this approach, called IQA-aug (or simply aug), includes valence-valence, core-core and core-valence interactions, and is computationally equivalent to an AE IQA calculation. In this approach, an intrinsic error is introduced by supposing orthogonality of a set of orbitals that is not rigorously orthogonal. Since the core-valence exchange-correlation terms ($\rho_{2,ecp-core}^{xc}$) obtained with this scheme may be untrustworthy, a problem may be traced back to the lack of both self-consistency and orthogonality between the core and the valence orbitals. For this reason, a third mixed strategy has been used in which all core-valence exchange-correlation matrix elements are neglected, i.e. $\rho_{2,ecp-core}^{xc} = 0$. With this, the core-valence interaction is reduced to its purely Coulombic terms, contained in the separated first order core (ρ_{core}) and valence (ρ_{ecp}) densities. All core-core and valence-valence terms are explicitly included. We will call this procedure IQA-noxc (or simply noxc). Although aug and noxc procedures allow us to perform IQA calculations from external ECP wave-functions, it should be noticed that no significant computational saving is achieved respect to an AE computation with these two techniques. In order to isolate core-removal effects from genuine alterations due to the ECP approximations, a pseudo-ECP (pECP) wavefunction was constructed deleting the appropriate core orbitals from the AE calculations. Results are reported in table 4.2.

X	Q X	E_{self} X	E_{def} X	E_{self} H	V_{cl} XH	V_{xc} XH	δ XH	V_{cl} HH	V_{xc} HH
Ge(AE)	1.7977	-2074.3005	0.9715	-0.4251	-0.2745	-0.1884	0.7959	0.0434	-0.0062
Ge(pECPl)	1.7230	1.6993	1.6604	-0.4752	-0.2469	-0.1766	0.7760	0.0394	-0.0063
Ge(pECPs)	1.7949	-44.7902	1.0109	-0.4292	-0.2736	-0.1871	0.7949	0.0432	-0.0062
Ge(ECPl)	1.7162	-3.1443	1.0427	-0.4718	-0.2464	-0.1789	0.7722	0.0393	-0.0063
Ge(ECPs)	1.7570	-47.9161	0.9804	-0.4253	-0.2633	-0.1913	0.8016	0.0416	-0.0063
Ge(augl)	1.7729	-2075.4851	-0.2131	-0.4244	-0.2678	-0.1965	0.8146	0.0424	-0.0062
Ge(augs)	1.7598	-2075.4606	-0.1886	-0.4211	-0.2644	-0.1949	0.8114	0.0418	-0.0063
Ge(noxcl)	1.7729	-2075.0803	0.1916	-0.4218	-0.2678	-0.1867	0.8007	0.0424	-0.0063
Ge(noxcs)	1.7598	-2067.6789	7.5931	-0.4210	-0.2645	-0.1917	0.8030	0.0418	-0.0063

Table 4.2: The all-electron results (AE) are to be compared with the three flavors of ECP and pseudo-ECP calculations (ECP, pECP, aug, and noxc) described in the text. All ECP and pECP wave functions have been obtained at the fixed AE geometries, and all interatomic surfaces are also frozen to those of the AE systems. The central atom deformation energies are measured with respect to 3P *in vacuo* references. For germanium, they are -2075.2720, -45.8011,0.0389, -48.8965, and -4.1870 au in the AE,pECPs, pECPl, ECPs, and ECPl order

Germane gives us the opportunity to examine all the above effects in large (28 electrons removed, ECP_l) and small core (18 electrons removed, ECP_s) cases and will be now briefly analyzed. First, being outer electrons in He, Ne, and Ar closed shell series less and less compact, core leakages are considerably larger than in methane (0.001e) and silane (0.027e) case. Notice that the large core leaks about 0.8 e into the ligands, and that this number is only halved by using the small [Ne] core. In other words, the 10 $3d$ electrons leak out about as much charge as the [Ar] core. This is in agreement with common wisdom, and the 3d sub-shell has a similar extension as the $3s$ and $3p$ ones. The effect of the ECP approximation is non-negligible in the small-core case, and the Ge ECP pseudo-valence orbitals have about 0.04 extra electrons in the core region as compared with the AE valence ones. Concerning the energy contributes, the small core yields a deformation energy value quite similar to that found at the AE level. Core reconstruction leads to very large deformation errors. On the other hand, the E_{self}^{H} ECP_l value is almost 30 kcal/mol larger than the AE one, but this error becomes very small for the ECP_s case. Core reconstruction reduces considerably the error for the large core leading to a converged value (within 1 kcal/mol) 2-3 kcal/mol above the AE value. The covalent contribution for the HH interaction, -3.9 kcal/mol, is almost one third of that in silane, and similar to that found in methane. It is already well simulated by ECP-only results. Coulomb effects are, as usual, larger. V_{cl}^{HH}differs in the large ECP calculation by 2.6 kcal/mol from the AE result, while only by 1.1 kcal/mol if the small core is used. If we examine the GeH pairs, a similar image arises. δ^{GeH} is too low in the ECP_l description, while reasonable in the ECP_s one. The errors in the V_{xc}^{SiH} contribution are +6.0 and -1.8 kcal/mol, respectively. The greater core leakages now induce larger deviations of V_{cl}^{GeH} from the AE value: -17.6 and -10.6 kcal/mol for ECP_l and ECP_s, respectively. Core reconstruction leads to an improvement of the GeH interaction terms,

although an error of about 7 kcal/mol remains in the classical contribution. This clearly points towards a mixture of core polarization, orthogonality and self-consistency effects affecting the particle charge distribution of the core. It is important to recognize at this moment that core reconstruction has a rather small energetic impact in the small core case, but a considerable one as the computational cost is regarded, if core-core electron repulsions are computed. Thus, the balance between accuracy and computational cost should be selected depending on the particular needs of the study that is undertaken.

How to perform an IQA-ECP analysis

Data in table 4.2 confirm that reasonably accurate results may be obtained by performing IQA integrations on pseudo-valence densities. Moreover, in terms of energetic accuracy *versus* computational cost, reconstruction of the core is really not necessary to account for chemical bonding issues, although the topology of the electron density, i.e. the interatomic surfaces defining the integration domains, has to be obtained from a suitable core reconstructed density.

The protocol (IQA-ECP) that should be used can be summarized in five step:

- select the ECP description of the molecular system;
- obtain the pseudo-valence description from any standard electronic structure code;
- construct adequate core densities for all atoms described by ECPs[54]
- construct the interatomic surfaces of the reconstructed density: $\rho_{aug} = \rho_{core} + \rho_{ecp}$
- integrate over the ρ_{aug} basins using first and second-order density matrices obtained from the pseudo-wavefunction only.

Let us take germane as our production example. Optimization of geometries at the ECP level leads to differences inherent to the pseudopotential approximation as summarized in table 4.3, while table 4.4 provides IQA results obtained with IQA-ECP protocol.

Both small and large core ECPs induce a significant contraction of the Ge-H distance, although the harmonic frequencies are not affected much. This may be due to the use of non-relativistic ECPs, since it is known that better geometries are obtained with the latter[55]. From the real space point of view, this Ge-H distance, shortening with no particular force constant change, is associated to a redistribution of charge without much variation in the exchange-correlation contributions. Force constants depend much more abruptly on changes on V_{xc} than on those on

[54] A simple option for this is to perform *in vacuo* atomic calculations with the same basis sets used in the molecular case, but others exist.

[55] P.Macchi, A.Sironi *Acta Crys. Sect. A* 2004 **60** 502

V_{cl}. The Ge atom is noticeably less charged in the optimized ECPs geometry than in the one corresponding to the AE calculation. This is relatively easy to rationalize. Since the Ge cores clearly leak into the valence, their absence, even with the projection operators that preclude collapse of the valence orbitals onto core states, induces an artificial lack of core pressure on the valence electrons, and Ge-H distance decreases. The effect of this decrease is clearly more important on the large core situation. The use of relativistic cores may prevent these effects and should be taken into account. The reduced net charge in Ge gives rise to smaller classical stabilization for the GeH pair. This is classical reasoning based on Coulomb's law, for the change in geometry does not compensate the larger change in charge transfer, the reduction being thus more important for the ECP_l case. Small perturbations in charge transfers are usually accompanied by similar, though opposite, changes in V_{xc}. In our case, the absolute value of V_{xc}^{GeH} increases with respect to table 4.2, and ECP_l and ECP_s result bracket AE energies. This is correlated to the equivalent bracketing in the GeH stretching frequencies. Flexion or bending modes are more related to the HH interactions, which are now dominated by the Coulombic terms. Now they are consistently larger in the ECP calculations than in the AE one, as corresponds to the smaller classical repulsions between the H atoms, particularly in the ECP_l case. Overall, the IQA/ECP description of germane gives rise to reasonably accurate covalent contributions for both the GeH and the HH pairs, and introduces a charge transfer bias related both to the too short Ge-H optimized distance and to core leakage as explained above. Fortunately, this effect may be clearly anticipated from the failure of the ECPs used to provide an accurate geometry. The charge amount that leaks from the core of an atom A may be bounded from above if one computes the number of electrons lying within a sphere with a radius equal to the average of the distances from the nucleus A to all of its associated BCPs. Since the atomic cores will be spherical almost always, this is a very easy task. For instance these radii are 0.678, 0.708 and 0.888 Å for the AE optimized geometries of CH_4, SiH_4 and GeH_4 respectively. The number of electrons of the core escaping their related spheres turn out to be 0.3, 86.9, 257.5, and 17.9 me, for the C, Si, Ge(l), and Ge(s) cores, respectively. Hence these numbers represent the upper bounds to the actual core leakages.

	d(Ge-H)	ν_1	ν_2	ν_3	ν_4
AE	1.5315	912.3	993.3	2229.9	2255.7
ECPl	1.5170	934.8	1015.5	2214.4	2250.3
ECPs	1.5174	917.9	1009.0	2249.9	2273.5

Table 4.3: Distance in Å, freq ν^{-1}

	Q X	E_{self} Ge	E_{def} Ge	E_{self} H	V_{cl} XH	V_{xc} GeH	δ GeH	V_{cl} HH	V_{xc} HH
ECPl	1.6898	-3.1680	1.0190	-0.4734	-0.2351	-0.1817	0.7784	0.0378	-0.0063
ECPs	1.7104	-47.9542	0.9423	-0.4306	-0.2457	-0.1944	0.8107	0.0390	-0.0061

Table 4.4: IQA decomposition for germane according to IQA-ECP protocol

Summarizing IQA analysis can be used with pseudovalence wave-function constructed under pseudopotential or effective core potential approximation. Depending on the size of excluded core, the topology of valence region, which defines the interatomic surface of the basin may be completely wrong. Thus, it is necessary to add a core density to the pseudovalence one in order to recover reasonable topologies from an ECP calculation. Under the IQA/ECP protocol this is done obtaining core densities from appropriate atoms (for instance from a free atoms calculations) and adding to the valence pseudodensities. Doing this reasonable results are obtained allowing the implementation of ECP approximation inside IQA analysis with a consequent cut of the computational time required for calculations.

PART II

Chapter 5: The metal carbonyl bond[56]

The metal (M) carbonyl (CO) interaction has probably arisen more interest than any other in metallorganic chemistry. M-CO interaction is generally explained using the classical model proposed by Dewar, Chatt, and Duncanson (DCD) in 1951[57]. Briefly, a synergistic interaction is proposed to occur between σ charge donation from the CO highest occupied molecular orbital (HOMO) and a consequent π-backdonation from the M d orbitals to the CO lowest unoccupied molecular orbital (LUMO). From a simple molecular orbital (MO) perspective, the CO HOMO is its 5σ orbital, while the LUMO is a relatively low lying $2\pi^*$ function. Similarly, metal frontier orbitals are the (crystal field splitted) d orbitals. The success of the DCD model is based on its simple, straightforward qualitative predictions. It has been repeatedly reported that, for the CO bond, the 5σ orbital is either nonbonding[58], or slightly antibonding[59], while the nature of the $2\pi^*$ is definitely antibonding. In this way, the flow of electrons into the latter easily rationalizes the weakening of the CO bond, with its consequent lengthening[60] and reduction of stretching frequencies[61]. These two effects are commonly used to quantify the backdonation and evaluate the (reduced) CO bond strength.

The model illustrated so far was first questioned in the 1970s when, for the first time, the metal carbonyl cations $Cu(CO)^{n+}$ ($n = 1,2$) were synthesized[62]. These examples were followed by other homoleptic noble metal carbonyls like $Ag(CO)^{n+}$ ($n = 1,2$) or $Au(CO)^{2+}$. Their common feature was a higher CO stretching frequency than that found in free CO (2143 cm^{-1}), so they were called "nonclassical" by Strauss[63]. The effect was ascribed to the absence of π-backdonation, such that the remaining weak σ-donation removed density from the antibonding 5σ orbital, this resulting in a shorter CO bond with a larger force constant. Criticisms about the

[56] D.Tiana, E.Francisco, M.A.Blanco, P.Macchi, A.Sironi, A.Martin Pendas *JCTC* 2010 **6** 1064
[57] M.Dewar *Bull. Soc. Chim. Fr.* 1951 **18** C79
J.Chatt, L.A.Duncanson *J. Chem. Soc.* 1953 2929
[58] B.J.Johnson, W.G.Klemperer *J. Am. Chem. Soc.* 1977 **99** 713.
[59] K.L.D.D'Amico, M.Trenary, N.D.Shin, E.I.Solmon, F.R.McFeely *J. Am. Chem. Soc.* 1982 **104** 5102.
[60] F.A.Cotton, R.M.Wing *Inorg. Chem.* 1965 **4** 314
[61] F.A.Cotton *Inorg. Chem.* 1963 **3** 702
[62] Y.Souma, H.Sano *J. Org. Chem.* 1973 **38** 3633
[63] K.P.Hurlbut, J.J.Rack, J.S.Luck, S.F.Dec, J.D.Webb, O.P.Anderson, S.H.Strauss *J. Am. Chem. Soc.* 1994 **116** 10003

arbitrariness of such an explanation soon arrived[64] being, for instance, the antibonding nature of the 5σ MO not definitely demonstrated. Not only some studies demonstrated that this orbital was not antibonding, but also the CO bond stiffenning was correctly reproduced by just modeling the electric field induced by the M cation. Slowly, an image in which the density redistribution induced by this field increased the covalency of the CO bond emerged[65]. It is now relatively clear that it is not so easy to correlate CO stretching frequencies or force constants to M-CO backdonation due to mode coupling, that Strauss' inverse correlation between M-C and C-O distances may fail[66]. Further, backbonding is basically dependent on the M-CO distance, so that a particular onset distance exists for nearly every system that may be larger or smaller than its particular equilibrium geometry[67]. It has even been shown that the amount of donation-backdonation cannot be used as an indicator of binding energies[68].

CHART 1: Schematic Representation of the Metal–CO Donor–Acceptor Interactions in Terms of OC → M σ Donation and M → CO π-Back-donation

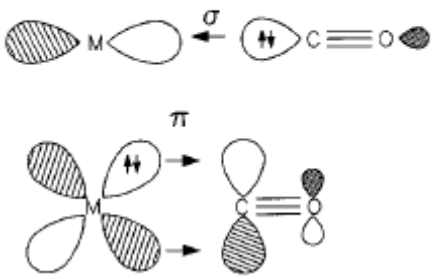

Figure 5.1: Lupinetti *et al.* J. Phys. Chem A 1997 **101** 9551

During the years, real space analyses of chemical bonding in transition metal carbonyls have also been commonplace, both in the QTAM and ELF flavors[69,70]. The MC bond is usually characterized by large positive laplacians at the bond critical point, with relatively large delocalization indexes δ^{AB} for the MC pair. According to QTAM indicators, the MC bond has characteristics similar to those found in dative interactions of main group elements. Attempts to validate the DCD model have also been made either by partitioning densities into σ and π

[64] C.Bach, H.Wilner *Angew. Chem. Int. Ed.* 1996 **108** 2104
A.Sierraalta, G.Frenking, *Theor. Chim. Acta* 1997 **95** 1
[65] A.S.Goldman, K.Krogh-Jespersen, *J. Am. Chem. Soc.* 1996 **118** 12159
[66] R.K.Szilagyi, G.Frenking, *Organometallics* 1997 **16** 4807
[67] A.J.Lupinetti, S.Fau, F.Frenking, S.H.Strauss, *J. Phys. Chem.* 1997 **101** 9551
[68] A.W.Ehlers, S.Dapprich, S.F.Vyboishchikov, G.Frenking, *Organometallics* 1996 **15** 105
[69] P.Macchi, A.Sironi *Coord. Chem. Rev.* 2003 **238-239** 383
F.Cortès Guzman, R.Bader *Coord. Chem. Rev.* 2003 **105** 3911
[70] J.Pilme, B.Silvi M.E.Alikhami *J. Phys. Chem. A* 2003 **107** 4506

contributions, by showing how the δ^{MO} correlates, as expected, with backbonding[71], or by using the domain averaged Fermi hole technique[72]. The solid theoretical foundation of these real space techniques is making them increasingly popular in the field of chemical bonding in transition metal (TM) chemistry[73]. However, a real space energetic image of these important bonds is lacking and interacting quantum atoms approach may clearly fill this gap.

In this chapter a number of classical and non-classical carbonyls will be examined. It will be showed how many of the accepted energy features of the DCD model can be recovered within IQA theory. Finally a particular attention will be dedicated to the possible difference between classical and non-classical systems.

IQA results

Bonding in T_d $M(CO)_4$ systems

Let us examine the isoelectronic $d^{10}\ T_d$ Fe, Co, Ni, Cu, and Pd tetracarbonyls whose results are summarized in table 5.1. All metals bear small positive topological charges, meaning that in the most simple DCD model, backbonding should be extremely large in the Fe compound. The geometric correlations of the model, generally used to quantify backdonation, do also come out easily from the computed data. For instance, the changes in the CO stretching frequencies upon bonding, the changes in $d(CO)$ and the total net charge of ligand correlate each other. Notice that the total charge of ligand is mostly absorbed by the C atom, so charge transfer is fairly localized in MC region.

M	Fe	Co	Ni	Cu	Pd
d(MC)	1.735	1.766	1.924	2.296	2.229
Δd(CO)	0.049	0.024	0.002	-0.010	0.000
Δν(CO)	-491	-295	-64	90	-32
Q_M	0.282	0.189	0.122	0.802	0.064
Q_L	-0.570	-0.297	-0.031	0.050	-0.016
ΔQ C	-0.439	-0.234	-0.086	-0.035	-0.025
δ_{MC}	1.347	1.153	0.798	0.313	0.623
δ_{MO}	0.198	0.166	0.097	0.024	0.075
δ_{CC}	0.130	0.084	0.039	0.012	0.016
Δδ(CO)	-0.318	-0.231	-0.046	0.037	-0.056

Table 5.1: Basic geometric and QTAM integrated properties $[Fe(CO)_4]^{2-}$, $[Co(CO)_4]^-$, $Ni(CO)_4$,$[Cu(CO)_4]^+$, $Pd(CO)_4$ $d^{10}\ T_d$ tetracarbonyls. HF data in atomic units, except distances in Å and frequencies in cm^{-1}. Parameters for the isolated CO molecule are as follows: $d(CO)$=1.114, $\nu(CO)$=2439, Q_C=1.403, δ^{CO}=1.508

[71] P.Macchi, L.Garlaschelli, A.Sironi *J. Am. Chem. Soc.* 2002 **124** 14173
[72] R.Ponec, G.Lendvay, J.Chaves *J. Comput. Chem.* 2008 **29** 1387
[73] E.Matito, M.Solà *Coord. Chem. Rev.* 2009 **253** 647

As explained in chapter 2, delocalization index provides a measure of bond order in real space. For $3d$ metals, the MC bond order decreases as the MC distance increases, as expected. In line with DCD, this increase is coupled to a lengthening of the CO distance and a decrease in the CO bond order. Not so obviously, however, it is also clear that δ^{CO} does also correlate with the overall CO (L) polarization. The only system in which the L net charge is positive is[74] $[Cu(CO)_4]^+$, meaning that charge transfer goes from ligand to the metal in a σ-like fashion. Another interesting point is related to the non-negligible δ^{CC} value that exists between adjacent L's in the Co and Fe compounds. This points towards an important multicenter character of the M-L bonding in those cases where backbonding is also deemed important (i.e. in electron rich compounds).

M	Fe	Co	Ni	Cu	Pd
E_{int} (ML)	-0.343	-0.277	-0.192	-0.070	-0.131
E_{int} (MC)	-0.215	-0.187	-0.142	0.122	-0.098
E_{int} (MO)	-0.128	-0.090	-0.050	-0.192	-0.033
ΔE_{int} (CO)	0.374	0.220	0.212	0.050	0.044
V_{Cl} (ML)	-0.008	0.001	0.005	-0.005	0.002
V_{Cl} (MC)	0.100	0.084	0.045	0.185	0.029
V_{Cl} (MO)	-0.108	-0.083	-0.040	-0.190	-0.027
ΔV_{Cl} (CO)	0.312	0.180	0.224	0.068	0.040
V_{xc} (ML)	-0.334	-0.288	-0.197	-0.067	-0.134
V_{xc} (MC)	-0.314	-0.271	-0.187	-0.065	-0.127
V_{xc} (MO)	-0.020	-0.017	-0.010	-0.002	-0.007
ΔV_{xc} (CO)	0.063	0.041	-0.011	-0.017	0.004

Table 5.2: IQA interactions for $[Fe(CO)_4]^{2-}$, $[Co(CO)_4]^-$, $Ni(CO)_4$,$[Cu(CO)_4]^+$, $Pd(CO)_4$ d^{10} T_d tetracarbonyls. HF data in atomic units. Parameters for the isolated CO molecule are as follows: $E_{int}(CO)$=-2.120, $V_{cl}(CO)$=-1.706, $V_{xc}(CO)$=-0.415

The energetic view provided by IQA in table 5.2 enlightens the above comments. Let us start with a fine-grained view, by examining the MC and MO IQA quantities. $E_{int}(MC)$ is large, and splits the T_d systems into two categories of negative (classic carbonyl) and positive (non-classic carbonyl) total MC interaction. The $V_{cl}(MC)$ contribution to the MC interaction is destabilizing, basically due to the positive net charge at the metal site. However, its particular value is the result of a complex balance among the MC distance, the positive net M and C charges, and the polarization of the charge distribution. The covalent contribution to the MC

[74] Note that this should be considered a non-classical carbonyl having smaller $d(CO)$ and larger δ_{CO} than those found in free CO.

bond, provided by $V_{xc}(MC)$, follows the total net charge of the complex. MC covalency is the basic stabilizing interaction in this series, and even in the Cu case, where backbonding is thought to have a minor role, it amounts to about -40 kcal/mol. Concerning $E_{int}(MO)$, it is obviously stabilizing, controlled by the negative electrostatic component which may be faithfully approximated by a point charge contribution, and its range of variation is smaller. Just as delocalization between the metal and the oxygen atom of each carbonyl provides a real space measure of the relative intensity of π-backdonation, $V_{xc}(MO)$ gives us its energetic signature. It is negligible in $[Cu(CO)_4]^+$ and ten times larger in the $[Fe(CO)_4]^{2-}$ anion. Being $V_{xc}(MO)$ always 7% smaller than $V_{xc}(MC)$, this property should not be interpreted as a direct measure of the total energetics associated to backdonation, which does also include the C atom of the ligand, but rather as an isolated energetic signature, not affected by the covalent contribution of σ donation. Moving to group interactions, the total $E_{int}(ML) = E_{int}(MC) + E_{int}(MO)$ is always negative, although in the Cu case it is relatively small (-44 kcal/mol). Notice that its classical component is small, its absolute value not exceeding 7 kcal/mol, and that it oscillates from positive to negative. Thus, even if each of the MC and MO electrostatic terms may be large, the polarization pattern of L conspires to overall small $V_{cl}(ML)$ values such that in the end covalency, not electrostatics, governs the ML bonding. Regarding the different properties involved in the CO deformation upon coordination, Δd_{CO}, $\Delta\delta^{CO}$, $\Delta V_{xc}(CO)$ are quite linearly correlated, whereas $\Delta V_{cl}(CO)$ is not. In agreement with previous IQA knowledge and with results by Lupinetti and coworkers[75] the CO distance basically responds to changes in covalency. These coordinated CO bonds display $V_{xc}(CO)$ values smaller than those in free CO (except in the Cu complex), so ML bonding decreases the covalence of the CO bond. Although $V_{cl}(CO)$ shows a relatively complex pattern, simple $\frac{Q_C Q_O}{d_{CO}}$ point charge term correlates rather well with it. In general, depolarization of a bond leads to a decrease in its electrostatic contribution, as may be rationalized from the smaller value of $(q-\varepsilon)(q+\varepsilon)$ with respect to $-q^2$ in Coulomb's law when charge is transferred from one point charge to the other in a ionic pair. We also note that although in the Cu compound the covalent CO interaction energy is comparable but smaller than that in the free CO molecule, its electrostatic interaction is considerably (by about 60 kcal/mol) larger. The combination of both facts justifies its $d(CO)$ 0.01Å smaller than the free value. A last comment about copper

[75] A.J.Lupinetti G.Frenking S.H.Strauss *J. Phys. Chem.* 1997 **101** 9551

tetracarbonyl must be done. Indeed in this molecule Δd_{CO}, Q_L, $\Delta\delta^{CO}$, $E_{int}(MC)$ and $\Delta V_{xc}(CO)$ change in sign. Thus the overall positive charge of the species has a deep impact on the molecule. Finally, the behavior of the neutral Pd complex is also noteworthy, at least when compared to the also neutral Ni case. This is probably related to its large ionization potential that justifies its smaller Q and the relatively small change in the net charges that it induces on the CO ligand. On the other hand, the effect of its diffuse d shell on ligand is not small, and the CO moiety suffers a rather big density polarization that increases its classical attraction.

Bonding in D_{3h} $M(CO)_5$ systems

The pentacarbonyls are characterized by well differentiated axial and equatorial ML bonds. It is well known that the equatorial link is generally stronger and shorter, but this gets reversed in the Co case. In this complex, the overall topological charge of the CO ligands is positive, as in $[Cu(CO)_4]^+$. It is also known, though nonetheless interesting, that the metal is quite positively charged even in the Mn complex. This means that the ligands in the complexes bear a considerable negative charge, larger in the equatorial positions. The values of the average MC delocalization indexes are similar to those found in the equivalently charged T_d molecules, and so does the covalent energy associated to the MC bond. There is however a tendency towards stronger (weaker) MC links for the negatively (positively) charged D_{3h} complexes when compared to their equivalently charged T_d counterparts. The V_{xc} and V_{cl} values validate that, in general, axial ML bonds are more ionic than the equatorial ones, although in some cases the difference is small. Interesting is the positive value of these axial $E_{int}(MC)$ for all systems but $Ru(CO)_5$. Thus it is the very stabilizing MO interaction which stabilizes the ML link. This is related to the combined effect of the larger positive charges of the M and the axial carbon atoms. Contrarily to the uniform MC electrostatic behavior, there is a clear change in the MC covalency. The axial links in the Mn and Fe moieties are less covalent than the equatorial ones, while the opposite holds in the $Ru(CO)_5$ molecule.

As regards the CO moiety, it is relatively interesting to notice that the equatorial CO distance is larger than the axial one, independently on the M-C distance behavior. This correlates reasonably with delocalization indexes and V_{xc} values. As in T_d compounds, $\Delta\delta$'s are considerably larger than ΔV_{xc}'s. In Mn and Fe complexes the axial carbonyls are slightly more covalent than the equatorial ones, but the situation is clearly reversed for $Ru(CO)_5$. As found in the tetrahedral cases, the total CO electrostatic interaction is related to the repolarization of the carbonyl group, increasing on average with $|\Delta Q_C|$. As in $[Cu(CO)_4]^+$ molecule, Δd_{CO}, Q_L,

$\Delta\delta^{CO}$, $E_{int}(MC)$ and $\Delta V_{xc}(CO)$ change sign for the cation $[Co(CO)_5]^+$. This consistency shows how intimately coupled the changes in the CO ligands are to the ML bonding features.

Finally, it is worthwhile noticing the similarity in the trends of the CO variations upon bonding for equally charged T_d and D_{3h} systems and the prominent CC delocalizations in Mn and Fe pentacarbonyls, which again point towards non-negligible multicenter bonding features among the carbonyls with covalent contributions as large as 10 kcal/mol. Results for pentacarbonyl are summarized in the below table 5.3.

M	Mn	Fe	Co	Ru	M	Mn	Fe	Co	Ru
$d(MC)_{ax}$	1.9370	2.0610	2.1760	2.0470	Q_M	0.6780	0.5700	0.8520	0.5150
$d(MC)_{eq}$	1.8220	1.8750	2.2510	2.0430	$Q_{L\text{-}ax}$	-0.1920	-0.0340	0.0360	-0.0610
$\Delta d(CO)_{ax}$	0.0130	-0.0020	-0.0110	0.0000	$Q_{L\text{-}eq}$	-0.4310	-0.1560	0.0250	-0.1390
$\Delta d(CO)_{eq}$	0.0300	0.0080	-0.0090	0.0060	$\Delta Q\ C_{ax}$	-0.1550	-0.1180	-0.0510	-0.1360
$\Delta\nu(CO)_{ax}$	-192	-11	140	-50	$\Delta Q\ C_{eq}$	-0.3690	-0.2320	-0.0500	-0.2090
$\Delta\nu(CO)_{eq}$	-360	-188	0	-113	$E_{int}\ (ML)_{ax}$	-0.2040	-0.1300	-0.0940	-0.2030
$\delta_{MC\text{-}ax}$	0.7500	0.5210	0.3650	0.8340	$E_{int}\ (ML)_{eq}$	-0.3180	-0.2310	-0.0870	-0.2260
$\delta_{MC\text{-}eq}$	1.1000	0.9330	0.3770	0.9550	$E_{int}\ (MC)_{ax}$	0.0090	0.0290	0.1250	-0.0420
$\delta_{MO\text{-}ax}$	0.1100	0.0590	0.0300	0.1060	$E_{int}\ (MC)_{eq}$	-0.0950	-0.0650	0.1190	-0.0780
$\delta_{MO\text{-}eq}$	0.1580	0.1230	0.0320	0.1260	$E_{int}\ (MO)_{ax}$	-0.2130	-0.1590	-0.2190	-0.1610
$\delta_{CC\text{-}axeq}$	0.1050	0.0690	0.0380	0.0550	$E_{int}\ (MO)_{eq}$	-0.2230	-0.1660	-0.2060	-0.1480
$\Delta\delta(CO)_{ax}$	-0.1860	-0.0280	0.0120	-0.0760	$\Delta E_{int}\ (CO)_{ax}$	0.1530	0.2140	0.0690	0.2260
$\Delta\delta(CO)_{eq}$	-0.2340	-0.0670	0.0180	-0.0550	$\Delta E_{int}\ (CO)_{eq}$	0.3090	0.3440	0.0590	0.3170
$V_{Cl}\ (ML)_{ax}$	-0.0240	-0.0100	-0.0120	-0.0070	$V_{xc}\ (ML)_{ax}$	-0.1800	-0.1200	-0.0810	-0.1950
$V_{Cl}\ (ML)_{eq}$	-0.0480	-0.0020	-0.0060	-0.0040	$V_{xc}\ (ML)_{eq}$	-0.2700	-0.2270	-0.0810	-0.2220
$V_{Cl}\ (MC)_{ax}$	0.1780	0.1430	0.2040	0.1440	$V_{xc}\ (MC)_{ax}$	-0.1690	-0.1140	-0.0780	-0.1850
$V_{Cl}\ (MC)_{eq}$	0.1590	0.1510	0.1970	0.1320	$V_{xc}\ (MC)_{eq}$	-0.2540	-0.2150	-0.0780	-0.2100
$V_{Cl}\ (MO)_{ax}$	-0.2020	-0.1530	-0.2160	-0.1510	$V_{xc}\ (MO)_{ax}$	-0.0110	-0.0060	-0.0030	-0.0100
$V_{Cl}\ (MO)_{eq}$	-0.2070	-0.1530	-0.2030	-0.1360	$V_{xc}\ (MO)_{eq}$	-0.0160	-0.0120	-0.0030	-0.0120
$\Delta V_{Cl}\ (CO)_{ax}$	0.1240	0.2250	0.0840	0.2300	$\Delta V_{xc}\ (CO)_{ax}$	0.0310	-0.0100	-0.0140	0.0030
$\Delta V_{Cl}\ (CO)_{eq}$	0.2690	0.3540	0.0740	0.3300	$\Delta V_{xc}\ (CO)_{eq}$	0.0410	-0.0090	-0.0140	-0.0120

Table 5.3: Basic geometric, QTAM integrated properties and IQA interactions for $[Mn(CO)_5]^-$, $Fe(CO)_5$,$[Co(CO)_5]^+$, $Ru(CO)_5$, d^8 D_{3h} pentacarbonyls. HF data in atomic units, except distances in Å and frequencies in cm^{-1}. Parameters for the isolated CO molecule are as follows: $E_{int}(CO)$=-2.120, $V_{cl}(CO)$= -1.706, $V_{xc}(CO)$=-0.415

Bonding in O_h $M(CO)_6$ systems

The octahedral d^6 hexacarbonyls follow similar basic rules. As we move from Ti to Fe, the MC distance increases with the exception of the Ti molecule, and the CO bond length decreases monotonically, getting shorter than in the isolated molecule for both Mn and Fe complexes, which also show positive Q_L values. Simultaneously, Q_M passes through a minimum in the Cr complex. Notice how, as Q_L goes from negative to positive, ΔQ_C becomes decoupled from it.

The double negative Ti anion has the largest positive metal charge and the most negatively charged CO species of all examples examined up to now. However, both δ^{MC}, δ^{MO} and their covalent energy counterparts clearly show that backbonding in this O_h complexes has

saturated at the vanadium complex, and that in titanium the approach of the six carbonyls is only possible at a slightly larger MC final distance. This is accompanied by a quite large inter-carbonyl delocalization, as measured by δ^{CC}. Another way to look at the same saturation stems from $\lambda_{Ti} = 18.39$. This parameter grows monotonously up to 23.69 in the Fe hexacarbonyl. Only about 18 electrons (its [Ar] core) are localized in the Ti atomic basin as far as two-center delocalizations are regarded, so all of the valence has been used in bonding to a first approximation. This effect may explain the unexpectedly large Ti-C distance. The O_h systems show very large M charges, thus positive total $E_{int}(MC)$ values independently of the value of Q_L. This behavior is different to that found in our previous example, and makes the MO interaction decisive to account for the negative $E_{int}(ML)$ values and the stability of the complexes. It should be noticed that, going from the tetra- to the hexa-carbonyls, $E_{int}(ML)$ turns out to be a function of the net charge of the complex and its coordination. For a given total charge of -2, -1, 0, +1, +2, its most negative value is obtained in $[Fe(CO)_4]^{2-}$, $[Mn(CO)_5]^-$, $Fe(CO)_5$, $[Mn(CO)_6]^+$ and $[Fe(CO)_6]^{2+}$ complexes respectively. Thus, ML interaction is most favorable for middle $3d$ metals, low coordinations and negatively charged complexes. However, as the total charge becomes positive, higher coordinations become preferable. Moreover the covalence of MC interaction decreases on going from anions to cations (as backbonding arguments suggest) for any coordination, except in $[Ti(CO)_6]^{2-}$ for which we have already suggested a saturation phenomenon. At last, MC V_{xc} decreases with coordination, and as we move from tetra- to hexa-carbonyls the ML link becomes more ionic, as measured by $V_{cl}(ML)$. This is a very well known bonding tendency in solid state physics, where larger coordination phases tend to be more ionic and, in fact, a simple consequence of Pauling's rules. With all the above arguments, the changes in the CO quantities of our $M(CO)_6$ molecules are easily rationalized. As seen in table 5.4, both $\Delta d(CO)$ and $\Delta V_{xc}(CO)$ are negative in the Mn and Fe molecules. Their stronger CO links do also display positive CO net charge with rather small negative oxygen charge and small δ^{MO}, thus very small backbonding.

M	Ti	V	Cr	Mn	Fe	M	Ti	V	Cr	Mn	Fe
d(MC)	2.036	1.986	2.012	2.159	2.225	Q_M	1.461	1.188	0.930	0.994	1.153
Δd(CO)	0.041	0.023	0.005	-0.008	-0.016	Q_L	-0.574	-0.361	-0.154	0.002	0.141
Δν(CO)	-495	-288	-108	57	148	ΔQ C	-0.509	-0.352	-0.162	-0.071	-0.118
δ_{MC}	0.622	0.739	0.680	0.444	0.374	E_{int} (ML)	-0.324	-0.267	-0.192	-0.113	-0.090
δ_{MO}	0.092	0.111	0.098	0.045	0.032	E_{int} (MC)	0.071	0.060	0.067	0.137	0.156
δ_{CC}	0.140	0.106	0.067	0.039	0.050	E_{int} (MO)	-0.395	-0.327	-0.259	-0.250	-0.246
Δδ(CO)	-0.225	-0.175	-0.124	-0.012	0.156	ΔE_{int} (CO)	0.416	0.343	0.150	0.082	0.218
V_{Cl} (ML)	-0.187	-0.096	-0.034	-0.013	-0.004	V_{xc} (ML)	-0.138	-0.171	-0.158	-0.099	-0.085
V_{Cl} (MC)	0.200	0.221	0.216	0.232	0.239	V_{xc} (MC)	-0.130	-0.161	-0.149	-0.095	-0.082
V_{Cl} (MO)	-0.387	-0.317	-0.250	-0.245	-0.243	V_{xc} (MO)	-0.008	-0.010	-0.009	-0.004	-0.003
ΔV_{Cl}(CO)	0.376	0.319	0.135	0.093	0.272	ΔV_{xc} (CO)	0.041	0.025	0.015	-0.010	-0.053

Table 5.4: Basic geometric, QTAM integrated properties and IQA interactions for d^6 O_h carbonyls: $[Ti(CO)_6]^{2-}$, $[V(CO)_6]^-$, $Cr(CO)_6$, $[Mn(CO)_6]^+$, $[Fe(CO)_6]^{2+}$. HF data in atomic units, except distances in Å and frequencies in cm^{-1}. Parameters for the isolated CO molecule are as follows: $E_{int}(CO)$=-2.120, $V_{cl}(CO)$=-1.706, $V_{xc}(CO)$=-0.415

Bonding in D_{4h} $[M(CO)_4]^{2+}$ systems

The analysis of cations $[Ni(CO)_4]^{2+}$ and $[Pd(CO)_4]^{2+}$ confirms the observations related to non-classical carbonyls in other words: shortening $d(CO)$, large metal and small ligand positive topological charges, relatively small MC delocalization indexes coupled to very small δ^{MO} or backbonding, and positive $\Delta\delta^{CO}$. Energetically, these compounds have positive (repulsive) MC interaction energies with large negative $E_{int}(MO)$. Another feature is the important MC ionicity and, regarding the CO ligand, larger covalency than in free CO. This provides an image in which almost all the characteristics of standard carbonyls have been reversed. Notice how, as we move from anionic to cationic species, the overall $V_{cl}(ML)$ changes from negative values to even destabilizing interactions, here exemplified by the $[Pd(CO)_4]^{2+}$ system. Its only overall stabilizing ML term is $V_{xc}(ML)$, clearly dominated by the MC contribution.

M	Ni	Pd	M	Ni	Pd
d(MC)	2.126	2.131	Q_M	1.490	1.104
Δd(CO)	-0.019	-0.020	Q_L	0.128	0.224
Δν(CO)	172	120	ΔQ C	-0.057	0.035
δ_{MC}	0.383	0.614	E_{int} (ML)	-0.091	-0.101
δ_{MO}	0.026	0.050	E_{int} (MC)	0.264	0.171
δ_{CC}	0.049	0.035	E_{int} (MO)	-0.355	-0.272
Δδ(CO)	0.092	0.069	ΔE_{int} (CO)	0.107	0.080
V_{Cl} (ML)	-0.004	0.042	V_{xc} (ML)	-0.087	-0.143
V_{Cl} (MC)	0.348	0.309	V_{xc} (MC)	-0.084	-0.138
V_{Cl} (MO)	-0.352	-0.267	V_{xc} (MO)	-0.003	-0.005
ΔV_{Cl} (CO)	0.146	0.118	ΔV_{xc} (CO)	-0.038	-0.036

Table 5.5: Basic geometric, QTAM integrated properties and IQA interactions for d^8 D_{4h} carbonyls: $[Ni(CO)_4]^{2+}$, $[Pd(CO)_4]^{2+}$. HF data in atomic units, except distances in Å and frequencies in cm^{-1}. Parameters for the isolated CO molecule are as follows: $E_{int}(CO)$=-2.120, $V_{cl}(CO)$=-1.706, $V_{xc}(CO)$=-0.415

Energetic orbital contributions

As explained in chapter 3, DAFH analysis provides a set of domain natural orbitals (DNOs) which are related to the statistic of electron population[76]. Applying IQA on these DNOs allows to decompose the covalent energy in orbitals contributes. This IQA-DAFH technique results extremely computational intensive. For this reason only T_d and D_{4h} systems were analyzed.

The T_d complex

Starting from $Ni(CO)_4$, only DNOs with occupation numbers (n_i) significantly different from zero (i.e. DNOs totally or partially localized on M) will be analyzed. There are 13 of them. The first four have $n_i > 0.999$ resulting almost fully localized in the metal basin. They may intuitively be associated (looking at figure 5.3) to the $3s$ and $3p$ valence orbitals of the Ni atoms[77]. They do not participate in bonding. The remaining nine functions can also be immediately classified. Four of them are σ orbitals delocalized over the metal and each of the four ligands, with an eigenvalue $n = 0.117$. These Φ_σ are rather polarized. If we obtain the domain integrals of Φ^2, the probability of finding the electron in the M basin turns out to be equal to 0.128, and 0.838 in the corresponding CO, so they are adequately interpreted as σ-donating carbonyl orbitals. Only 0.033 electrons described by Φ_σ are delocalized among the other three remaining ligands. Another rationalization path would say that each ligand Φ_σ donates 0.117*2=0.234 (being DNO one electron function) electrons to the metal, making a grand total of about 0.935 electrons. The total delocalization index between M and L is 0.895 of which 0.407 comes from Φ_σ. This value is only slightly smaller than half the total δ^{ML}. The rest up to 0.895 is due to the contribution of the five remaining DNOs, which, as seen in figure 5.3 are d-like functions very localized in the Ni basin (i.e. π-backdonating orbitals). A first point regarding these backdonating functions is that, as deduced by δ^{CC}, they do not localize over one particular CO moiety, contrarily to what the four σ functions do. This points towards a very important difference in these tetracarbonyls between σ-donation and π-backdonation. In the former case, four isolated ML_i functions linking two-groups exist, while in the latter ML bonding must involve several ligands at a time revealing a multilingand nature of π-contribute.

[76] E.Francisco, A.Martin Pendas, M.A.Blanco *J. Chem. Phys.* 2007 **126** 94102
[77] Let us not forget that the [Ar] core has been substituted by an ECP

The five d DNOs come out to be slightly split in a 3+2 fashion with occupation numbers equal to 0.892 and 0.894, respectively. This splitting reminds the $T_2 + E$ decomposition in T_d symmetry. Actually (see below), none of the five slightly split DNOs bind equally the four CO ligands, so that care is to be taken when labelled according to T_d irreps. Each of the five d functions backdonates 0.213 electrons to each of the ligand, making a total of 1.058 electrons. The topological charge of the metal in the complex is +0.122 and can be viewed as coming from the balance of a d^{10} system backdonating 0.122 more electrons than those received by σ-donation from ligands. On average, each of the d functions provides a total bond order with the rest of the system of 0.381, where about 85% of which is due to bonding with two out of the four carbonyls. Each d function thus links preferentially the metal to two L's, as seen in figure 5.2, where the expanded $|\Phi| = 0.03$ au isosurfaces of one representative Φ_d function have been plotted. Any Φ_d may be described, roughly speaking, as an in-phase combination of one metal d and two π^* orbitals from two ligands, again in agreement with the DCD picture. However, since 5 (d functions) is not congruent to 4 (carbonyls), the procedure freezes one out of 6 several equivalent resonance structures: since there are six different ligand pairs, and considering all five DNOs equivalent among themselves, we get one ligand pair not bonded by any DNO. This pair may be selected in six ways. We have thus a considerable multicenter character in backdonation. Adding the contribution of all the d functions to a given ML bond order we get a value of 0.381* 5/4=0.477.

Concerning the energetic profiles of interactions, the covalent interaction energy associated to each ML link is $V_{xc}(ML)$ = -123 kcal/mol. Only 5% of this value is due to the MO interaction, as opposed to a larger 10% contribution in δ_{ML}. A decomposition into our DNOs works as expected, and 87% of the total $V_{xc}(ML)$ is accounted for by the diagonal contributions of its corresponding Φ_σ and the five Φ_d functions. If non-diagonal interactions between this set of six functions are included, this percentage grows to 95%. This means that not only ML bond orders, but also covalent energies, are recovered from the set of appropriate σ and π contributions. Out of the -108 kcal/mol due to V_{xc}(ii) (which are diagonal terms of V_{xc} matrix), -60 are solely due to Φ_σ, or to σ-donation. The energetic share of each σ bond is therefore similar, though slightly larger, than its equivalent share in δ. The remaining -47

kcal/mol comes from backdonation. Since, on average, 2.5 Φ_d functions link the metal to each ligand, each of these links providing about -19 kcal/mol to the covalent ML interaction energy. Summarizing, a σ-donating ML bond is about one and a half times stronger than any of the five three-center π-backdonations. Similarly, σ delocalization is more effective than π delocalization. The former accounts for 45% of the total ML δ, a figure that is amplified to a 55% as the covalent energy is regarded. Overall, our real space results are pretty compatible with MO arguments[78] but provide a far more detailed, invariant picture of bonding in this system.

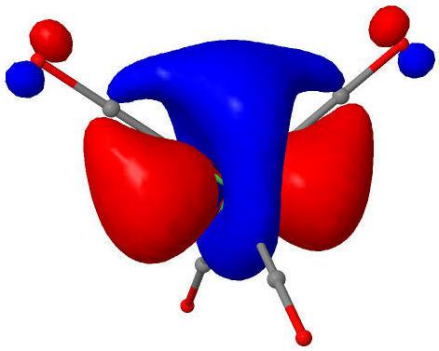

Figure 5.2: Representative d isopycnic DNO orbital for the $Ni(CO)_4$ tetracarbonyl. The isosurface has been expanded up to the $|\Phi| = 0.05$ au level. Notice how the orbital is a combination of metal d and π^* carbonyl functions, and that it preferentially links only two of the ligands

[78] A.W.Ehlers, S.Dapprich, S.F.Vyboishchikov, G.Frenking *Organometallics* 1996 **15** 117

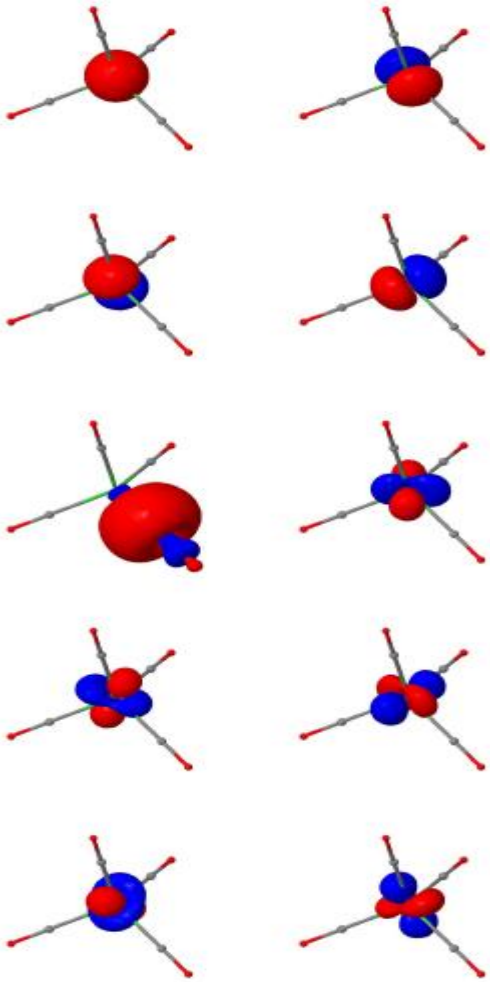

Figure 5.3: Isopycnic DNO orbitals that are significantly localized on the Ni basin for the $Ni(CO)_4$ tetracarbonyl. Isosurfaces displayed at the $|\Phi| = 0.1$ au level

After presenting a detailed picture in the Ni tetracarbonyl, let us now briefly turn to how all the above parameters change with M in T_d systems. In table 5.6 the more important results are reported. A first point regards the general nature of the DNOs. The same general structure found for the Ni case is repeated in all the systems. We have found extremely localized $3s$ and $3p$ functions that do not participate in bonding, plus a set of four equivalent localized Φ_σ donating and five delocalized Φ_d backdonating orbitals. Going from copper to cobalt complex DNOs occupation numbers evolution can be summarized as follows:

- n_σ increases, thus the σ-donating functions become more delocalized over the metal;
- n_d decreases and the π-backdonating orbitals delocalize better over the ligands;

- T_2-E splitting increases such that $n_d(T_2)$ becomes smaller and the participation of T_2-like functions in ML bonding more important, as we should intuitively expect from standard molecular orbital arguments related to ML overlap.

As in $Ni(CO)_4$, the d functions delocalize over more than one ligand. The pattern found in $[Cu(CO)_4]^+$ is exactly the same already presented in $Ni(CO)_4$, but as the T_2-E-like gap increases, a shift is seen towards another pattern. In $[Co(CO)_4]^-$, the E-like functions link the four ligands at a time in a symmetric manner, while the T_2 ones do only delocalize over three ligands. Thus the multicenter (multiligand) character of backdonation increases as the formal charge of the complexes becomes more negative. From the point of view of electron population, it is clear that both σ-donation and π-backdonation increase in the Cu to Co direction. This is clearly related to the decrease in MC distance. Overall, the topological charge on the metal may be seen as a balance between donation and backdonation over the ideal d^{10} configuration. As we shift from copper towards cobalt molecule, more electrons (thus stronger ML interaction) are delocalized both in the donating and backdonating channels. However, their mutual ratio changes completely. In the Cu case, the number of σ-donated (N_d) electrons almost doubles those π-backdonated (N_b). These numbers are roughly equal in the Ni molecule, but N_b more than doubles N_d in the Co complex. Thus, the positive topological charge of cobalt is the result of backdonating 2.235e, but receiving only 1.047e from the ligands on top of its ideal -1 oxidation state.

M	Co	Ni	Cu
d(MC)	1.766	1.924	2.296
Δd(CO)	0.024	0.002	-0.01
Δν	-295	-64	90
QM	0.189	0.122	0.802
n_i σ	0.131	0.117	0.056
n_i d(T_2)	0.729	0.892	0.974
n_i d(E)	0.848	0.894	0.975
δML	1.319	0.895	0.337
δMC	1.153	0.798	0.313
δML(Φ_σ)	0.423	0.407	0.196
δML(Φ_π)	0.850	0.477	0.124
V_{xc}ML	-0.320	-0.197	-0.067
V_{xc}MC	-0.302	-0.187	-0.065
V_{xc}ML($\Phi_\sigma\Phi_\sigma$)	-0.139	-0.096	-0.042
V_{xc}ML($\Phi_\pi\Phi_\pi$)	-0.129	-0.075	-0.020
V_{xc}ML($\Phi_\sigma\Phi_\pi$)	-0.033	-0.026	-0.005

Table 5.6: DAFH-IQA results for $[Co(CO)_4]^-$, $Ni(CO)_4$,$[Cu(CO)_4]^+$ T_d tetracarbonyls. HF data in atomic units. Parameters for the isolated CO molecule are as follows: $E_{int}(CO)$=-2.120, $V_{cl}(CO)$= -1.706, $V_{xc}(CO)$=-0.415

Quantification of electron sharing (or electron delocalization) provides a similar picture, although backdonation (if not too large) is slightly more effective than donation to delocalize electrons. For that reason, the ratios of the π to σ contributions to δ^{ML} are slightly larger than their equivalents obtained from the total number of electrons transferred, except in the $[Co(CO)_4]^-$ case. In this latter system, the number of electrons shared via π-backdonation doubles those shared via σ channels.

The energetic scale is again a product of these considerations, if we take into account that, as explained above, π links do provide smaller bond energies than σ ones. First, we notice that diagonal orbital terms account for about 90% of the total ML covalent energy. This fact corroborates the goodness of our approximations.

The D_{4h} complex

Concerning non-classical d^8 square planar, only 12 isopycnic functions show non-negligible occupancies at the metal site as shown in figure 5.4. As above, four of them (that may be made to correspond to the metal $3s$ and $3p$ valence) display $n_i > 0.998$ values, and do not contribute to bonding. We also recognize four equivalent σ-donating orbitals (only one shown), and four occupied d-like functions. The d space spans the $A_{1g} \oplus B_{1g} \oplus B_{2g} \ominus E_g$ set of representations in

D_{h4} symmetry, but the B_{1g}-like representative is lacking from our DNOs. This indicates that the system may be described as a d^8 one, again in agreement with formal electron counting. More interestingly, the unrepresented function ($d_{x^2-y^2}$) is the only one having a zero overlap with a π ligand contribution, reinforcing the intuitive role of the d functions as backbonding entities. The four equivalent localized Φ_σ's display $n = 0.086$, and are again very polarized. The probability that one of these effective electrons lies in the M basin is equal to 0.100, and 0.853 that it is found in its corresponding carbonyl, so about 0.047 electrons are found over other basins, basically in the *trans* carbonyl ligand (0.032 of them). As delocalization is concerned, $\delta^{ML} = 0.409$, and its contribution coming from Φ_σ is 0.294. Only 6% of this value is due to MO delocalization. The other three σ functions contribute very little to the ML δ, a mere total of 0.016. The d functions are very localized in the M basin, with n equal to 0.976 for d_{xz} and d_{yz}, 0.988 for d_{z^2} and 0.969 for d_{xy} respectively. They contribute to ML delocalization with 0.107. Backdonation is therefore not large, but non-negligible. The four occupied d functions contribute differently to this value, the largest contribution being 0.041 for d_{xz} if L lies along the x axis, for instance, and the smallest, 0.012 for d_{z^2}, all in entire agreement with chemical intuition. Overall, 0.693 electrons are σ-donated to the metal, and only 0.184 backdonated to the ligands, making the total topological charge of the metal equal to 1.490. The multicenter character of backdonation is again clear, the d_{z^2} and d_{xy}-like DNOs backdonating equally to all the four ligands, while the d_{xz}, d_{yz} backdonate exclusively to two ligands *trans* to each other. Interestingly, σ-donation is also affected by this multicenter delocalization, and each Φ_σ, as stated before, delocalizes slightly over its *trans* situated ligand. All these features are shown in figure 5.5. Notice that what is found here is the existence of direct delocalization channels that affect *trans* located ligands so that a perturbation at a given L will be transmitted directly to its *trans* partner. This effect may hold clues about the origin of the famous *trans* effect and deserves further exploration.

Finally, the total $V_{xc}(ML)$ = -55 kcal/mol is partitioned in the following way: -43 kcal/mol are due to Φ_σ, with only -1 kcal/mol coming from the MO contribution, and -10 kcal/mol are provided by the four Φ_d functions, so backdonation provides less than 20% of the total ML

stabilization energy. Even more interesting is that 80% of backdonation stabilization is due to two d functions: the d_{xy} and the appropriate d_{xz} or d_{yz} component. So as far as covalence is regarded, backdonation is energetically small, but it clearly plays a role in bonding in these non-classical systems, in agreement with modern thinking.

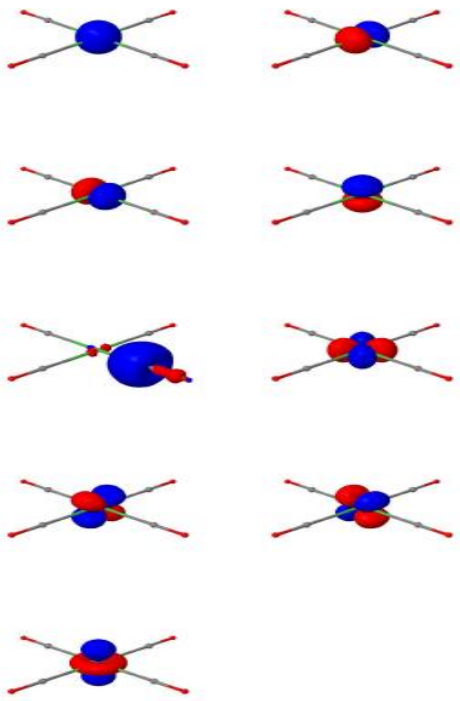

Figure 5.4: Isopycnic DNO orbitals for $[Ni(CO)_4]^{2+}$. Isosurfaces displayed at $|\Phi|$=0.1au

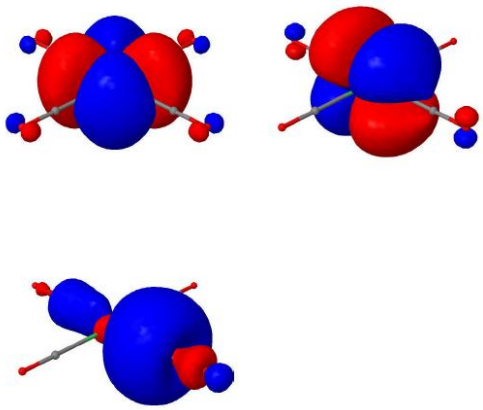

Figure 5.5: Multicenter character of relevant DNO's in $[Ni(CO)_4]^{2+}$. Isosurfaces displayed at $|\Phi|$=0.07 and 0.05 au for d and σ contributes respectively

Chapter 6: The metal-metal interaction

The metal-metal (MM) interaction in policarbonyl metal cluster is one of the most challenging issues in metal-organic chemistry. Since the discovery of the first dimetal policarbonyl $M_2(CO)_n$ molecules, $Fe_2(CO)_9$[79] and $Mn_2(CO)_{10}$[80], a debate on the existence of a direct metal metal bond has arisen. Indeed, it was soon realized that the 18-electrons rule could fail in $M_2(CO)_n$ systems. This was especially true in molecules like $Fe_2(CO)_9$ in which the presence of bridging carbonyls (μ-CO) increases the complexity of the problem[81]. Furthermore, also in case of simpler $Mn_2(CO)_{10}$, early experimental[82] and theoretical[83] studies doubted about the presence of MM bond giving the stability of this compound by a Mn...CO long interaction.

The situation improved with the advent of QTAM which, as read in chapter 2, states that a sufficient and necessary condition for atoms to be bonded is the existence of a bond path (BP) linking them[84] implying the presence of a bond critical point (BCP) between atoms if a direct chemical bond exists. Thus, using QTAM, a better theoretical explanation of MM interaction in $M_2(CO)_n$ was proved. It was found that while "unsupported" (with no bridging carbonyl) molecules have a BCP (a direct MM bond exist), molecules with bridged ligand have not (no direct MM bond)[85]. On the other hand, it is well known that QTAM analysis between transition metal (TM) atoms can be tricky. For instance although the classic Lewis rule predicts a direct bond in bridged $Co_2(CO)_8$, no BCP was found between two cobalts[86]. Despite this, using another topological index like the energy density H(r), Finger [87] found a minimum where the direct CoCo bent-bond should be placed, concluding there was an interaction between two cobalts. The peculiarity of MM interaction and the difficulty to study it was confirmed during the years. Even in case of simple $Mn_2(CO)_{10}$, where a BCP between the two manganeses is present, different hypotheses concerning MM bond were made. Both Bianchi[88] and Farrugia [89] made an experimental measure of ρ and analyzed MM in terms of $\nabla^2\rho$ which is usually used in QTAM to classify a bond. Despite both studies found a BCP between manganeses and similar values of

[79] M.H.Powell, R.V.G.Ewens *J. Chem. Soc.* 1939 **16** 419
[80] L.F.Dahl R.E.Rundle *Acta Cryst.* 1963 **16** 419
[81] C.W.Bauschlicher *J. Chem. Phys.* 1986 **84** 872
[82] M.Martin, B.Rees, A.Mitscheler *Acta Cryst.* 1982 **B38** 6
[83] M.B.Hall P.Coppens *Electron distribution and the chemical bond*. Plenum Press 1982
[84] R.Bader *J. Phys. Chem. A* 1998 **102** 7314
[85] A.A.Low K.L.Kunze P.J.McDougall *In. Chem.* 1991 **30** 1079
[86] P.Macchi, A.Sironi *Coord. Chem. Rev.* 2003 **238-239** 383
[87] M.Finger, J.Rehinold *In. Chem.* 2003 **42** 8128
[88] R.Bianchi, G.Gervasio *In. Chem.* 2000 **39** 2360
[89] L.J.Farrugia P.R.Mallison, B.Stewart *Acta Cryst.* 2003 **B59** 234

ρ_{bcp} and $\nabla^2\rho_{bcp}$, Bianchi described Mn Mn interaction like a closed-shell whereas Farrugia stated that the interaction between metals was a mixture of covalent (shared) and ionic (closed-shell) interactions. It has been proved that using $\nabla^2\rho$ as a bond indicator can be misleading in metallorganic chemistry[90]. Moreover a study[91] based on the source function (SF)[92] reveals how most of the topological indexes fail describing MM bonds. Trying to overcome the ambiguity arisen from QTAM concepts Ponec[93] studied $M_2(CO)_n$ systems through DAFH analysis finding a direct MM bond only for "unsopported" molecules whereas a multicenter 3c2e bond was found for the bridged ones. In the former systems an interaction amongst metal and carbon was also found. This supports the idea that in unbridged $M_2(CO)_n$ molecules a more complicate interaction between two single $M(CO)_{n/2}$ blocks exists[94] rather than a simple MM bond. In summary, despite the big amount of studies made, an exhaustive and final explanation of MM interactions in those types of molecules has not been provided yet. In this chapter the metal metal interaction in dimetal polycarbonyl dimers will be analyzed using the combined IQA-DAFH for brigded ($Co_2(CO)_8$), semibridged ($[FeCo(CO)_8]^-$) and unbridged ($Co_2(CO)_8$, $[Fe_2(CO)_8]^{2-}$) systems.

Bridged systems

The bridged M(μ2-CO)M bond in $Co_2(CO)_8$

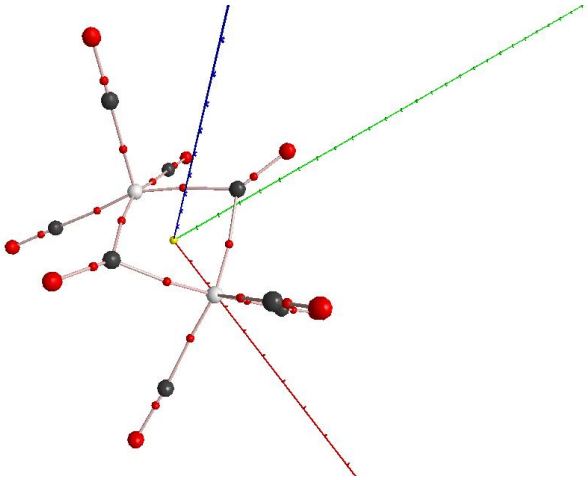

Figure 6.1: Molecular graph of bridged $Co_2(CO)_8$

[90] P.Macchi, D.Proserpio, A.Sironi *JACS* 1998 **120** 13429
[91] C.Gatti, D.Lasi *Faraday Disc.* 2007 **135** 55
[92] R.BAder, C.Gatti *Chem. Phys. Lett.* 1998 **287** 233
[93] R.Ponec,G.Lendvay, J.Chaves *J. Comp. Chem.* 2007 **29** 1387
R.Ponec,G.Lendvay, M.R.Sundberg *J. Phys. Chem. A* 2008 **112** 9936
R.Ponec, C.Gatti *Inorg. Chem.* 2009 **48** 11024
[94] P.Macchi, L.Garlaschelli, A.Sironi *JACS* 2002 **124** 141173

The distance between metals results quite long indicating a weak overlap between metals shells. Indeed, as stated above, no BCP is present between MM in "supported" molecules and so direct metal-metal bond should be excluded. Such hypothesis is also corroborated analyzing the delocalization index between cobalts which is only 0.328e. On the other hand each cobalt shares 0.824 electrons with the bridged carbonyl giving a total of 3.624e shared amongst the four centers. The multicenter nature of the interaction becomes evident analyzing the Fermi hole. Being interested in the bridged bond the basin was defined including cobalts and bridged carbonyls. Twenty DNOs completely localized inside the basins (occupation number = 1) were found. Such DNOs are not bonding resulting attributable to s and p orbitals of metals and to carbonyls one. Analyzing the other eigenvalues related to the basins ($n_i \neq 0$), there are two DNOs with $n_i = 0.96$ and one with $n_i = 0.94$ which are involved in the M(μ_2-CO)M bond. Figure 6.1 shows such orbitals: the former (on the right) is a σ-bond between cobalts and CO whereas the latter (on the left) represents the π-bond which is delocalized amongst the whole bridge system. It should be noticed that occupation numbers are not 1 revealing these bonds are basically but not fully localized inside the bridge. Other 14 bonding orbitals were found. Six of them are σ bonding while the other 8 are π backbonding between Co and $C_{terminal}$. Concerning the second ones, as saw in the previous chapter, they are delocalized between metal and ligands. The energetic profile of the MM interaction reveals a small repulsive energy ($E_{int} = 0.025H$) between cobalts. Indeed, the lack of a direct metal metal bond is reflected in the low covalent energy contribution ($V_{xc} = -0047H$) which cannot fully compensate the electrostatic repulsion ($E_{cl} = 0.071$) between the two positive charges of cobalts. On the other hand such destabilizing interaction is more than compensated by the Co-$(CO)_{bridge}$ one ($E_{int} = -0.203 * 2 = 0.406H$). Thus bridged carbonyls force the dimers together. Analyzing the metal bridge carbonyl interaction, the 33% (-0.067H) of this is due to interaction between cobalt and carbon. Of the remaining 66% (-0.136H) about 90% (-0.121H) is due to the Coulombic attraction between Co and O which results the main component of the bridged bond.

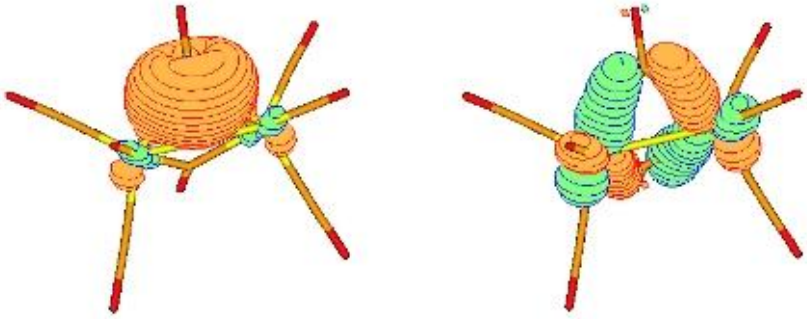

Figure 6.2: Representative isopycnic DNOs for $Co_2(CO)_8$ bridged system. n_i=0.96 and 0.94 respectively reveal there is a minimum of interaction shared with terminal CO. The isosurface has been expanded up to the $|\Phi| = 0.06$ au level.

M	$[Co_2(CO)_8]_{br}$	$[FeCo(CO)_8]^-$	M	$[Co_2(CO)_8]_{br}$	$[FeCo(CO)_8]^-$
d MM	2.546	2.626	Q Co	0.551	0.554
d Co C_{br}	1.954	1.832	Q Fe		0.677
d Fe C_{br}		2.193			
δ MM	0.328	0.294	V_{cl} MM	0.071	0.075
δ CoC_{br}	0.676	0.897	V_{cl} CoC_{br}	0.094	0.101
δ FeC_{br}		0.442	V_{cl} FeC_{br}		0.091
δ CoO_{br}	0.148	0.183	V_{cl} CoO_{br}	-0.121	-0.133
δ FeO_{br}		0.101	V_{cl} FeO_{br}		-0.146
E_{int} MM	0.025	0.030	V_{xc} MM	-0.047	-0.045
E_{int} CoC_{br}	-0.067	-0.117	V_{xc} CoC_{br}	-0.161	-0.218
E_{int} FeC_{br}		-0.006	V_{xc} FeC_{br}		-0.098
E_{int} CoO_{br}	-0.136	-0.150	V_{xc} CoO_{br}	-0.015	-0.018
E_{int} FeO_{br}		-0.156	V_{xc} FeO_{br}		-0.010

Table 6.1: Basic geometric, QTAM integrated properties and IQA interactions for bridged molecules. DFT:PBE data in atomic units, except distances in Å

The semi-bridged M(μ-CO)M bond $[FeCo(CO)_8]^-$

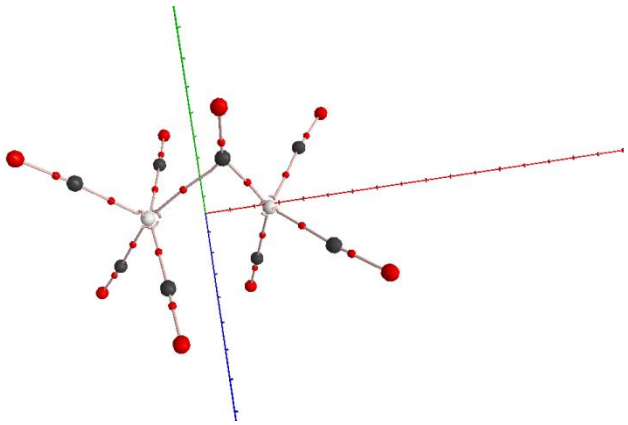

Figure 6.3: Molecular graph of semi-bridged $[FeCo(CO)_8]^-$

As above a direct bond path which joins metals is absent. Unlike the previous case, now, there is only one carbonyl that forces the dimers to be joined. This yields a bigger MM distance than the previous case of about 1Å. Concerning the MC_{br} distance, it results quite long (2.19Å) in FeC case. On the other hand CoC_{br} is 1.83Å resulting shorter than the one in $Co_2(CO)_8$. This is not the case of the Co charge which instead remains constant (0.55au) and lower than the iron one (0.68au) in the two molecules. Regarding the delocalization index of the bridged system, it is 1.917e comparable with 1.976e of the previous case[95]. A decomposition in single contributes reveals how, compared to the previous case, metals shared less electrons ($\delta_{FeCo} = 0.294e$, $\delta_{CoCo} = 0.328e$) whereas, there is a big enhancement of electrons shared between Co and the bridged carbonyl (from 0.824e to 1.080e respectively). Hence, of 1,917e shared inside the bridge, only 0.443e is related to δ_{FeCObr} revealing a different interaction between Fe-CO_{br} respect to Co-CO_{br}. Despite related to different systems (terminal and bridge respectively), a comparison with metal carbonyl molecules analyzed in the previous chapter reveals how δ_{CoCObr} is comparable to neutral molecules while δ_{CoCObr} is on the same magnitude of cations.

The diagonalization of the Fermi hole G-matrix yields the DNOs similar to the previous case and are showed in figure 6.2.

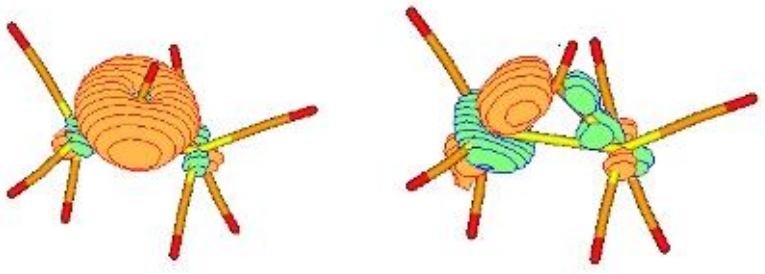

Figure 6.4: Representative isopycnic DNOs for the semi-bridged system. $n_{i-\sigma} = 0.93$, $n_{i-\pi} = 0.79$. The isosurface has been expanded up to the $|\Phi| = 0.1$ au level

The IQA reveals some interesting features. As said above the cobalt charge is equal to $[Co_2(CO)_8]_{bridge}$ and the iron one is bigger. This provides an electrostatic repulsive energy bigger (0.075H instead of 0.071H) than in the previous case. Moreover there are less electrons shared between atoms which consequently lower (in absolute value) covalent energy. This implies a total interaction energy between metals more repulsive than in the bridge $Co_2(CO)_8$.

[95] In bridge $Co_2(CO)_8$ 3.624e is referred to the total bridged system which is composed of 2carbonyls. In order to compare with $[FeCo(CO)_8]^-$ it must be summed only one CO giving the correct value 0.328+0.676+0.148=1.976

Looking at the M-CO components the different nature of interaction between Co-CO and Fe-CO is now evident. Indeed $E_{int}(CoC)$ is -0.117 revealing a classic metal carbonyl interaction whereas $E_{int}(CoC)$ is -0.006 can be considered almost a non-classic one. On the other hand the interaction between metals and oxygen is in both cases attractive and of the same magnitude. Analyzing the single contribute of the interaction energy allows us to understand what is the force which puts together the dimers in this molecule. Concerning Co-CO interaction, being Co-C distance shorter than in $[Co_2(CO)_8]_{br}$, the Coulombic part is a bit more repulsive (0.101H) than in the previous case (0.094). On the other hand, this also increases the stabilization due to M and O electrostatic attraction (which is -0.133H respect previous -0.121H). The enhancement of shared electrons is obviously correlated to the covalent part is -0.236H bigger than in the previous case (-0.176H). Thus, the interaction between Co and the bridge carbonyl is stronger in $[FeCo(CO)_8]^-$ than $[Co_2(CO)8]_{br}$. The interaction between Fe and CO is quite different. Now the bond distance is bigger and so there is less repulsion between Fe and C (0.091H). The iron charge (0.677au) is higher than the cobalt one (0.554au) giving more electrostatic attraction between Fe and O (-0.146H) than in Co-O case (-0.133H). The difference between Fe-CO and Co-CO interaction is much more evident looking covalent terms. In Fe-CO case V_{xc} is only -0.108H of the contribute due to Fe-C (-0.098H) which is less than the half of the one related to Co-C (-0.218H).

Summarizing, as in the previous case the bridge carbonyl is the responsible of the existence of the molecule. The asymmetricity introduced substituting one Co with Fe affects the nature of the bridge bond. Now the cobalt is stronger with CO_{br}. This interaction is characterized by a big covalency. This is not the case of Fe-CO whose bond result mainly due to electrostatic contributes. Somehow the molecule can be seen as a block constituted of $Co(CO)_4$ monomer ($Co(CO)_{3\text{-terminal}} + CO_{bridge}$) which “electrostaticaly bind” the iron one.

Unbridged systems

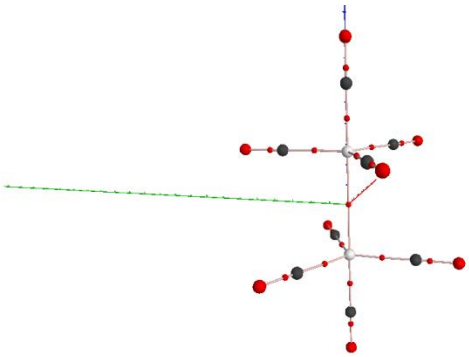

Figure 6.5: Molecular graph of unbridged $[Fe_2(CO)_8]^{2-}$

Now a direct MM bond exists as showed by the presence of a bond path in figure 6.5. The absence of a bridge allows the two dimers to relax lengthening their distances to 2.648Å and 2.847 Å in $[Co_2(CO)_8]_{unbr}$ and $[Fe(CO)_8]^{2-}$ respectively. The iron-iron longer distance affects the charge density at the metal-metal BCP which results more concentrated for $[Co_2(CO)_8]_{unbr}$ ($\rho_{MM_{BCP}} = 0.0335e$) than $[Fe(CO)_8]^{2-}$ ($\rho_{MM_{BCP}} = 0.0259e$). The same feature is provided by the $\nabla^2\rho_{MM_{BCP}}$ which is more negative (-5.9E-3) in the former molecule than in the latter (-2.9E-3).

The elongation of the MM distances also affects the delocalization index between metals. Indeed, although now a direct bond is present, δ_{MM} is quite small in both cases. As found by Macchi[96](figure 6.6) these numbers ($\delta_{CoCO} = 0.425e$, $\delta_{CoCO} = 0.0314e$) should be summed with the small but not negligible contribute coming from the delocalization between one metal and the opposite (proximal) carbonyl. Indeed, each CO shares about 0.1 electrons with the opposite metal giving a delocalization index between one metal and the other monomer of about[97] 1e.

The IQA enlightens the above comments. The charge density lying between the two metals is not so high and cannot completely hide the positive charges of metals. This is particularly true for $[Fe(CO)_8]^{2-}$ which has a total interaction energy between positive metals (0.013H). Indeed, although there is a bond between metals they are quite distant and cannot overlap well. This gives a small covalent contribute comparable to the bridged cases. What binds the molecules now is the interaction amongst metal and proximal carbonyls which, logically, is due to the M-O electrostatic attraction.

[96] P.Macchi, L.Garlaschelli, A.Sironi *JACS* 2002 **124** 141173

[97] Adding all the contributes yields a number of electrons shared between the two monomers of about 1.7electrons

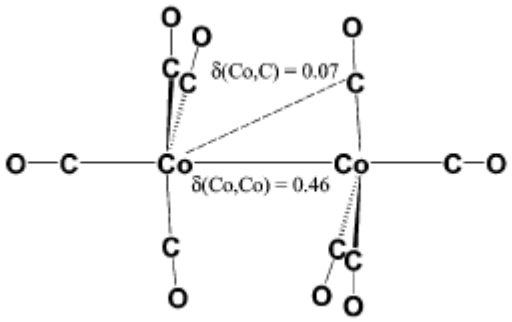

Figure 6.6: P.Macchi, L.Garlaschelli, A.Sironi *J.Am.Chem.Soc.* 2002 **124** 14173

M	$[Co_2(CO)_8]_{un}$	$[Fe_2(CO)_8]^{2-}$	M	$[Co_2(CO)_8]_{un}$	$[Fe_2(CO)_8]^{2-}$
d MM	2.648	2.847	Q M	0.605	0.603
δ MM	0.425	0.314	E_{int} MM	-0.006	0.013
δ MC_{opp}	0.075	0.078	E_{int} MC_{opp}	0.066	0.053
δ MO_{opp}	0.026	0.029	E_{int} MO_{opp}	-0.094	-0.100
V_{cl} MM	0.062	0.060	V_{xc} MM	-0.068	-0.047
V_{cl} MC_{opp}	0.078	0.064	V_{xc} MC_{opp}	-0.012	-0.011
V_{cl} MO_{opp}	-0.092	-0.097	V_{xc} MO_{opp}	-0.002	-0.002

Table 6.2: Basic geometric, QTAM integrated properties and IQA interactions for unbridged molecules. DFT:PBE data in atomic units, except distances in Å

The metal-metal multiple bond

Despite it is not an observable, the bond order (BO) is one of the key concept used by chemists and it is defined as the number of electrons shared between two atoms. Until 1964 it was thought the maximum BO was three; in that year Cotton[98] reported the crystal structure of $[K_2Re2Cl_8]_2H_2O$ with a formal bond order of four. This opened a new frontier in the chemistry world and a lot of molecules with BO four were synthesized.

From the molecular orbital (MO) theory molecules with BO greater than four can exist. With 6 valence orbitals, $5d$ and $1s$, transition metal can reach a BO up to six (2σ, 2π, 2δ). Due to their valence configuration, metals of period 6 (VIB) are the best candidates for this possibility[99]. Theoretical and spectroscopic studies made in the past[100] revealed that dimers as CrCr can

[98] F.A.Cotton, C.B.Harris *Inorg. Chem.* 1965 **4** 3072

[99] U.Radius, F.Breher *Angew. Chem. Int. Ed.* 2006 **45** 3006
G.Frenking *Science* 2005 **310** 796

[100] E.P.Kunding, N.Moskovits, F. Brynda, G.A.Ozin, P.P.Power *Nature* 1975 **254** 503
M.D.Morse *Chem. Rev.* 1986 **86** 1049
E.A.Boudreaux, E.Baxter *Int. J. Quantum Chem.* 2001 **85** 509
G.L.Gustev, C.W.Bauschlicher Jr *J. Phys. Chem. A* 2003 **107** 4755
J.L.Jules, J.R.Lombardi *J. Phys. Chem. A* 2003 **107** 1268

exist but are not stable at room temperature. Ligands can be used to stabilize the dimer reducing the BO to five. After forty years of failed attempts, finally, in 2005 Nguyen[101] successfully synthesized a kinetically stable Ar'CrCrAr' molecule with a formal BO of five. As the bond order is not observable, some criticism arose concerning the real nature of high multiple bond. One claim arose from the bent geometry found in such compounds. The origin of the non linear geometry was explained[102] by the tendencies of sd hybridization to give the strongest σ bond[103]. This was also confirmed with a Walsh diagram[104] showing how in molecules as HMMH the bent geometry is energetically favored. On the other hand, concerning the MM dimers, a clear explication has not been given, particularly for the CrCr case. Its experimental bond length is very short (1.679Ang) but its dissociation energy is quite low (1.66eV). In literature it is described as a sextuple bond[105], a single bond[106] or also an absence of bond between the chromium atoms[107]. The main question concerns the weakness of the delta bond and if this can be considered as a true bond instead of a weak interaction. Moreover, it was proved that the ground state is a singlet[108] but it is not sure if this state arises from a "real multiple bond" instead of an anti-ferromagnetic coupling. Roos *at al.*[109] showed the low dissociation energy of the chromium dimers is due to the size difference between the $3d$ and $4s$ orbitals which generates a $4s$ bond "repulsive" at the equilibrium distance and gives weaker $3d$ bonds, and the repulsive interaction between $3p$ orbitals and the $3d$ ones. Going down to the period, relativist effects change the situation giving a dissociation energy of 4.41ev for MoMo and 5.37eV for WW. Thus a final description about such MM interaction has not been provided yet. Armed with IQA and DAFH techniques I analyzed the bond in dimers of group 6 (VIB). Table 6.3 shows the main results.

[101] T.Nguyen, A.D.Sutton, F. Brynda, G.J.Long, P.P.Power *Science* 2005 **310** 844
[102] M.Brynda, L. Gagliardi, P.Widmark, P.P.Power, B.O.Ross *Angew. Chem. Int. Ed.* 2006 **45** 3804
[103] C.R.Landis,F.Weinhold *JACS* 2006 **128** 7335
[104] G.Merlino, K.J.Donald, J.S.D'Acchioli, R.Hoffmann *JACS* 2007 **129** 15295
[105] E.A.Boudreaux, E.Baxter *Int. J. Quantum Chem.* 2005 **105** 199
[106] E.J.Thomas, J.S.Murray, C.J.O'Connor, P.Politzer *Theochem* 1999 **487** 177
[107] M.M.Goodgame, W.A.Gooddard III *J. Phys. Chem.* 1981 **85** 215
[108] D.L.Michalopoulous, M.E.Geusic, S.G.Hansem, D.E.Powers, R.E.Smalley *J. Phys. Chem.* 1982 **86** 3914
[109] O.B.Roos, A.C.Borin, L.Gagliardi *Angew. Chem. Int. Ed.* 2007 **46** 1649

M	dist	ρ_{bcp}	δ_{MM}	E_{int}	E_{cl}	E_{xc}
CrCr	1.6397	3.00E-01	3.1800	-0.4186	0.1682	-0.5868
MoMo	1.9919	2.18E-01	2.7732	-0.3643	0.1238	-0.4881
WW	2.0510	2.05E-01	3.5534	-0.4963	0.1164	-0.6126

Table 6.3: Bond distance, QTAM integrated properties and IQA interactions for MM molecules. CASSCF data with an active space of 12e-12 orbitals. All data in atomic units, except distances in Å

The bond distances increase going down to the period and are correlated to charge density at BCP. As long is bond as the ρ_{BCP} decreases. Although such results would seem to indicate a strongest bond for CrCr, looking at the interaction energies reveals how this is not the case. Indeed Wolframium dimer is the strongest one with an $E_{int} = -0.496H$. The reason arises from the valence shell of metals as stated by Roos. Cr has $3d$ and $4s$ orbitals which are not so expanded in the space. Thus, metals must be quite close (1.64Å) to be bounded yielding a repulsion amongst the different shells. On the other hand W has a very diffuse $5d$ and $6s$ orbitals which can overlap each other at a longer distance (2.05 Å) reducing in this way the orbitals repulsion. IQA provides a quantification of such effects. Looking at classic energy (which in this case is obviously repulsive), it is higher for CrCr following a linear trend with MM distances. Concerning the covalent part of interaction energy (which is always stabilizing) it is bigger for WW than for CrCr and MoMo respectively. Such trend can be attributed to $ns - (n-1)d$ gap energy and so to relativistic effects. Analyzing the delocalization indexes, which can be viewed as a BO in real space, all of them are lower than 6 questioning the existence of the sextuple bond.

Its absence is also corroborated by DAFH analysis. Indeed, although it is true six DNOs were found to be shared between metals, only four of them (2σ and 2π) can be fully ascribed to real bond. In fact, the remaining 2 DNOs (which are δ interactions as showed in figure 6.7) have $n_i \neq 0.5$ which, because of symmetry, must be in case of a pure bond. Thus, analyzing the occupation numbers (0.32 and 0.68 for CrCr, 0.36 and 0.64 for MoMo, 0.38 and 0.62 foe WW) the delta interaction should be considered as an anti-ferromagnetic interaction instead of pure bonds. It should be noticed how going from Cr to W n_i becomes more close to the bond value of 0.5 increasing their covalent nature. This is apparently in contrast with the delocalization indexes trend deserving further studies in future.

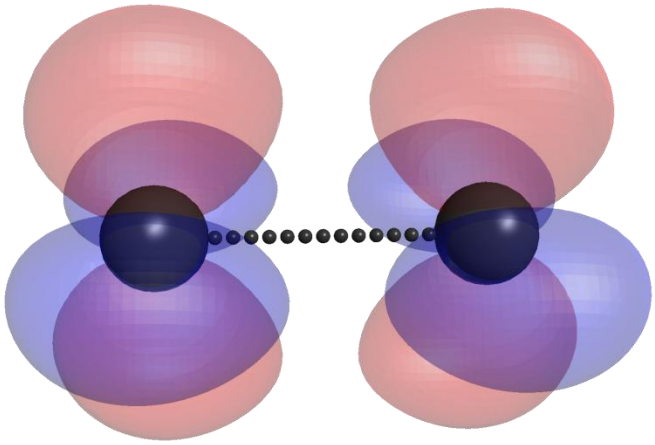

Figure 6.7: Eigenvectors related to delta interactions. The occupation numbers (0.32 and 0.68 for CrCr, 0.36 and 0.64 for MoMo, 0.38 and 0.62 foe WW) reveal how such interactions should be considered as an anti-ferromagnetic interaction instead of pure bonds.

Chapter 7: The metal hydrogen bond

The M-H bond plays a very important role in organometallic chemistry because metal hydrides can undergo insertion with a wide variety of unsaturated compounds to give stable species or reaction intermediates containing M-C bonds[110]. Hieber was the first to report a metal hydride complex with the discovery of $H_2Fe(CO)_4$ in 1931[111]. His claim that this compound contains an Fe-H bond remained controversial until sixties when polyhydride $K_2[ReH_9]$ was synthesized and the reality of the M-H bond as a normal covalency become widely accepted. In spite of its simplicity, during the years, such bond has become important from a pure theoretical point of view[112]. Indeed hydride, the least computational costly atom, can only make σ bond and has negligible steric effect on the bond. Thus, the replacement of a large variety of σ-ligands (in particular alkyls) by a hydride is a common practice. It was also used to define concepts like coordination spheres and isolobal analogy.

The discovery of molecular hydrogen complexes in 1984[113] stimulated intense activity, which continues today. The bonding of a dihydrogen ligand to a TM can be described adapting the donation backdonation model saw in chapter 5. In this case it is the H-H σ bond which donates electrons to the metal and the backdonation occurs into the H-H σ^* orbital. As for CO, removing electrons from a bonding orbital and putting into an antibonding one yields a lengthening of H_2 bond. An important difference exists between M-CO and M-H_2 bond; now, if the two interactions are strong, the H-H bond could be cleaved forming two metal-hydride bond. The possibility of activating an hydrogen bond is very important in industry and so, such balance has been deeply studied during the years. A systematic study[114] of the influence of the L ligand *trans* to H_2 in $[M(CO)_4L]H_2$ revealed there is a nearly linear correlation between the calculated bond energies and the H-H distance. Thus, the stronger is M-H_2 bond the longer is the H-H distance. Ligands that are π acceptors weaken the M-(H_2) bond, whereas ligands that are poor π acceptors tend to strengthen it. Thus, π-acceptor ligands as CO and NO subtract electrons from the metal decreasing the M-H_2 backdonation hampering the H_2 cleavage. On the other hand, since going down into a triad d orbitals become higher in energy and more diffuse, dihydride form is favorite for heaviest metals as proved by Dapprich[115]. Studying the factors

[110] R.H.Crabtree *The Organometallic Chemistry of the Transition Metals*. John Wiley & Sons
[111] W.Hieber, F.Leutert *Naturwissenschaften* 1931 **19** 360
[112] F.Maseras, A.Lledos, E.Clot, O.Einstein *Chem. Rev.* 2000 **100** 601
[113] G.J.Kubas, R.R.Ryan, B.ISwanson, P.J.Vergammi, H.J.Wasserman *JACS* 1984 **106** 451
[114] S.Dapprich, G.Frenking *Organometallics* 1996 **15** 4547
[115] S.Dapprich, G.Frenking *Ang. Chem. Int. Ed.* 1995 **34** 354

which influence classic over non-classic structure, Lin and Hall[116], postulated that a diagonal line splits the d-block. Early TM will assist the break of H-H bond whereas the opposite will be for late metals.

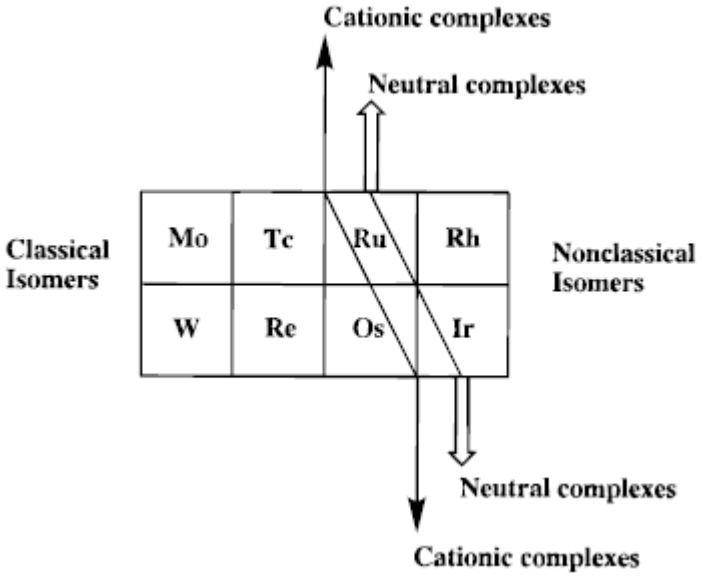

Figure 7.1: F.Maseras, A.Lledos, E.Clot, O.Einstein *Chem. Rev.* 2000 **100** 601

At last, hydrides have an high tendency to bridge two or more metals[117]. Resembling BHB bridge, metals hydride complexes are commonly in octahedral coordination with an easy calculation of metal orbitals used to achieve M-H-M overlap. Moreover, unlike boranes, MHM does not present neutron scattering problem. Thus, such feature makes M-H-M bridge bond particularly interesting in order to study the electron-deficient three-center-two-electron bonds.

In this chapter first the σ bond in simple metal hydride molecules will be explained under IQA approach. Then, the non-classic polihydrides and the bridged system will be studied[118]. Finally, the chapter will end showing a study on H_2 cleavage by transition metal[119].

Metal hydride bond

H^- can bind transition metals donating its negative charge providing a simple σ bond. The following classic hydride were analyzed:

[116] Z.Lin, M.B.Hall *Coord. Chem. Rev.* 1994 **135-136** 845
[117] R.Bau, R.G.Teller, S.W.Kirtley, T.F.Koetzle Acc. *Chem. Res.* 1979 **12** 176
[118] D.Tiana, E.Francisco, A.Martin Pendas, P.Macchi, A.Sironi *to be pubblished*
[119] D.Tiana, C.A.Morrison, P.Macchi *to be pubblished*

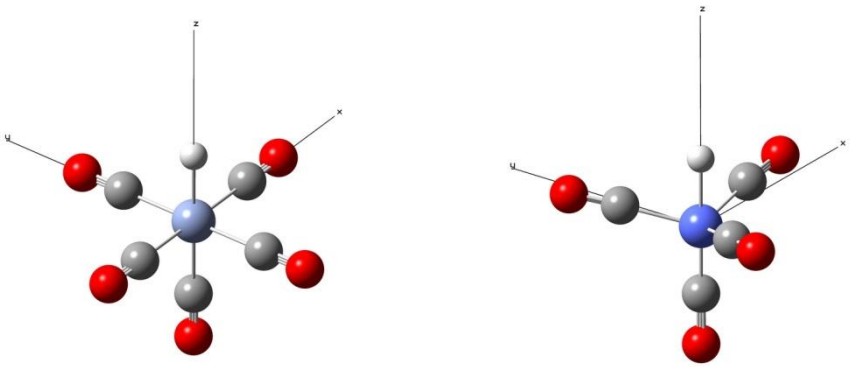

Figure 7.2: Symmetry C_{4v}: $[Cr(CO)_5]^-$, $[Mn(CO)_5]$, symmetry C_{3v}: $[Fe(CO)_4]^-$

The metal hydrogen bond distance decreases from Cr to Fe. The M-H bond critical point is close to the middle of MH bond. In Cr and Mn cases it is closer to H while the opposite is for Fe. Regarding charges, all metals bear a quite positive one which, for C_{4v} systems, resembles the corresponding carbonyl molecule (remembering for instance in $Cr(CO)_6$ Q_{Cr} was 0.930) while it is higher in C_{3v} case (in $Fe(CO)_5$ Q_{Fe}=0.57). The total negative charge of Cr and Fe molecules seems to affect the H charge which is more negative in these cases. QTAM quantities as the charge concentration at BCP and the delocalization index between M and H are correlated to MH distance and increase from Cr to Fe. In all cases these values are lower the M-CO ones indicating that in the molecule M binds stronger with CO than H. The electrons shared between M and CO is about 1e. Comparing such value to homoleptic δ_{M-CO} (in classic O_h metal carbonyls was about 0.7e) molecules the effect of hydrogen σ-donation is clear. Putting electrons into the metal indirectly enhances the back-donation from M to CO increasing the electrons shared between them.

Finally IQA results confirms the above comments. Indeed, as saw before, MH shorter distance in iron molecule yields a number of electrons shared between M and H bigger with a consequently stronger covalent energy between them. On the other hand, the charges are more pronounced in Cr case providing a M-H Coulombic attraction more than double of the other cases for such molecule. Thus, even if $[Cr(CO)_5]^-$ has the weaker M-H covalent bond, it is the molecule where hydrogen has the strongest bound with the metal. Using IQA it is also possible to quantify the effects of M-H bond upon the molecule. Indeed, since H donates electrons to M, this one increases its backdonation to CO. This yields a stronger interaction between M and CO as expected from the classical chemical concepts.

M	$[Cr(CO)_5]H^-$	$[Mn(CO)_5]H$	$[Fe(CO)_4]H^-$
d M-H	1.647	1.569	1.528
d M-BCP	0.831	0.810	0.756
Q M	0.991	0.877	0.638
Q H	-0.251	-0.149	-0.160
ρ_{bcp} MH	0.095	0.114	0.121
δ MH	0.582	0.656	0.678
E_{int} MH	-0.175	-0.165	-0.162
V_{cl} MH	-0.050	-0.018	-0.010
V_{xc} MH	-0.125	-0.147	-0.152

Table 7.1: Basic geometric and QTAM integrated properties. DFT:PBE data in atomic units, except distances in Å. d M-H measures M-H bond distance, d M-BCP provide the distance from metal and the M-H bond critical point

Non classic metal hydrogen interaction

The bond between transition metal and H_2 is a subtle balance between σ donation and π backdonation which has continued to attract an increasing amount of attention since their discovery in dihydrogen complexes in Eighties.

CHART 1: Schematic Representation of the Metal–CO Donor–Acceptor Interactions in Terms of OC → M *σ* Donation and M → CO *π*-Back-donation

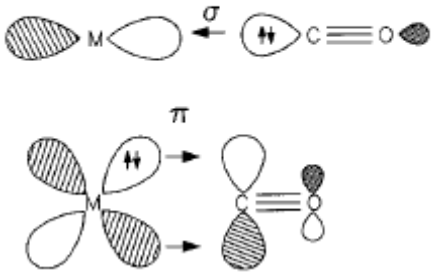

Figure 7.3: Lupinetti *et al.*, *J. Phys. Chem. A* 1997 **101** 9551

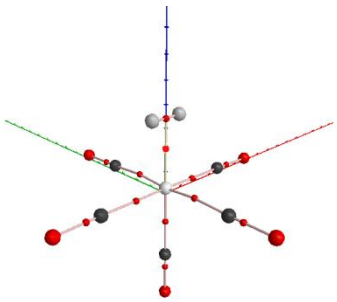

Figure 7.4: Molecular graph of $Cr(CO)_5H_2$

In order to analyze the non classic metal hydride molecules, the C_{2v} symmetry molecule $[M(CO)_5]H_2$ (from now called MH_2) with M=Cr,Mo,W were studied(figure 7.4). Moreover, with the aim of studying the effect of the ligand H_2, the M-H_2 bond was also analyzed in $[H_2Cr(CO)_4]H_2$ changing the axial CO with another H. Results are summarized in table 7.2.

The distance between metal and the middle of H_2 (where the BCP of H_2 lies) has not a linear trend and it is subject to relativistic effect being d(W-H_2) shorter than d(Mo-H_2). The same trend (Cr>W>Mo) is followed by the distance between M and the M-H_2 BCP (lying in the M-H_2 bond path) which in all cases is closer to H than to M. At variance from the MCO case, hydrogen molecule is formed by a single σ bond. Withdrawing electrons from this and putting them into σ^* gives rise to an increasing of the bond length, more than what occurs to a carbonyl. Looking at the changes in H_2 bond length, it is possible to estimate the aptitude of metal to back-donate. Thus, the atoms mostly prompted to back-donate electrons from d-orbitals are W, Cr and Mo in this order. The charges show a different behavior with a linear increase in Q_M and more negative Q_{H2} values going down the group. As usual, the charge concentration at BCP follows the bond distance: the shorter is this the bigger is ρ. More interesting is $\Delta\rho_{BCP}(H_2)$ which provides the ρ hydrogen changes where it binds a metal ($\Delta\rho = \rho_{bind} - \rho_{free}$). All values are obviously negative indicating the weakness of H_2 bond when it is bounded. Since metal backdonation goes in H_2 σ^* orbital (which for its nature is not concentrate in the middle of H_2), these numbers can be used to give a roughly evaluation of the σ donation. The delocalization indexes are in contrast with ρ_{BCP} confirming that the charge density value alone can be misleading and requires further parameters. Indeed, despite CrH_2 has more charge density at BCP, WH_2 is the bond which shares more electrons and as we will see below from IQA it is also the strongest bond. The opposite correlation between M-H_2 and ΔH_2 values is interesting. Indeed $d(\mathrm{M-H_2})$ and $\rho_{BCP}(\mathrm{M-H_2})$ follow the same trend (Cr>W>Mo) of $\Delta\delta(\mathrm{H_2})$ whereas $\Delta d(H_2)$ and $\Delta\rho_{BCP}(H_2)$ correlate (W>Cr>Mo) with $\delta(\mathrm{M-H_2})$. The same happens with the total interaction energy which is bigger for W-H_2 than Cr-H_2 and Mo-H_2 respectively. A detailed analysis of E_{int} components shows how the M-H_2 is mainly due to covalent interaction between M and H_2. V_{xc} is almost equal for Cr and W but, in the former case, the M-H_2 distance is too short giving a small repulsion between M and H_2 resulting in a Cr-H_2 interaction weaker than W-H_2 one. Looking at changing in H_2 it should be noticed how, despite H-H distance is longer,

the repulsion between two H is bigger. This is due to the donation of electron density from H_2 to the metal with, consequently, smaller shielding between hydrogens nuclei.

M	$[Cr(CO)_5]H_2$	$[Mo(CO)_5]H_2$	$[W(CO)_5]H_2$
d M $H_{2\text{-BCP}}$	1.728	1.933	1.881
d M BCP	1.057	1.193	1.171
$\Delta d(H_2)$	0.078	0.064	0.084
Q M	1.024	1.280	1.572
Q H_2	-0.006	-0.027	-0.059
ρ_{BCP} M-H2	0.073	0.058	0.065
$\Delta\rho_{BCP}$ H2	-0.046	-0.040	-0.050
δMH_2	0.546	0.533	0.587
$\Delta \delta H_2$	-0.339	-0.280	-0.318
E_{int} MH_2	-0.112	-0.111	-0.139
ΔE_{int} MH_2	0.057	0.047	0.053
V_{cl} MH_2	0.008	-0.003	-0.017
ΔV_{cl} H_2	0.072	0.060	0.069
V_{xc} MH_2	-0.120	-0.108	-0.122
$\Delta V_{xc}H_2$	-0.015	-0.013	-0.016

Table 7.2: Basic geometric and QTAM integrated properties. DFT:PBE data in atomic units, except distances in Å. Parameters for the isolated H_2 molecule are as follows: $d(H_2)$=0.749, ρ_{BCP}=0.264 , δ^{H2} =1.0, E_{int}=-0.219, V_{cl}=0.041, V_{xc}=-0.260

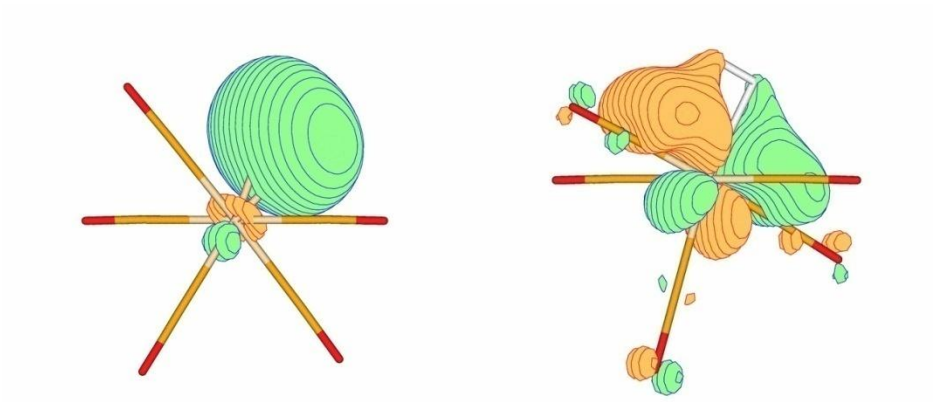

Figure 7.5: DAFH eigenvectors shared between H_2 ans $M(CO)_5$. The occupation number for $Cr(CO)_5H_2$, $Mo(CO)_5H_2$, $W(CO)_5H_2$ were n_i= 0,086, 0.075, 0.096 for σ orbitals and n_i= 0.865,0.889,0.878 for π ones. As for metal carbonyl bond a delocalization character of the π interaction is present.

Finally table 7.3 compares results of $[H_2Cr(CO)_4]H_2$ with $Cr(CO)_5H_2$. Changing the axial carbonyl with an hydrogen molecule has the effect to reinforce the M-H_2 interaction. Indeed CO is an acceptor (which withdraws electrons from molecule) while, as saw above, H_2 is a donor (which pushes electrons into the molecule). This yields a increment of the backdonation from Cr to the other H_2 with, consequently, a weakening of H-H bond. Briefly, the net effect is to move electrons from H-H into M-H_2 as the delocalization indexes change shows. For this reason

$d(\mathrm{M}-\mathrm{H}_2)$ becomes shorter while $d(\mathrm{H}-\mathrm{H})$ becomes longer and there is an enhancement of electron density at M-H2 BCP whereas its decrease is smaller for H-H and, more important, the covalent contribute to M-H_2 interaction increases with a consequent destabilization of H-H bond.

M	$[Cr(CO)_5]H_2$	$[H_2Cr(CO)_4]H_2$
d M $H_{2\text{-BCP}}$	1.728	1.621
d M BCP	1.057	0.989
$\Delta d(H_2)$	0.078	0.092
Q M	1.024	0.963
Q H_2	-0.006	-0.010
ρ_{BCP} M-H2	0.073	0.080
$\Delta\rho_{BCP}$ H2	-0.046	-0.052
$\bar{\delta}$ MH_2	0.546	0.642
$\Delta\ \delta H_2$	-0.339	-0.368
E_{int} MH_2	-0.112	-0.126
ΔE_{int} H_2	0.057	0.063
V_{cl} MH_2	0.008	0.013
ΔV_{cl} H_2	0.072	0.081
V_{xc} MH_2	-0.120	-0.138
$\Delta V_{xc}H_2$	-0.015	-0.018

Table 7.3: Basic geometric and QTAM integrated properties. DFT:PBE data in atomic units, except distances in Å. Parameters for the isolated H_2 molecule are as follows: $d(H_2)$=0.749, ρ_{BCP}=0.264 , δ^{H2} =1.0, E_{int}=-0.219, V_{cl}=0.041, V_{xc}=-0.260.

Metals bridge hydrogen interaction

In chapter 6 the MM interaction was studied in unbridge and bridge carbonyls. Another possibility to bind metals in molecules is bridging them with hydrides. Molecules like $[Cr_2(\mu_2\text{-}H)(CO)_{10}]^-$ are interesting as examples of three center two electron bonds (3c2e). In literature such molecules are considered like σ complexes with a M-H donating to the other M. Even if the reason why the molecule is bent seems to be clear, there is not a definitive explanation for the MHM to be in open (i.e. no M-M bond) or closed (i.e. with a M-M bond) configuration. Indeed, there is no bond path linking the two metals although, looking at Walsh diagram (figure 7.6), a direct bond should be present in bent geometries.

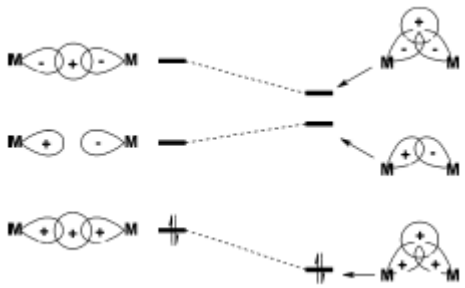

Figure 7.6: According to Walsh diagram the molecule should be bent in case of a significant MM overlap in the MHM moiety

$[Cr_2(\mu 2\text{-}H)(CO)_{10}]^-$ can crystallize in two different conformations: one linear eclipsed (geometry D_{4h}) and one staggered bent (C_s). A linear bent conformation (D_{4d}) was also assumed as a possible transition state on the potential energy surface (PES) as showed by Macchi[120] (figure 7.7). Going down into the group only C_s configurations are present in solid state.

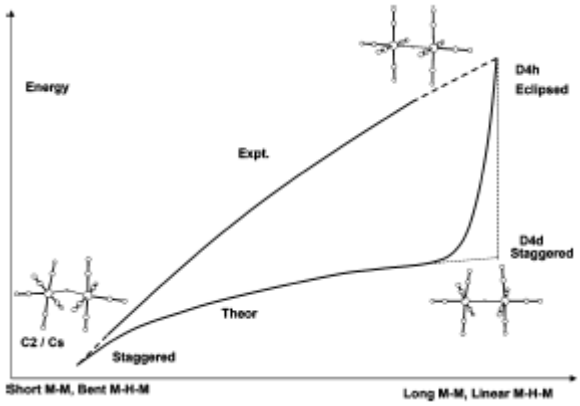

Figure 7.7: $[Cr_2(\mu 2\text{-}H)(CO)_{10}]^-$ PES. The most stable conformations result the C_s bent molecule

In order to clarify the nature of MM interaction in such molecules, $[Cr_2(\mu 2\text{-}H)(CO)_{10}]^-$ was studied at all three geometries while $[Mo_2(\mu 2\text{-}H)(CO)_{10}]^-$ and $[W_2(\mu 2\text{-}H)(CO)_{10}]^-$ at D_{4h} and C_s only.

[2] P.Macchi, A.Sironi *JACS* 2005 **127** 16494

$[Cr_2(\mu 2\text{-}H)(CO)_{10}]^-$

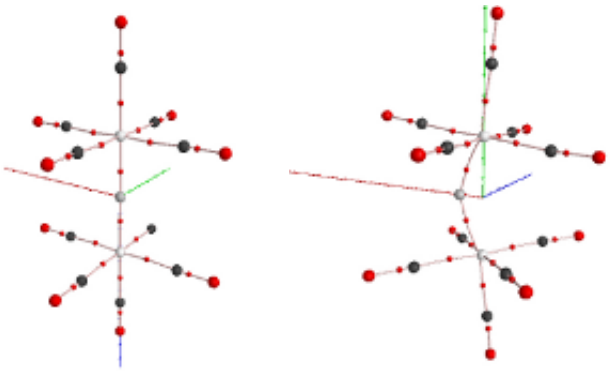

Figure 7.8: Molecular graph for $[Cr_2(\mu 2\text{-}H)(CO)_{10}]^-$ in C_s and D_{4h} geometries respectively

Figure7.8 shows the molecular graphs of molecules for different conformations. As stated above, no BCP is present between metals in C_s configurations. Changing from bent to linear MM distance obviously increases going from 3.29Å to about 3.5Å. This is not the case of $d(MH)$ which is about 1.75Å for C_s and D_{4h} while it is shorter (1.75Å) for D_{4d}. In all molecules $d(MH)$ is longer compared to $d(MH)$ of classic hydride.

Changing from bent to linear molecules shows two different features for H and Cr. Moving H between metals increases its negative charge, while changing from bent to linear geometries does not affect the metal charge which remains constant ($Q_M = 0.97au$) amongst different conformations. Almost constant but with a slightly decrease going from C_s to D_{4d} and D_{4h} is also the charge density concentration at the BCP between Cr and H which is low in every molecules (0.069e, 0.068e, 0.065e). The delocalization index between M and H, obviously negligible in linear systems, is 0.371e in bent molecules corroborating the absence of a direct MM bond. On the other hand the electrons shared between Cr and H are about 0.370e in each conformation. Summing δ_{MM} with δ_{MH} in C_s molecule gives a total number of electrons shared amongst metals and hydrogen (0.371+ 2*0.369) of about 1e.

Analyzing IQA profiles provides an exhaustive explanation of MHM interaction. With a charge of 0.970au the electrostatic repulsion between chromiums is quite high despite the long MM distance. Furthermore, the lack of a BCP between them implies low δ_{CrCr} and then low covalent energy ($V_{xc}(CrCr)$). This gives a quite repulsive CrCr total interaction energy $E_{int}(MM)$ (0.145H, 0.134H and 0.133H for C_s, D_{4d} and D_{4h} respectively). As in "supported"

carbonyl molecules is the interaction amongst metals and bridged atoms which joins together the monomers. Indeed, summing $E_{int}(MM)$ with two times $E_{int}(MH)$ provides a global $E_{int}(MHM)$ (-0.168H, -0.177H and -0.180H for C_s, D_{4d} and D_{4h} conformations respectively) of the same magnitude of $E_{int}(MH)$ in classic hydride. A partition of $E_{int}(MH)$ reveals how, unlike the carbonyl bridge bond which was prevalently electrostatic in nature, in this case both terms (electrostatic and covalent) contribute to the bond with a slightly prevalence of V_{xc}.

Summarizing , since positive charges there is a repulsive interaction energy between metals. This is less destabilizing in linear molecules. Indeed, although in such systems the covalent interaction between metals almost disappears, the hydrogen can shield better the coulombic repulsion. Being the interaction between M and H (which is attractive) almost constant amongst the different conformations, the final result is a MHM interaction more stabile in D_{4h} cases[121]. Finally, since the covalent interaction between MM is very low also in bent configurations, the QTAM idea of a lack of a direct bond between metals is confirmed.

M	Cr Cs	Cr D_{4d}	Cr D_{4h}	Mo C_s	Mo D_{4h}	W C_s	W D_{4h}
d MH	1.750	1.737	1.756	1.901	1.873	1.892	1.866
d MM	3.286	3.475	3.512	3.470	3.745	3.461	3.732
ang MHM	139.8	180.0	180.0	131.7	180.0	132.2	180.0
Q H	-0.288	-0.308	-0.324	-0.370	-0.421	-0.423	-0.470
Q M	0.970	0.970	0.972	1.300	1.292	1.617	1.595
ρ_{BCP} MH	0.069	0.068	0.065	0.066	0.067	0.070	0.070
δ_{HM}	0.369	0.374	0.373	0.419	0.432	0.425	0.431
δ_{MM}	0.371	0.069	0.068	0.107	0.073	0.103	0.069
E_{int} HM	-0.157	-0.155	-0.157	-0.209	-0.222	-0.266	-0.278
V_C HM	-0.075	-0.073	-0.076	-0.118	-0.129	-0.171	-0.183
V_{xc} HM	-0.082	-0.082	-0.081	-0.091	-0.093	-0.095	-0.095
E_{int} MM	0.145	0.134	0.133	0.234	0.222	0.365	0.345
V_C MM	0.156	0.142	0.140	0.248	0.230	0.379	0.353
V_{xc} MM	-0.011	-0.007	-0.007	-0.014	-0.008	-0.014	-0.008

Table7.3: Basic geometric and QTAM integrated properties. DFT:PBE data in atomic units, except distances in Å

Metals hydride bridge interaction in Mo and W cases

Due to the relativistic contraction the longest distances are for Mo: $d(MoH) > d(WH) > d(CrH)$ and $d(MoMo) > d(WW) > d(CrCr)$. An enhancement of charges is observed going down into the group, as metal becomes more positive as H becomes

3 Note this is related only to the MHM bridge interaction. The total energy of the anions are: -1035.6776au, -1035.6753au, -1035.6740au for C_s, D_{4d} and D_{4h} respectively

more negative. Analyzing the $\rho_{BCP}(MH)$ it seems to be not affected by metal change remaining almost constant with only a slight increment in W molecules. This is not the case of delocalization indexes between M and H. In C_s conformation it raises from 0.369e for Cr to 0.419e for Mo and 0.425e for W whereas in D_{4h} it increases from 0.373e to 0.432e and 0.431e respectively. The opposite happens for δ^{MM} which in bent molecules is bigger for Cr (0.371e) than for the others (0.107e for Mo and 0.103e for W). IQA results show the same trend observed in Cr molecules. The main difference is due to the higher charges involved which provide bigger electrostatic energies.

Breaking the H_2 bond. A study of the complex $(PH3)_3FeH_2(\eta^2\text{-}H_2)$

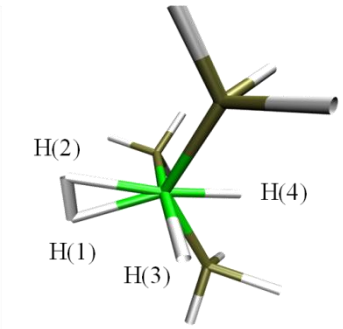

Figure 7.9: $(PH3)_3FeH_2(\eta^2\text{-}H_2)$

Molecular hydrogen complexes play a very important role in industries because of their activation of hydrogen molecules. Through intramolecular exchange these molecules can be used to make-cleavage strong H-H bond. This interesting mechanism was modeled with a molecular dynamic simulation on the complex $(PH_3)_3FeH_4$. As showed in figure 7.10, within 30ps, a flipping process occurred amongst the ligand H_2-2H. Defining the transition state configuration as time 0, a time line study of the phenomenon was made taking geometric configurations arisen during MD and analyzing them in terms of QTAM and IQA.

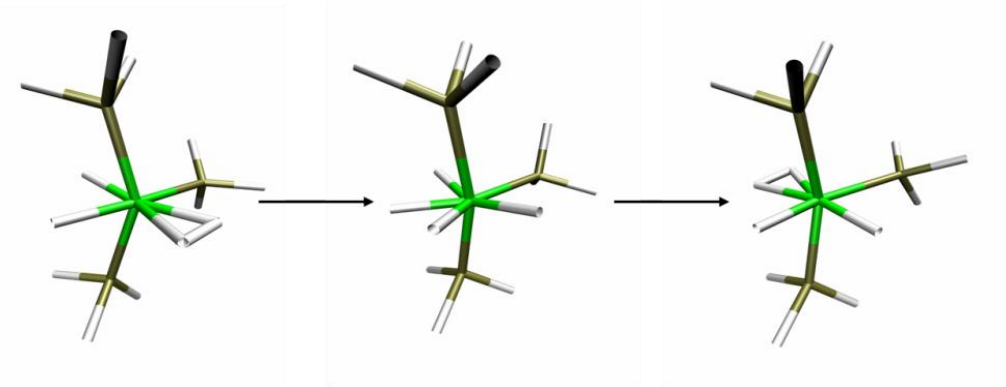

Figure 7.10: During the simulation $(PH3)_3FeH_2(\eta^2\text{-}H_2)$ breaks H_2, goes into a TS where it becomes a classic hydride and then reform H_2between the other H's

The QTAM analysis reveals there are three topological configurations (called A,B,C in figure 7.8). Two of them (A,B) are related to non classical hydride. The difference between them is that one (B) has got a RCP amongst Fe and H_2. Depending on H-H distance, during the simulation, there is a change between them. In detail the ring is formed when H_2 bond length is bigger than 0.92Å. In the timeline -50fs → -25fs H(1)-H(2) distance starts to grow continuously; thus, since after time -50fs H-H distances is always bigger than 0.96Å, a final transition between A and B is observed. The system remains in B configuration until -22fs. After this point, with a H(1)-H(2) distance of about 1.3Å, the BCP between hydrogens is broken and the system goes to classical form (configuration C) with no bond amongst any hydrogen. Obviously the same happens, after t=0, for H(3) and H(4). The bond is formed between them after 14fs when the distance becomes less than 1.3Å.

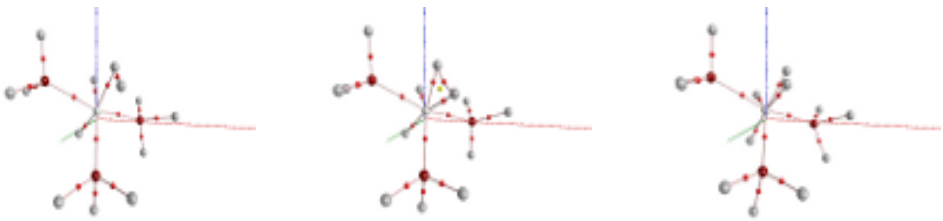

Figure 7.11: Non classic molecule open configuration A, non classic ring B and classic hydride C

While the topological charge of iron remains almost constant during all the simulation with an average value of 0.37au, big changes that require some comments occur for hydrogens. First it is clear the difference between the hydrogens bound in H_2 molecule and the ones that are in hydride form. For instance, at the beginning of the simulation, the negative charge of H(1) and H(2) are small, about -0.05au, whereas for H(3) and H(4) it is lower than -0.2au. It should be noticed that before -22fs H(1) and H(2) should be considered like a single H_2 molecule instead of two different H atoms, the same for H(3) and H(4) after 14fs. Summing H(1) and H(2) charges gives a correct value for the ligand of about -0.1au. This means backdonation from Fe to H_2 σ^* is bigger than donation from H_2 σ to iron d-orbital.

Looking at the graph reported in figure7.12 it is possible to see how the situation evolves over time. A first change arises at about -50fs. After that point H(1) and H(2) start to become more negative while the other two hydrogens lose their charge. This "charge rearrangement" continues till -22fs where, for some time, H(1) and H(3) do not change their charges. After step1235 the change restarts even for these two atoms and finally leads to a total charge of about -0.1au for H(3)-H(4) and -0.2au for H(1) and H(2).

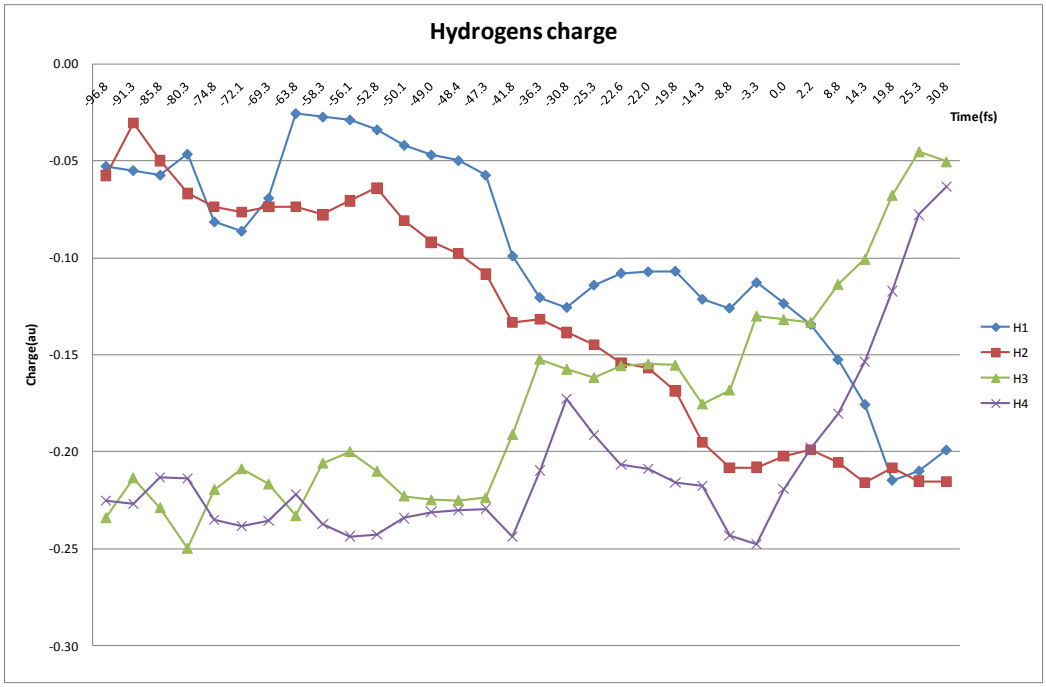

Figure 7.12: Timeline of the hydrogens topological charges

Concerning the delocalization index figure 7.13 and figure 7.14 report the behavior of δ_{Fe-H} and δ_{H-H} respectively. The former shows different situations. When Fe is bonded with an hydride like, for instance, Fe-H(3) and Fe-H(4) until 14fs, δ_{Fe-H} is about 0.75 au. When instead hydrogen is part of an H_2 molecule summing the contribute of the two hydrogens to give the total delocalization index between Fe and H_2, δ_{Fe-H2} we obtain a bigger value with a mean of 0.9au. The chart also reveals that, from a metal bond point of view, change from non-classic to classic occurs in the systems from -50fs → 14fs.

Concerning figure 7.14, the behavior of δ_{H1-H2} was expected. It goes from about 0.55au when two hydrogens are bonded in H_2 molecule to 0.05au when they are isolated H^- hydride ligand. As for topological configuration, the situation starts to change after -50fs and δ_{H1-H2} starts to decrease, passing for a "flat zone" around -22fs, up to the transition state where it is 0.16au. On the other hand δ^{H3-H4} starts to increase during the timeline 50fs → 0fs, it passes through a small flex at about -30fs when its value grows up to 0.19au, goes to the same value of δ_{H1-H2} at t=0fs and finally it grows to about 0.55au when H(3) and H(4) become an hydrogen molecule.

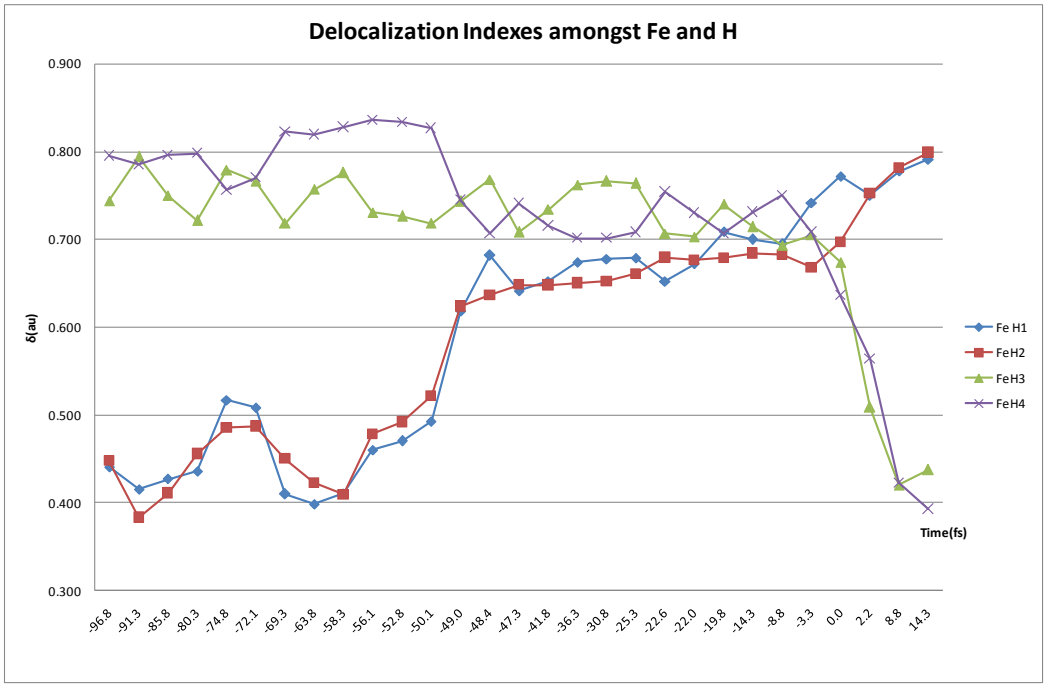

Figure 7.13: $\delta_{Fe\text{-}H}$ timeline

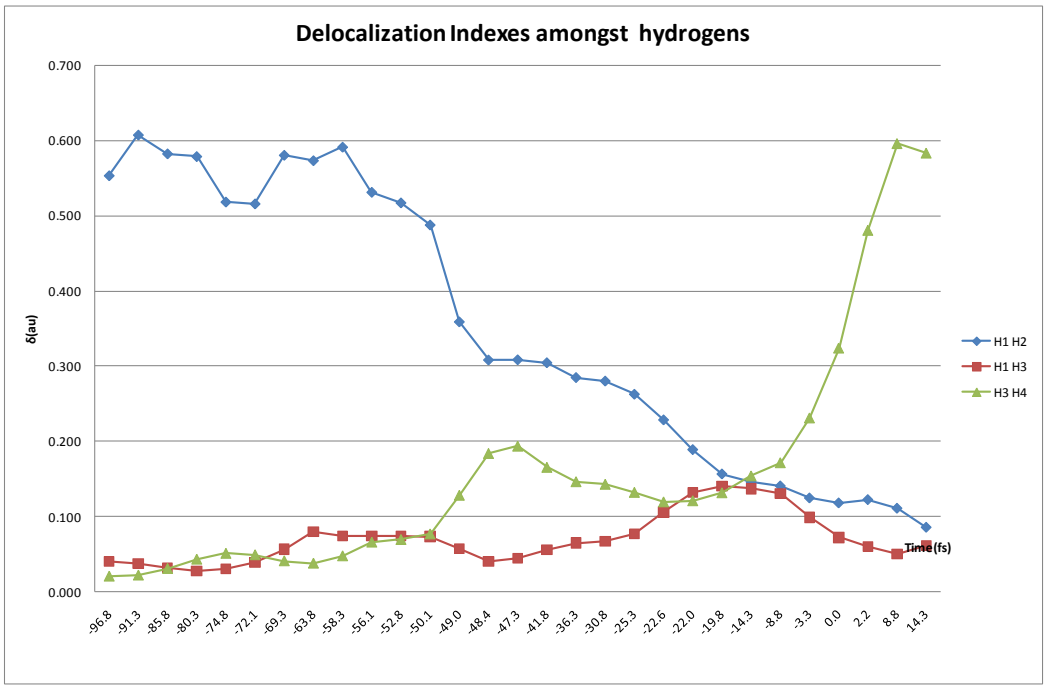

Figure 7.14: $\delta_{h\text{-}H}$ timeline

More interesting is δ_{H1-H3}. Here a first evidence of the so-called *cis*-effect[122] appears. This was introduced[123] for the first time to explain the orientation of H2 in $FeH_2(H_2)(PEtPh_2)_3$ whose conformation is a balance among backdonation between Fe and H_2 and interaction between H_2

[122] J.Riehl, M.Péllisier, O.Eisenstein, *Inorg. Chem.* 1992 **31** 3344
[123] L.S.Van der Sluys, J.Eckert, O.Einstein, J.H.Hall, *JACS* 1990 **112** 4831

and *cis* Fe-H σ bond. From a molecular orbital point of view it was explained[124] as a donation from Fe-H σ bond to H_2 σ^*. During the simulation, H_2 molecule flops and H(1) goes closer to H(3) than H(2). Just before H(1)-H(2) bond is broken, H(1) starts to increase the shared electrons with H(3) arriving at the same value of δ_{H1-H2} and δ_{H3-H4} at time 0fs. Then this value decreases to negligible quantities with reform of non-classic molecule.

It is well-known that δ is related to the covalent energy. We found that there are significant interactions amongst hydrogens only for this pairs: H(1)-H(2), H(1)-H(3) and H(3)-H(4). Figure 7.15 reports the interaction energy for H(1)-H(2) with its partition in coulombic and covalent terms.

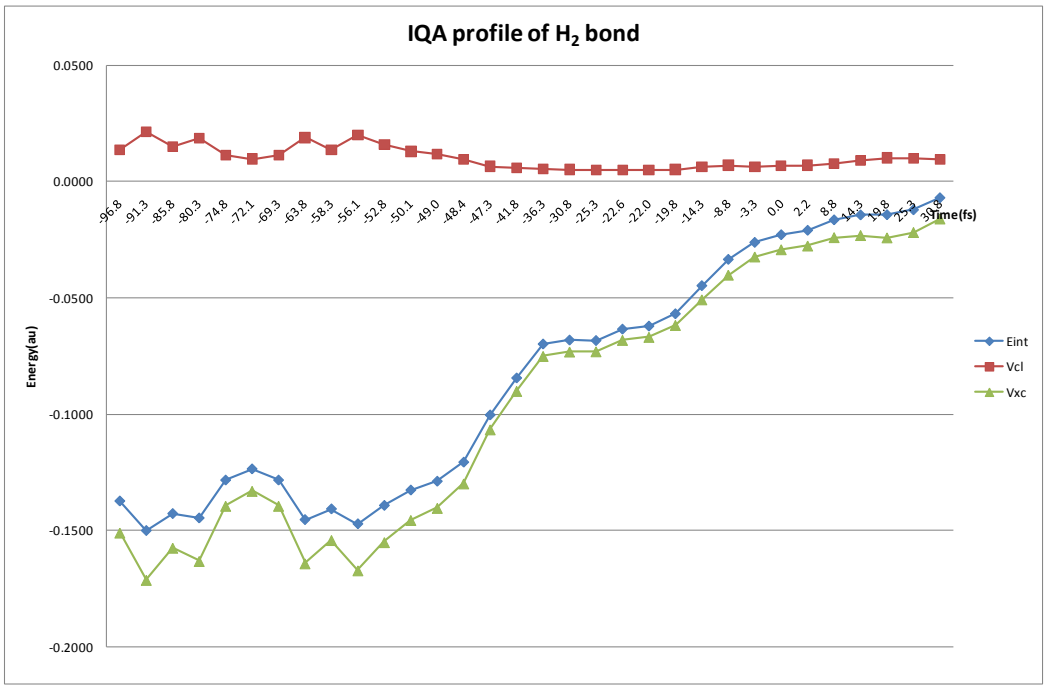

Figure 7.15: IQA profile for H_2

The negative charges on hydrogens (q_H) give a repulsive V_{cl}. Due to the relatively small value of q_H, the coulombic term, it does not affect very much the total interaction energy, thus its shape is mainly determined by the V_{xc}. change. This reflects the quantum nature of H_2 bond[125] and it is confirmed for all the others H-H interactions. Finally, figure 7.16 shows the feature of E_{int} amongst hydrogens. Now the importance of the *cis*-effect in the H_2 breaking is evident.

[124] F.Maseras, A.Lledòs, E.Clot, O.Einstein, *Chem. Rev.* 2000 **100** 601
[125] A.Martín Pendás, M.A.Blanco, E.Francisco, *J. Chem. Phys.* 2006 **125** 184112

After the BCP between H(1) and H(2) disappears, H(1) starts to interact with H(3), arriving to -0.023H (-16.880 kcal/mol) just before t=0fs.

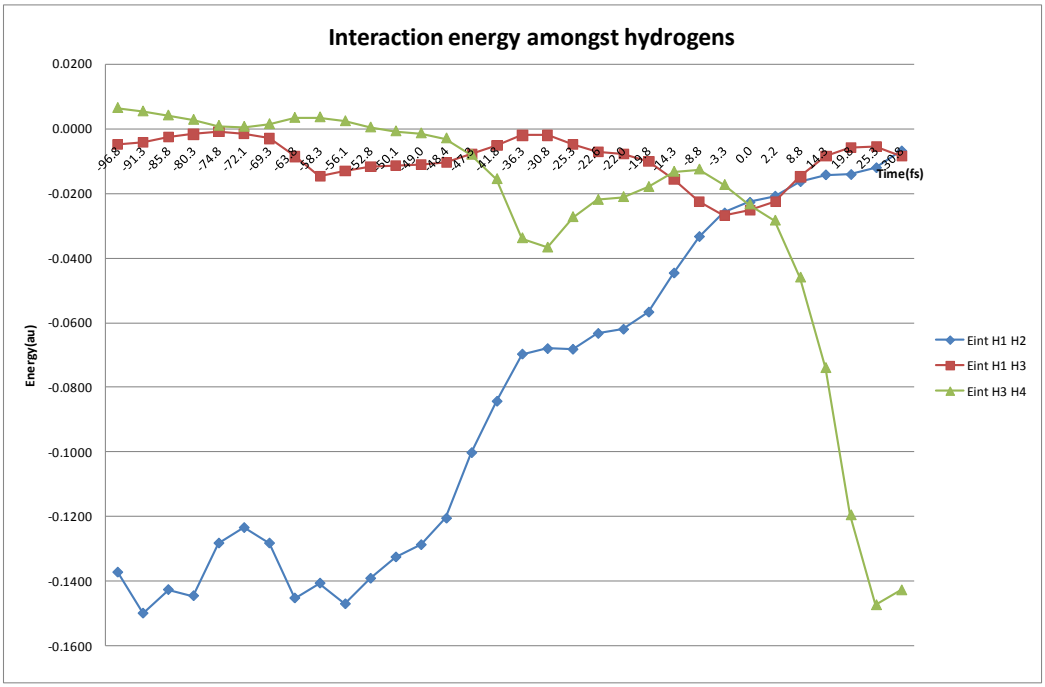

Figure 7.16: Interaction Energy amongst hydrogens

Summarizing, during the simulation the molecule is subject to thermal motion implying a continuous change in distances amongst hydrogens. It can happen that H(3) and H(4) approach each other with an enhancement of interaction and shared electrons between them. This yields a decrease of the delocalization index between them and Fe which, consequently, can increase its donation to H_2, weakening it. This happens three times during the simulation and it is not enough to break the H_2 bond alone. Only when *cis* interaction can arise, the system manages to break H_2 and goes to the transition states. This happens at time -50fs when phosphines motion forces H_2 molecule and an hydrogen (H(3)) to be in the correct configuration. This gives rise to an interaction between H(1) and H(3) with further electrons shifting from H(1) - H(2) to H(1) - H(3) with the consequent cleavage of H_2 bond.

Conclusions and perspectives

In this thesis most of common chemical concepts used in metal-organic chemistry were recovered within a real space description. In detail the main result can be summarized as follow:

- The role of back-donation was quantified and a clear definition of classic and non classic systems was made.
- M_2 fragments (M = Cr, Mo, W) were analyzed revealing how these dimmers are bounded by a quadruple (not a sextuple!) bond assisted by 'anti-ferromagnetic' interactions.
- The presence of multicenter bonds was confirmed (and quantified) for Carbonyl bridged species while the importance of the long range M—CO interaction was recognized for unbridged $[M_2(CO)_n]^x$ molecules.
- Direct MM bonds were ruled out in closo Hydrido bridged molecules, like $[M_2(\eta 2\text{-}H)(CO)_{10}]$.
- The importance of cis-effect for the H-H cleavage in $(PH3)_3FeH_4$ was demonstrated opening a new perspective on hydrogen activation.

Concluding we can say that: by a topological analysis of the electron density it is easy to explain concepts like the DCD model, the 3c2e bond and the charge transfer. The IQA quantifies this interaction providing a clear description of atoms interactions giving the electrostatic and the covalent contribute to the chemical bond in molecules. At last the Lewis concept of chemical bond can be described using DAFH orbitals. Combining QTAM and DAFH with IQA, provides a complete and detailed picture of chemical interactions. Being ρ an experimental measurable quantity allows to introduce a more realistic and easy language in the metal-organic community.

In order to make IQA feasible for TM compounds, the IQA approximation and an openMP parallelization[126] were implemented inside the code. By reducing the time consuming, such parallelization widens the molecular complexity which can be handled with IQA analysis which is now a mature technique ready to be used by the scientific community.

[126] HPC European project n° 228398

Despite of this, some limitations due to the computational cost remain and will be improved in the near future. For instance, Slater type orbital (STO) can be used to add the core to the ECP wavefunction. This not only will improve the treatment of core but also, being STO an analytical function, will fasten the integration during the surface calculation. Maybe more important, another improvement concerns the parallelization. OpenMP speeds up the integration making studies in molecules like Co_2CO_{10} feasible; nevertheless, at the moment, the big amount of memory required limits studies in the dimension of molecules. Indeed, nowadays a good cluster has got about 8 processor per node and up to 32GB of RAM memory. Hence, despite compared to the static version the openMP one is much faster[127], a limit due to the share memory and the number of processors remains. Due to the cost of enhancing the shared memory, the near future will see an increase in the number of nodes in a cluster rather than the number of processors or shared memory in a single node. Thus, the parallelization requires to be extended to an hybrid MPI-openMP. With such improvement it will be possible to split a molecule of x atoms in y nodes and, inside each node, run a openMP calculation extended up to the max number of processor. With this branching the calculation not only will become very faster but also the problem limitation will be removed allowing the extension of IQA theory to big system as macromolecules and metal clusters. Another problem regards how to include the electronic correlation. Indeed, even it seems that DFT wavefunctions(wfn) give reasonable results, the problem of the approximated 2nd order density matrix remains (see Appendix A) and a better solution should be searched. The use of CASSCF or, even worse, CI wfn would repropose the computational cost problem. A possible solution, which is now under test, could be arisen using CAS-MP2 wavefunctions which provide a correlated monodeterminant wfn with a properly 2nd order density matrix defined.

[127] Due to the cycle structure of the code it scales linear

Appendix A: Computational details

All the electronic structures were optimized with Gamess. The QTAM and IQA-DAFH[128] analyses were performed with our Promolden and EDF codes. The basis-set (BS) employed consists of the HAY-WADT[129] small relativist ECP with its standards basis-set for TM. p-Block elements were simulated using a 6-31G(d) basis-set. The same BS[130] was used for simple hydrogen whereas one more polarization function was added for hydrogen bonded with metal. The calculations were done at DFT level with functional PBE. Few words must be spent about DFT. IQA partitioning, necessarily based on numerical integration techniques, is computationally intensive and needs to be fed with well defined 1st and 2nd order density matrices. The 2nd order density matrix constructed from Khon Sham (KS) orbitals is different from the HarteeFock (HF) one. A real theoretical justification lacks. Hence δ and V_{xc} values calculated with DFT are approximated. Probably due to the similarity of KS and HF wavefunctions, it was found[131] DFT value are equiparable to the HF one and DFT techniques provide a realistic description of MM bond[132]. For this reason the first systems studied (metal carbonyl bond) were done at HF level. The literature on M-CO systems is huge, much is known about performances and limitations of HF in comparison to higher-level approaches for the treatment of electron correlation. For instance, Sherwood and Hall[133] showed that 97% the total energy is recovered at the HF level for $Cr(CO)_6$. At this moment, it is well known that MP2 results parallel those trends found at the SCF level, with only quantitative differences. Single determinant approaches give rise to lower binding energies, thus longer MC, and shorter CO distances[134] and to underestimated π-backdonating but reasonable σ-donating effects[135].

Summarizing a simple HF wave function provides a reasonable account of the major binding forces acting on simple transition metal carbonyls. Comparing HF results with DFT ones we found that, in spite of the above problem, DFT gives reasonable results. Actually this is not true for metal-metal dimers. In these high correlated systems DFT results to fail. Counting the valence orbitals like HF it calculates a wrong delocalization index of 6. Strictly related to V_{xc}

---

[128] D.Tiana, E.Francisco, M.A.Blanco, A.Sironi, P.Macchi. A.M.Pendas subm. to *Phys. Chem. Chem. Phys.*
[129] P.J.Hay W.R.Wadt *J. Chem. Phys.* 1985 **82** 299
[130] Hydrogen has got only one electron thus the basis-set was equal to a -31G(p)
[131] G.Y.Wang, C.Matta, N.H.Werstiuk *J. Comp. Chem.* 2003 **24** 379
[132] R.Ponec J.Chaves *J. Comp. Chem.* 2005 **26** 447
R.Ponec, *G.Yuzhakov, R.Carbo Dorca J.Comp. Chem.* 2003 **24** 1829
R.Ponec, F.Feiaxas *Organometallics*, 2004 **23** 1790
[133] D.E.Sherwood, M.B.Hall *Inorg. Chem.* 1983 **22** 93
[134] A.Barnes, C.W.Bauschlicher Jr. *J. Chem. Phys.* 1990 **93** 609
[135] A.W.Ehlers, S.Dapprich, S.Vyboishchikov, F.Frenking *Organometallics* 1996 **15** 105

this result produces a value of the interaction energy completely wrong. Thus, those systems were studied at CASSCF level using an active space of 12 electrons in 12 orbitals.

Appendix B: Code manuals

Promolden

Promolden is the code used to calculate QTAM and, more important, IQA in this thesis. The program read an input made of different lines. An example of input file can be as follows:

```
CAS.wfn
ecp 0
orthowfn
doexchange
tes
        int 1 2
        epsilon 1e-5
        nr 501
        rotate 1 1 2
        lebedev 2810
        lmax 10
        radialquad 1
        rmapping 2
        betasphere
        nobsizetest
        nrb 257
        lebedevbeta 304
        lmaxbeta 6
        radialquadbeta 4
        rmappingbeta 2
        betarad 14 1.4
        betarad 17 1.0
        rbragg  14 2.27010
        rbragg  17 1.03050
endtes
```

As we can see the first line contains (and must be) the name of the wavefunction (written in AIM wfn format) that will be used in calculation. Another evident feature is that the text is included inside tes (theory of electrons separability) and endtes keywords. Such block is related to the IQA analysis. Notice that each keyword is optional. If not present Promolden will use the default value. A summary of options and input keywords will be report in the following paragraph.

Input keywords

- Ecp 0: the program will add core during the surface calculation. A core wavefunction, called core.wfn, is required. This option must be utilized if a large ECP is used and can improve the accuracy in case of small ECP (default = not used).
- Orthowfn: It orthogonalizes the wavefunction (not used)
- Doexchange: this option can be used with a CI or CASSCF wfn (written as a determinant expansion as explained in chapter 2). It separates V_{xc} in exchange and correleate contributes.
- Rmaxsurf n.m ($n = 10.0$): specifies the largest value of the radial coordinate in the integrations.
- Bigoutput (false): provides a big output.
- TES: Promolden makes an IQA calculation.
    - AOM: the program computes only the atomic overlap matrix (AOM) between all the canonical orbitals within the QTAM basins writing the output.wfn.QTAM-summary file.
    - Int atom_i atom_j: only interactions between atom i and j are computed. It is possible calculating as many couple as one need.
    - Exact_surf: if this order is given, the QTAM atomic surface of an atom is determined with an EPSILON precision. Otherwise, it is determined with the precision of the defined radial grid. Usually the precision of this keyword is not required.
    - Cutoff n ($n = 1e - 16$): any Gaussian primitive and Gaussian derivative is assumed to be zero if it smaller than 'cuttz'.
    - Epsilon: precision demanded in the determination of the boundaries of the atomic basins. Default is $1e - 5$. This parameter is only used in this task when the Exact_surf keyword has been activated. Otherwise, the boundaries are obtained with the precision of the radial grid.
    - Epsorb n ($n = 1e - 4$): with this order we change the value of the ‘epsorb’ parameter that determines if molecular orbitals in 'transor.f' routine breaks symmetry or not.
    - Epssym n (n=1e-6): with this order we change the value of the 'epssym' parameter that determines if molecular orbitals in 'transor.f' routine are considered linearly independent or not.

- Tolsym n ($n = 1e-6$): with this order we change the value of the 'tolsym' parameter that is used in symmetry modules and measures the tolerance for identity of points, matrices, and so on.
- Rotate x y z: this keyword rotates the molecule respect to the Cartesian axes. It can be useful in high symmetry molecules as T_d, O_h where the presence of spike lying on a Cartesian axe can make misleading in the atomic basins charge integration.
- Nr n ($n = 100$): number of points in the radial grid outside B-spheres.
- Nphi n (used. $n = 100$): number of phi points outside B-spheres.
- Ntheta n (used. $n = 100$): number of theta points outside B-spheres(100).
- Lebedev n (not used): a bidimensional Lebedev angular quadrature is used outside beta spheres. As only some predetermined numbers of angular points are possible, the program will take the next which is lower than or equal to the selected one. If this keyword is used the values of ntheta and nphi are not used at all. This type of angular quadrature are preferable to theta and phi one.
- Lmax n ($n = 10$): defines the maximum value of the angular momentum number used outside the B-spheres.
- Radialquad n: defines the radial quadrature used in the integrations outside β spheres. The possible choices are:
  - n = 1 Trapezoidal
  - n = 2 Euler-McLaurin
  - n = 3 Clenshaw-Curtis
  - n = 4 Gauss-Chebychev 2nd kind
  - n = 5 Gauss-Chebychev 1st kind
  - n = 6 Perez-Jorda (Gauss-Chebychev) 2nd kind
  - n = 7 Gauss-Legendre
- Thetaquad: defines the theta quadrature used in the integrations, both inside and outside the B-spheres. The possible choices are:
  - n = 1 Gauss-Legendre
  - n = 2 Clenshaw-Curtis
  - n = 3 Gauss-Chebichev 1st kind
  - n = 4 Gauss-Chebicev 2nd kind
  - n = 5 Perez-Jorda
- Rmapping n: defines the mapping function r(u) ($-1 \leq u \leq +1$) outside the β-spheres. Amongst the different mapping functions it has been found the best one is related to option 2 and should not be changed.

- Nobetasphere (default): don't use beta sphere.
- Betasphere (not used): use β sphere in the calculation.
  - Nphibeta n ($n = 100$): number of phi points inside B-spheres (100).
  - Nthetabeta n ($n = 100$): number of theta points inside B-spheres (100).
  - Nrb n:number of points in the radial grid outside B-spheres (100).
  - Lebedevbeta n: a bidimensional Lebedev angular quadrature is used outside beta spheres. As only some predetermined numbers of angular points are possible, the program will take the next which is lower than or equal to the selected one. If this keyword is used the values of ntheta and nphi are not used at all. Note that different kind of quadrature can be used inside and outside sphere.
  - Lmaxbeta n ($n = l_{max}$): defines the maximum value of the angular momentum number used inside the β-spheres.
  - Radialquadbeta n: defines the radial quadrature used in the integrations within β-spheres. The possible value are the same as Radialquad.
  - Rmappingbeta n: as rmapping but referred to β spheres.
  - Betarad atomnum newrad: it reassigns a new β radius value for the atom related to the atomic number read in the wavefunction. The default radius is 0.6Ang. This number should be set from 80% to 90% of the nucleo- BCP distance of atoms.
  - rbragg n: reassigns a new Slater-Bragg radius value for the atom related to the atomic number read in the wavefunction. For instance, in case of an ECP calculation it should be used to set the correct value related to the new protons number of atom in wfn (for instance Ni small ECP will be 28-10=18).
- ENDTES: it finish the TES block

Output

The output is composed of different blocks which report information about the wavefunction used, the system studied and, obviously, provide results. If a normal calculation is made the monoatomic quantities are reported at the end of the output (the atom number is referred to as the wavefunction):

RELEVANT RESULTS FOR ALL THE ATOMS WITH LMAX = 10

Atom	Charge	Eadd	Enet	Eeff	Kin	Loc Index
1	0.990673	-97.851595	-97.021490	-98.681700	42.698304	9.886060
2	0.781369	-37.793369	-36.927866	-38.658872	37.003494	3.627388
3	-1.191550	-74.885159	-74.187324	-75.582993	75.303222	8.260556
4	0.839891	-37.785269	-36.907872	-38.662667	36.989899	3.591359
5	0.839891	-37.785269	-36.907872	-38.662667	36.989899	3.591359
6	0.839891	-37.785269	-36.907872	-38.662667	36.989899	3.591359
7	0.839891	-37.785269	-36.907872	-38.662667	36.989899	3.591359
8	-1.174312	-74.896960	-74.196300	-75.597620	75.301578	8.241258
9	-1.174312	-74.896960	-74.196300	-75.597620	75.301578	8.241258
10	-1.174312	-74.896960	-74.196300	-75.597620	75.301578	8.241258
11	-1.174312	-74.896960	-74.196300	-75.597620	75.301578	8.241258
12	-0.250608	-0.516029	-0.415407	-0.616652	0.574186	0.650506

Concerning the two body contributes ($E_{int}, V_{xc}, V_{cl}, \delta^{AB}$) they are reported inside the TES module and can be easily found looking for “interaction with”:

========== Interaction with atom: 2 ==========

(NN,EN,NE,EE,Inter)	24.147220	-22.351460	-22.074016	20.194556	-0.083700
EE wself : (coul,XC,self)	20.434174	-0.239618	0.166891		
EE woself: (coul,XC)	20.267283	-0.072727			
Coul comp.: (longr, shortr)	-0.116710E+04	0.118753E+04			
Classical Int. (Long,Total)	-0.118791E+04	0.155918E+00			
RHO_2 Integ comp (TOT,J,XC)	67.360223	67.890874	0.530651		
F_AB (XC)	1.061302				

Interaction components as a function of LMAX

	EE	EEwcoul	EEwexch	EEwself	EEwocoul	EEwoexch	EN	NE
LMAX= 0	20.027054	20.189744	-0.162690	0.145149	20.044595	-0.017541	-22.433192	-20.989545
LMAX= 1	20.325208	20.536650	-0.211442	0.160471	20.376179	-0.050972	-22.411775	-22.675773
LMAX= 2	20.267216	20.503947	-0.236731	0.167777	20.336170	-0.068954	-22.475221	-22.208513
LMAX= 3	20.214919	20.457350	-0.242430	0.167123	20.290226	-0.075307	-22.408767	-21.986512

In detail:

In the first row, the last value, Inter, is the interaction energy (-0.0837).

In the second row the second value, XC, is V_{xc} (-0.239618).

In the fifth row the second value, Total, is V_{cl} (0.155918E+00

In the last row there is the delocalization index, F_AB(XC) (1.061302)

In case of int keyword the output change and the results are reported as follows. The pairs that will be analyzed are reported at the beginning of TES module:

```
-------------------------------------------------------------------------
THE FOLLOWING ATOM PAIRS WILL BE ANALYZED
-------------------------------------------------------------------------
ATOM PAIR (  1  2), EQUIVALENT TO PAIR (  1  2)
ATOM PAIR (  1  3), EQUIVALENT TO PAIR (  1  3)
ATOM PAIR (  2  3), EQUIVALENT TO PAIR (  2  3)
-------------------------------------------------------------------------
THERE ARE   0 REDUNDANT PAIRS
```

The atom charge can be obtained subtracting the total charges from proton numbers. To find this quantity inside the output an user first has to move in the part related to the correct atom. This can be done moving to “Monocentric analysis”:

```
 +++ Monocentric analysis on neq atom:  3
 +++ Numbers in parenthesis are (NO B-sphere,B-sphere)
     Number  3  Nuc. charge:    14.0000
 +++ kinetic energy                 :    21.6923 (     8.1089    13.5834  )
 +++ self nuc-el energy             :  -146.0571 (   -41.9623  -104.0948  )
 +++ energy elec( 3)-nuc( 1)        :    -3.5297 (    -1.5520    -1.9777  )
 +++ energy elec( 3)-nuc( 2)        :   -27.1851 (   -12.0097   -15.1754  )
```

Then going down to “TOTAL Charge Multipoles”:

```
++++++   TOTAL Charge Multipoles (Qlm)
                      NO B-sphere      B-sphere         TOTAL
                     ============   ============   ============
        lm   0  0     :  0.55933E+01    0.71069E+01    0.12700E+02
        lm   1 -1     :  0.13329E+00    0.89367E-02    0.14223E+00
        lm   1  1     : -0.24001E-01    0.85568E-03   -0.23146E-01
        lm   2 -2     : -0.13539E+00    0.12540E-02   -0.13413E+00
```

In this case the atom was a Cr simulated using a small ECP. Thus the proton number was 24-10=14 and the chromium charge was 14-12.7= 1.3

Regarding IQA quantities and delocalization index, the pair which is to be analyzed can be located searching “BICENTRIC ANALYSIS ON PAIR” inside the output:

```
 +++++++++ BICENTRIC ANALYSIS ON PAIR    1 ===> Atoms    1 and    2

 NO B-sphere OF ATOM    1 WITH NO B-sphere OF ATOM    2

 ++++++++   lm Convergence   ++++++++++++++++++++++++
       Coulomb     Exch+Corr       Self
 0  0.20115E+01 -0.42482E-01  0.28396E-01
 1  0.20299E+01 -0.63008E-01  0.35017E-01
 2  0.20004E+01 -0.72831E-01  0.37798E-01
 3  0.19994E+01 -0.75360E-01  0.38461E-01
 4  0.19842E+01 -0.75614E-01  0.38175E-01
 5  0.19828E+01 -0.74809E-01  0.37851E-01
 6  0.19826E+01 -0.74299E-01  0.37701E-01
 7  0.19826E+01 -0.74120E-01  0.37654E-01
 8  0.19829E+01 -0.74048E-01  0.37651E-01
 9  0.19830E+01 -0.74052E-01  0.37663E-01
10  0.19830E+01 -0.74051E-01  0.37666E-01
```

And then moving until this summary screen is reached. :

```
                     ----------  TOTAL --- NOBsph-NOBsph ---- Bsph-NOBsph ---- NOBsph-Bsph ------ Bsph-Bsph
COUL with self (COULw)       =       4.719572        1.982987        0.093022        2.524792        0.118770
COUL without self (COULwo)   =       4.666587        1.945321        0.091275        2.511695        0.118295
LONG  RANGE COUL with self   =   -.122680E+01     -.396350E+01     0.949077E-01     0.252302E+01     0.118770E+00
SHORT RANGE COUL with self   =   0.594637E+01     0.594649E+01     -.188543E-02     0.176895E-02     0.000000E+00
Exch-Corr with self (XC)     =      -0.091164       -0.074051       -0.002964       -0.013669       -0.000479
XC without self              =      -0.038179       -0.036385       -0.001218       -0.000572       -0.000005
TOTAL El-El REPULSION (EE)   =       4.628408        1.908936        0.090058        2.511123        0.118290
LONG RANGE TOTAL INTERACTION =   -.609195E+01     -.396350E+01     -.148667E+01     -.244480E+01     0.180302E+01
SELFINT = COULW-COULwo       =       0.052985        0.037666        0.001747        0.013097        0.000474
RHO_2int (J)                 =      17.372107        7.304653        0.334571        9.306616        0.426266
RHO_2int (XC)                =       0.209732        0.155718        0.006735        0.045470        0.001809
DELOCALIZATION INDEX (F_AB)  =       0.419465

(NN,EN,NE,EE,TotalInt)       =       3.897287     -5.205633     -3.529300      4.628408     -0.209238
(TotalInt,Elstat,XC)         =      -0.209238     -0.118074     -0.091164
```

Appendix C: Publications

- Using Pseudopotentials within the Interacting Quantum Atoms Approach.
  J. Phys. Chem. A, 2009, 113 (27), pp 7963–7971
- Bonding in Classical and Nonclassical Transition Metal Carbonyls: The Interacting Quantum Atoms Perspective.
  J. Chem. Theory Comput., 2010, 6 (4), pp 1064–1074
- Restoring Orbital thinking from real space description: Bonding in classical and non-classical transition metal carbonyls.
  submitted to *Physical Chemistry Chemical Physics*
- Breaking the dihydrogen bond: a first principles study of the complex $(PH_3)_3FeH_4$
  to be submitted to *Dalton Trans*
- 'Madelung Effects' on the crystal electron density of metal carbonyl clusters.
  to be submitted to *Acta Crys. A*
- An Interacting Quantum Atoms analysis of metal-metal bonds in $[M_2(CO)_8]^n$ system.
  to be published
- Does the sexutple bond exist? A final answer from the Interacting Quantum Atoms theory.
  to be published
- A real space description of classical and nonclassical metal hydride bond: a theoretical study of the M-H-M bridge bond.
  to be published